Curtin University

Department of Chemical Engineering

Ash Cenosphere Formation, Fragmentation and its Contribution to Particulate Matter Emission during Solid Fuels Combustion

Yi Li

This thesis is presented for the Degree of

Doctor of Philosophy

of

Curtin University

March 2012

Declaration

To the best of my knowledge and belief this thesis contains no material previously published by any other person except where due acknowledgment has been made.

This thesis contains no material which has been accepted for the award of any other degree or diploma in any university.

Signature: ……

Date: ……...…….

To my beloved family

ABSTRACT

Electricity generated from stationary coal-fired power stations has been playing an important role in powering the global economy and is projected to continue its key role in the foreseeable future. However, substantial quantities of fly ash are produced from coal-fired power stations as solid wastes every year, not only exerting significant pressure on waste management but also having adversely impacts on environment. Therefore, there has been considerable R&D to develop technologies for minimizing these adverse impacts of fly ash via various routes e.g. fly ash utilisation.

Ash cenospheres are light-weight, thin-walled and hollow ash particles as part of the fly ash produced from solid fuels combustion. These light-weight ash particles are considered to be valuable materials for manufacturing various value-added products. Since almost half a century ago, substantial R&D was conducted to characterize ash cenospheres and understand their formation mechanisms during the combustion of pulverised solid fuels e.g. coal. Unfortunately, the fundamental mechanisms responsible for ash cenosphere formation during pulverized solid fuels combustion are still largely unclear.

Therefore, the research program in this PhD study aims to carry out a systematic investigation on ash cenosphere formation, fragmentation behaviour and its contribution to ash and particulate matter formation during solid fuels combustion. The specific objectives are to 1) investigate the possible formation mechanisms of ash cenospheres via characterizing the properties of ash cenospheres collected from a coal-fired power station; 2) reveal the fundamental formation mechanism of ash cenospheres during solid fuels combustion using pyrite as a model fuel; and 3) demonstrate the phenomenon of ash cenosphere fragmentation during solid fuel combustion and provide direct experimental evidence on its role in ash and particulate matter formation during solid fuels combustion.

To accomplish these objectives, ash cenosphere samples were collected from a coal-fired power station. A systematic experimental program was also designed and

conducted in a DTF system under various conditions using pyrite as a model fuel. The ash cenosphere samples and ash samples collected from laboratory experiments (including ashes collected in the cyclone and PM_{10} collected by a DLPT) were characterized by various analytical methods. The specific objectives have been successfully achieved in this PhD study.

Firstly, the characterization of narrow size-fractioned ash cenospheres collected from a coal-fired power station indicates that SiO_2/Al_2O_3 ratio decreases with the increase of ash cenosphere size, accompanied with an increase in the sum of TiO_2 and Fe_2O_3 contents. The gas products locked inside various ash cenosphere size fractions are dominantly CO_2 and some N_2. The average gas pressure decreases from 0.227 atm to 0.172 atm (NTP) as particle size increases from 63−75 μm to 150−250 μm. Thermomechanical analysis further shows that ash cenospheres of different size fractions do not melt at 1600 °C, suggesting that these ash cenospheres from coal-fired power station are impossible to be formed at temperatures < 1600 °C. Ash chemistry of individual cenospheres indicates that the optimum particle temperature for cenosphere formation is ~1640 – 1800 °C. Under these conditions, molten ash droplets can be formed and grow by trapping a certain amount of gas generated within the ash droplets. The growth of cenosphere precursors is governed by the wide range of viscosity of molten cenosphere precursors together with the force of surface tension, which is demonstrated to be inversely proportional to the viscosity of molten droplets, producing ash cenospheres with various wall thicknesses. The data also appear to suggest that apart form Fe_2O_3, TiO_2 may play a role in the formation of ash cenospheres during pulverized coal combustion.

Secondly, a systematic experimental program was designed to fundamentally investigate the formation mechanism of ash cenosphere during solid fuels combustion in a drop-tube furnace (gas temperature: 530 – 1100 °C; residence time: 1.1 s) using pulverized pyrite (38-45 μm) as a model fuel. The results show that the formation of ash cenosphere commences at a furnace temperature as low as 580 °C. At furnace temperatures ≥ 600 °C, ash products of pyrite combustion consist of dominantly large ash cenospheres (up to 130 μm in diameter) with thin shells (1−3 μm) and ash cenosphere fragments of various sizes. An increase in furnace temperature leads to enhanced ash cenosphere fragmentation. The presence of O_2 is

found to be essential to the formation of molten Fe-S-O droplets. The sulphur oxides gaseous products produced within the droplets inflate to form cenospheric precursors, followed by further oxidation and resolidification transforms these cenospheric Fe-S-O precursors into final ash cenospheres that also experience fragmentation and contain dominantly iron oxides.

Thirdly, a set of experiments were also carried out to combust pulverised pyrite at 600 °C in the drop-tube furnace system but at various residence times (0.4, 0.7, 0.9 and 1.1 s). Substantial amounts of PM_{10} (dominantly PM_{1-10} and also some PM_1) are produced during the combustion of pulverised pyrite. The PSDs of PM_{10} have a bimodal distribution, i.e. a fine mode with a mode diameter of 0.26 µm and a coarse mode with mode diameters from 4.4 µm to 6.8 µm. At 0.4 s residence time, the production of ash cenospheres is limited. As the residence time increases, the formation of complete ash cenospheres and their fragments increases substantially, suggesting the enhanced fragmentation of ash cenospheres. As a result, there is a substantial increase in the yield of PM_{10} at a longer residence time (e.g. 1.1 s). Therefore, the results in this study provide direct experimental evidences to demonstrate the important role of ash cenosphere fragmentation in PM_{10} formation.

Overall, the present study provides original and new insights into the formation mechanism of ash cenospheres during solid fuels combustion using pulverized pyrite as a model fuel. As the first time in the field, it clarifies the role of ash cenosphere fragmentation and its significant contribution to particulate matter emission. The characteristics of ash cenospheres of various size fractions also provide essential insights into ash cenosphere formation during pulverized coal combustion. Most importantly, the research methodology taken in this PhD study, particularly the design of the systematic experimental program using pyrite as a model fuel provides a simple (but not simpler) solid fuel combustion system for investigating complicated thermochemical process of ash cenosphere formation. This approach makes it possible to thoroughly understand the fundamental formation mechanism of ash cenosphere during solid fuels combustion.

ACKNOWLEDGEMENTS

I gratefully acknowledge the Curtin International Postgraduate Research Scholarship (CIPRS) from Curtin University to support my PhD study.

I would like to express my sincere and deepest appreciation to my supervisor, Professor Hongwei Wu, for providing me the opportunity for this research in his group. I am extremely grateful for his invaluable advice, guidance, patience, and inspiration during my PhD study. Without his persistent support and supervision, my PhD research would not be possible.

Additionally, I am also grateful to have various opportunities in Prof Wu's research group to participate into research activities on other topics such as biomass pyrolysis, biochar etc.

I would like to acknowledge the Centre for Materials Research at Curtin University's Faculty of Science and Engineering for facilities assessment. I would like to thank Ms. Elaine Miller and Mr. William Richard for their technical assistance.

I also would like to express my gratitude to Ms. Karen Haynes and Mr. Jason Wright for their laboratory assistance and Mr. Andy Vierecki for his technical assistance in the lab. Thanks also go the staff from Department of Chemical Engineering for their assistance.

Special thanks go to Dr. Xiangpeng Gao, Dr. Yun Yu, Dr. Kongvui Yip, Dr. Hanisom binti Abdullah, Mr. Alan Burton, Mr. Dawei Liu, Mr. Muhammad Usman Rahim, Mr. Syamsuddin Yani, Mr. Sui Boon Liaw, Ms. Yanwu Yang, Ms. Zhaoying Kong and Ms. Mingming Zhang in our research group for their help in various ways.

Last but not least, I am deeply indebted to my beloved family, for their support and encouragement during my PhD study. I especially would like to express my greatest appreciation to my husband, Mr. Zuhua Hu, for his love, support and encouragement, and my son, Master Xutao Hu, for his love, understanding and encouragement during my PhD study.

PUBLICATIONS

Yi Li and Hongwei Wu. Ash Cenosphere from Solid Fuels Combustion. Part 1: An Investigation into its Formation Mechanism Using Pyrite as a Model Fuel. *Energy & Fuels* **2012**, 26 (1), 130-137.

Yi Li, Xiangpeng Gao, and Hongwei Wu. Roles of Ash Cenosphere Fragmentation in the Formation of Ash and Particulate Matter during Pulverized Pyrite Combustion. *The 7th International Symposium on Coal Combustion* ***2011***, 17-20th July, Harbin, China.

Yi Li and Hongwei Wu. Formation of Ash Cenosphere during the Pyrolysis and Combustion of Pyrite in a Laboratory-Scale Drop-Tube Furnace. *Asia Pacific Conference on Sustainable Energy & Environmental Technologies* **2011**, 10-13th July, Adelaide, Australia.

Hongwei Wu, William Hendrawinata, Yun Yu, Xiangpeng Gao, **Yi Li**, John Bartle, and Peter Grayling. Effect of Hydrodistillation on 1,8-Cineole Extraction from Mallee Leaf and the Fuel Properties of Spent Biomass, *Industrial & Engineering* Chemistry Research **2011**, 50: 11280–11287.

TABLE OF CONTENTS

LIST OF FIGURES

LIST OF TABLES

CHAPTER 1 INTRODUCTION

1.1 Background and Motive

Coal is an important primary energy source for electricity generation and it will continue its significant share in the global energy mix for the foreseeable future. It is projected in the International Energy Outlook 2010 that coal-fired generation is expected to account for 43% of world electricity supply in 2035.[1] However, electricity generation from stationary coal-fired power stations leads to the production of considerable amount of fly ash as solid wastes. The large quantify of fly ash not only poses seriously adverse impacts on environment and human health but also causes significant pressure on waste management.[2-6] Therefore, considerable R&D has been carried out globally to minimise these adverse impacts of fly ash, via extensive and effective fly ash utilisation in various industry, agriculture and construction applications.[7-9]

In Australia, around 12 millions tonnes of fly ash were produced annually from coal-fired power generation during the last five years.[10] However, only about 10 % of the fly ash was utilised, leaving Australia unfortunately being one of the countries of the lowest ash utilisation.[10-12]

As part of the fly ash produced from solid fuels combustion, ash cenospheres are lightweight, thin-walled and hollow spherical particles,[13-23] which typically have bulk densities of 0.2-0.5 g/cm and sizes of 20-200 μm.[13, 15, 19, 20, 24, 25] Ash cenospheres have superior physical, chemical, mechanical, and thermal properties so that these materials are widely used for manufacturing various value-added products, such as lightweight construction products and lightweight composites.[26-31]

The past several decades have witnessed a substantial amount of research, which went into characterising ash cenospheres and understanding the behaviour and mechanisms of ash cenospheres formation during pulverised coal combustion. The thin-shelled, hollow and spherical nature of ash cenospheres suggest that ash cenosphere formation requires a source of gas enclosed within the molten ash

droplets of inorganic residues during coal combustion, followed by resolidification of these particles as a result of rapid quenching in the later stage of combustion. Unfortunately, in despite of the substantial past research, the mechanisms responsible for ash cenosphere formation during pulverised coal combustion is still largely unclear. Yet, such knowledge is of great need and interests of coal-based power generation companies for maximising the production of ash cenosphere of desired quality without affecting the main business of electricity generation.

The previous work on the characterisation of ash cenospheres produced from coal-fired power stations was largely based on bulk samples. A recent work from our research group[19] clearly demonstrates the difference in the structure of ash cenospheres of various size fractions. Further work is required to understand the possible mechanisms leading to such a difference, considering differences in ash chemistry and gas locked in the ash cenosphere of different size fractions.

Fundamentally, it is also desired to design an experimental program, which enables an investigation into the formation and behaviour of ash cenospheres during solid fuels combustion. As coal as a fuel generally contains a mixture of various mineral particles, a simple fuel needs to be used, which should only contain one mineral and can produce ash cenospheres during combustion. Pyrite (FeS_2) as an iron-bearing mineral widely present in coal is a good option. It was observed that ash cenospheres can be possibly formed from pyrite combustion,[32, 33] however little was discussed in those studies on ash cenosphere formation.

In addition, it has been long speculated that fragmentation of ash cenospheres during pulverised coal combustion can be potentially an important mechanism for ash formation.[34-36] Such reasoning seems to be plausible given the nature of these particles. However, to the author's knowledge, there is little work done so far in understanding the roles of ash cenosphere fragmentation in the formation of particulate matter with aerodynamic diameter of 10 μm (PM_{10}).

1.2 Scope and Objectives

The present study is to fundamentally investigate ash cenosphere formation, fragmentation behaviour and its contribution to particulate matter emission during

solid fuels combustion through a systematic experimental program. The specific objectives are to:

(1) further investigate possible formation mechanism of ash cenospheres from pulverised coal combustion via the characterisation of thermal behaviours, ash chemistry and properties of gas locked inside ash cenosphere particles of different size fractions.

(2) design a systematic program for investigating formation mechanisms of ash cenospheres during solid fuels combustion under various conditions using pyrite as a model fuel.

(3) investigate ash cenosphere fragmentation and its significant role in the formation of ash and particulate matter during pulverized pyrite combustion.

1.3 Thesis Outline

This thesis is organized into total seven chapters as outlined detailed below. The structure of this thesis is illustrated in Figure 1-1.

- **Chapter 1** introduces the background and motive, objectives, and structure of this thesis.
- **Chapter 2** reviews the current research progress on ash cenospheres formation from solid fuels combustion, pyrite transformation during combustion and PM_{10} formation during pulverised-coal combustion. Based on the literature review, key research gaps are identified and research objectives are clarified.
- **Chapter 3** summaries the research methodology (including experimental and analytical techniques) deployed to achieve the research objectives.
- **Chapter 4** characterises the properties of size-fractioned ash cenosphere samples from a coal-fired power station, for investigating possible formation mechanism of ash cenospheres during pulverised coal combustion.

- **Chapter 5** reports the results obtained from a set of systematic experiments for investigating the formation of ash cenosphere during combustion, using pyrite as a simple model fuel.

- **Chapter 6** presents the clear evidence on the significant role of ash cenosphere fragmentation in the formation of ash and particulate matter during pulverised pyrite combustion.

- **Chapter 7** summarises the conclusions of the present study and recommends future work.

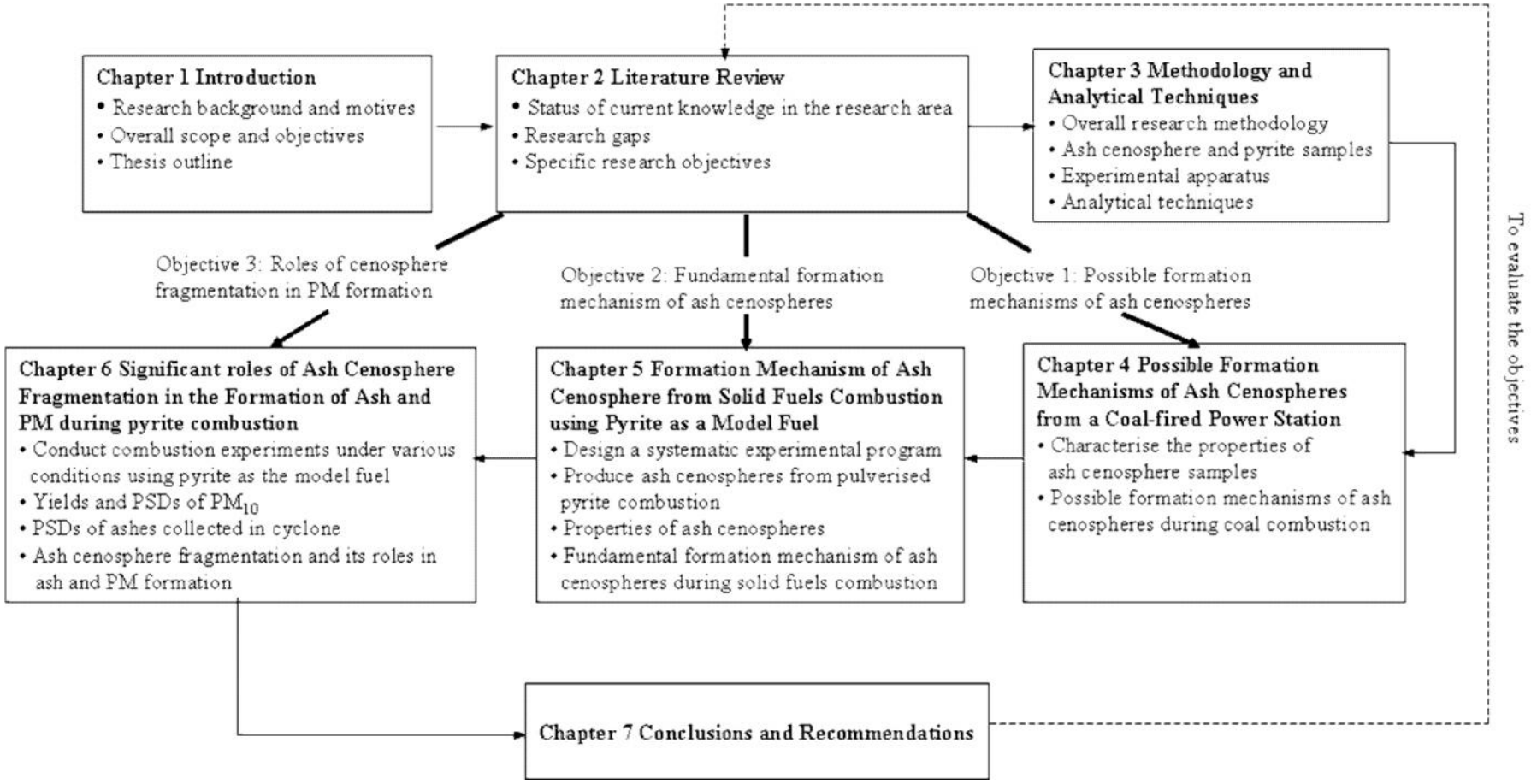

Figure 1-1: Thesis map

CHAPTER 2 LITERATURE REVIEW

2.1 Introduction

Ash cenosphere is part of fly ash produced from pulverised-coal combustion in coal-fired power stations. The term cenosphere was originated from Greek kenos (hollow) and sphaira (sphere), firstly used by Sinnatt's research group[37-39] to describe hollow char particles formed during coal pyrolysis. Ash cenospheres refer to ash particles that are hollow, of a low bulk density (lower than that of water), and typically collected from the surface of ash lagoon.

This chapter firstly reviews the up-to-date research progress in the characterisation, formation and utilisation of ash cenospheres from pulverised fuel combustion. It then summarises the existing evidence on the observation of ash cenosphere during pyrite (FeS_2) combustion as pyrite will be used as a model fuel for investigating ash cenosphere formation and behavior in this study. This chapter is then followed by a section on the mechanisms responsible for PM_{10} formation during pulverised coal combustion because this PhD thesis will investigate the roles of ash cenosphere fragmentation in PM_{10} formation. This chapter concludes with the key research gaps identified and the research objectives listed.

2.2 Ash Cenospheres from the Combustion of Pulverised Fuel

2.2.1 Properties of Ash Cenospheres

The properties of ash cenospheres are generally characterised into four aspects: physical (and morphological) structure, mineralogy, chemistry, and thermal properties.

Physical (and Morphological) Properties. While the real density of ash materials in ash cenospheres is > 2.0 g cm^{-3}, the apparent density of ash cenosphere is generally in the range of 0.4 to 0.8 g cm^{-3} and the bulk density varies from 0.2 to 0.5 g cm^{-3} (much lower than that of water).[13, 17, 20, 21, 26, 30, 40-48] Therefore, ash cenospheres can

be easily separated and collected from fly ash in ash lagoons as ash cenospheres have low apparent density and float on the lagoons' surface.[20, 24, 25] Ash cenospheres may have particle sizes ranging from 5 to 500 µm, typically 20 – 200 µm.[13, 17, 19-22, 25, 30, 42, 43, 45, 46, 48-53] The particle surface is generally smooth, with uneven texture or having blisters on. The shell thickness of ash cenospheres can vary from 1 to 20 µm. The apparent ratio of wall thickness to particle diameter is 3 – 16%, calculated based on the estimation of bulky ash cenosphere samples.[20, 21, 30, 45, 48, 51, 53, 54] However, the direct measurement of true diameter and shell thickness of ash cenospheres on a particle-by-particle basis via a novel technique developed recently show that such a ratio is limited between an upper bound of ~10.5% and a lower bound of ~2.5%, irrespective of ash cenosphere size.[19] Table 2-1 summarizes the typical physical properties of ash cenospheres.

Table 2-1: Typical physical properties of ash cenospheres

Item	Description
Appearance	Spherical particle with smooth or uneven surfaces (see references[20, 21, 30, 41, 43-45, 47, 50])
Apparent density (g	0.4 – 0.8 (see references[20, 21, 30, 43-46])
Bulk density (g cm^{-3})	0.2 – 0.5 (see references[13, 17, 20, 21, 26, 40, 42, 43, 47, 49, 52])
Particle size (µm)	20 – 200 (see references[13, 19-21, 30, 42, 46, 48-50, 52])
Shell thickness to diameter ratio	2.5 - 10.5% based on particle-by-particle analysis[19]

The common perception is that ash cenospheres are generally hollow with thin shells so that the cross-section of an ash cenosphere has a ring structure.[19, 20, 30, 43, 44, 48, 54] However, the recent study by our research group[19] has showed that the ash cenospheres separated from fly ash via density separation using water as a media consist of two different types of structures. One is spherical and of a single-ring structure (see Figure 2-1a) and the other is irregular and of a network structure (see Figure 2-1b).

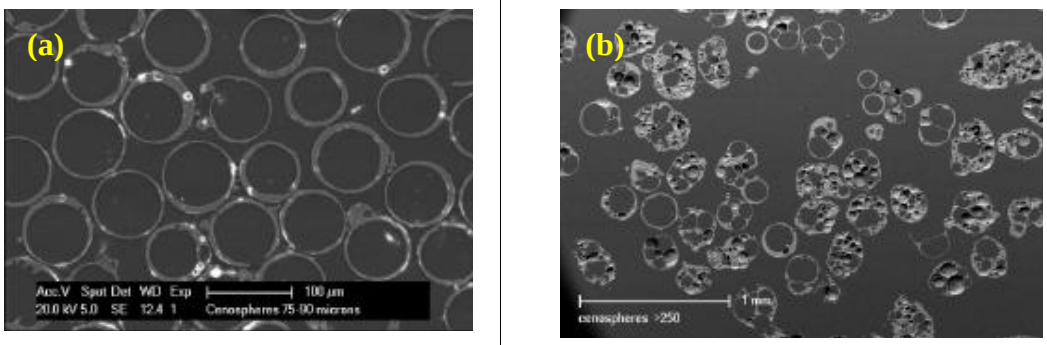

Figure 2-1: Morphology of ash cenospheres with (a) spherical shape with a single-ring structure; (b) non-spherical shape with a network structure.[19]

Mineralogy. The mineralogy of ash cenospheres varies from sample to sample. It is reported that mullite and/or quartz are the main crystalline phases identifiable in the shells of ash cenospheres, based on XRD analysis.[17, 41, 44, 46, 50, 55] The minor or accessory mineral phases in the shells of ash cenospheres are plagioclase, K-feldspar, dolomite and some gypsum and Fe oxides.[22] However, ash cenospheres from the combustion of solid fuels are generally amorphous aluminosilicate glass phases (70-90 wt%).[22]

Chemistry. The chemical compositions of ash cenospheres also vary from sample to sample, depending on the power station where the sample was collected. Table 2-2 lists the chemical compositions of bulk ash cenospheres reported in the literature. As generally FeO_x, SiO_2 and Al_2O_3 are dominant in the chemistry, the compositions are normalized to 100% and plotted in Figure 2-2 as a ternary diagram.

There are three important observations can be made based on Table 2-2 and Figure 2-2. Firstly, the chemistry of ash cenospheres varies from power plant to power plant. Such variations in the chemistry of ash cenospheres are expected, depending on mineralogy of ash-forming species in the parent coals and combustion conditions.

Secondly, Si and Al oxides are dominant (> 80% by weight) in the chemistry of ash cenospheres, with SiO_2/Al_2O_3 ratio varying from 1.3 to 2.5. Such chemistry is in

accordance with the mineralogy of ash cenospheres which contain commonly aluminosilicate glass phases plus mullite and quartz as the main crystalline phases.

Lastly, there has also been debate on whether iron species are essential to ash cenosphere formation. Raask[20] suggested that a minimum ~5% ferric oxide (Fe_2O_3) is essential to ash cenosphere formation, as it provides the required source of oxygen for gas generation inside the molten silicate particles for expansion. This conclusion appears to be suggested by the majority of the published data in the literature, as summarized in Figure 2-2 and Table 2-2. However, there were several studies[19,51], in which it is clearly shown that high yield of ash cenospheres were produced when iron oxide was very low (<0.5%). It is therefore clear that during pulverised fuel combustion, there are different mechanisms responsible for ash cenosphere formation. Iron may be one of the important factors for enabling gas generation within the molten precursor droplets. Other possible sources of gas generation including decomposition of carbonates, dehydration and dehydroxylation of clay minerals, evaporation of pore water and fusion of silicates should be considered as suggested in the literature.[20, 21, 25, 56]

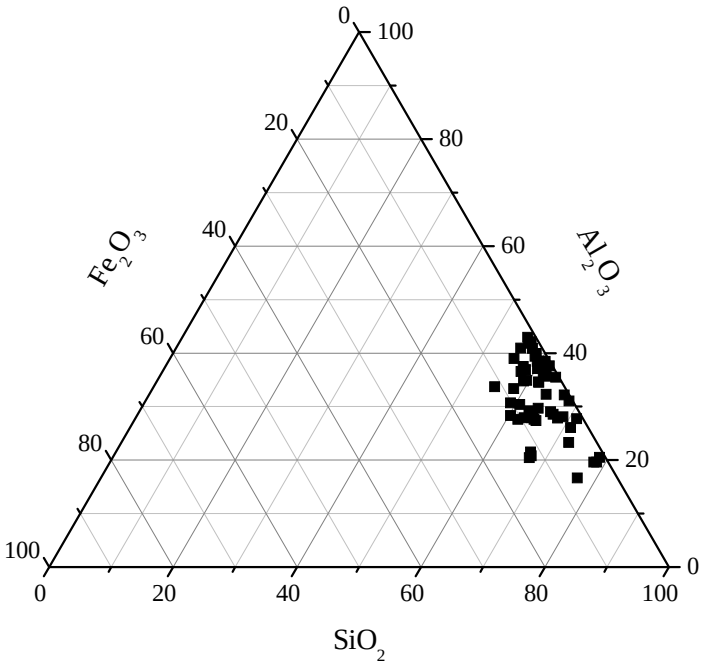

Figure 2-2: SiO_2-Al_2O_3-Fe_2O_3 ternary diagram of chemical compositions of ash cenospheres from literature data in Table 2-2.

Table 2-2: Summary of bulk chemical compositions (wt %) of ash cenospheres from various sources reported in the literature.

Reference	Source of Cenosphere samples	SiO_2	Al_2O_3	Fe_2O_3	CaO	MgO	Na_2O	K_2O	TiO_2	SO_3	P_2O_5
Anshits et al.[13]	Nonmagnetic cenospheres H	64.64	20.85	4.05	2.24	1.85	0.93	3.19	0.31	0.24	
	Nonmagnetic cenospheres M	63.66	25.93	2.84	1.19	0.86	0.48	2.90	0.74	0.25	
	Magnetic cenospheres MH -0.18+0.08	52.00-66.76	16.75-21.25	1.96-3.08	1.96-3.08	1.90-2.30	0.60-0.90	2.58-2.85	0.23-0.45	0.10-0.36	
	Magnetic cenospheres MH -0.5+0.25L	55.32-67.72	16.90-20.27	2.10-4.77	2.10-4.77	1.91-4.33	0.54-0.98	2.05-2.80	0.29-0.54	0.09-0.42	
	Magnetic cenospheres MM -0.125+0.1	56.76-63.26	18.40-23.40	1.60-2.20	1.60-2.20	1.50-2.10	0.41-0.97	2.12-2.32	0.00-0.12	0.12-0.22	
	(from fly ash during coal combustion (Kuznetsk Basin Russia)										
Kruger and Toit[17]	South African power plant MATLA	42.6	31.5	1.30	11.6	0.7		1.23	0.65	0.25	0.17
	South African power plant KRIEL	45.8	28.9	3.67	9.51	1.6		1.93	1.63	0.22	1.19
	South African power plant DUVHA	35.2	25.9	2.18	16.4	0.6		2.90	0.74	0.25	0.79
Ngu et al.[19]	Collie power station	51.60	36.20	5.10	0.88	0.87	0.23	1.70	1.50		0.84
	Wallerawang power station	57.90	34.80	1.20	0.29	0.35	0.31	3.50	1.10		0.10
	Mount Piper power station	58.10	36.70	0.73	0.19	0.22	0.23	2.70	0.85		0.04
	Tarong power station <25µm	67.40	26.20	0.94	0.03		1.30	0.30	1.08	<0.1	<0.01
	Tarong power station 63-75µm	62.40	34.60	0.49	0.04		0.30	0.35	1.31	<0.1	<0.01
	Tarong power station 125-150µm	60.60	36.80	0.50	0.07	0.20	<0.1	0.35	1.43	<0.1	0.03
Raask[20]	Skelton Grange cenospheres	55.0	28.5	9.5	0.5	1.6	1.8	1.7			
	Ferrybridge cenospheres	59.0	29.5	8.6	0.6	1.4	0.3	0.2			
	High Marnham cenospheres	60.7	26.5	4.2	0.2	2.1	1.2	3.8			
	Carrington cenospheres	57.3	26.9	10.8	0.6	1.1	0.6	1.3			
	(all from power stations' lagoons)										

Table 2-2 (continued).

Reference	Source of Cenosphere samples	SiO_2	Al_2O_3	Fe_2O_3	CaO	MgO	Na_2O	K_2O	TiO_2	SO_3	P_2O_5
Vassilev and Vassileva[25]	Bulgarian TPS[a] with coal combustion	59.7	27.6	5.8	0.7	2.5		2.9	0.7	non	
Anshits et al[40]	0.4-0.2; ρ=0.36-0.52 0.2-0.16; ρ=0.36-0.52 0.16-0.1; ρ=0.36-0.52 (All from coal-fired power plants)	60.2-61.0 59.8-60.6 59.7-60.7	18.4-19.0 18.2-18.3 19.0-19.6	10.1-11.1 10.7-11.3 9.7-11.1	2.8-3.1 3.1-3.3 2.4-2.9	2.6-2.9 2.6-3.0 2.6-2.7				0.0-0.1 0.0 0.0-0.1	
Blanco et al[41]	1 [a]Q 2 [a]Q 3 [a]Q 4 [a]Q 5 [a]Q 6 [a]Q (all from Narcea Coal-Burning Power Plant)	56 56 55 55 57 56	26 24 24 24 24 25	7.0 6.9 6.8 7.1 6.8 6.9	4.7 4.1 4.3 4.4 4.3 4.2	1.9 2.1 2.2 2.2 2.2 2.2	0.53 0.50 0.49 0.48 0.37 0.35	3.2 3.5 3.4 3.4 3.3 3.4	1.2 1.1 1.1 1.1 1.2 1.2		
Drozhzhin et al[42]	power station burnt Kuznetsk coal power station burnt Ekibastuz coal power station burnt Near Moscow coal	57-69 55-58 56	18-37 37-39 33	0.8-4.7 1.2-1.5 1.9	0.7-2.7 0.5-1.0 1.6	0.4-1.5 0.2-0.4 1.7	0.2-0.9 ~0.1 0.5	2.4-6.0 1.0-1.7 1.9	0.5-1.0 0.9-1.2 1.0		
Ignaszak et al[43]	Fly ash from bituminous coal combustion	49-61	26-30	4-10							

Table 2-2 (continued).

Reference	Source of Cenosphere samples	SiO_2	Al_2O_3	Fe_2O_3	CaO	MgO	Na_2O	K_2O	TiO_2	SO_3	P_2O_5
Sarkar et al[46]	As received cenospheres	54.95	36.87	1.77	0.39	0.79	0.249	2.76	0.708	0.015	0.034
	B1 Acetone float (-350)	56.22	35.10	1.95	0.44	0.78	0.213	2.65	0.765	0.016	0.043
	B2 Acetone float (+350)	55.62	35.88	1.88	0.48	0.79	0.189	2.73	0.821	0.012	0.036
	C1 further acetone float	58.20	39.58	1.41	0.30	0.76	0.215	2.79	0.573	0.008	0.03
	C2 sink of acetone float	52.61	40.51	1.25	0.26	0.82	0.216	2.93	0.421	0.016	0.028
	(all from ash pond of a TPP[b])										
Kolay and Singh[50]	Ash lagoon of TPP[b]	52.53	30.01	7.53	1.15	0.32	0.02	1.98	1.79	0.02	0.45
Pedlow[51]	Floater	51.88	38.52	1.04	0	2.62	0	4.75	1.15	0	
	Dry separated spheres	54-55.15	25-30.9	0.46-1.73	7.87-10	2-3.11	0-1.38	1.2-2.81	0.78-1.15	1.24-2	
	(both from pulverised fuel power plants)										
Russak et al[52]	Domestic source	59.5	30.0	3.4	0.9	0.3	1.2	3.2	1.5		
Sokal et al[54]	Fraction of glass silicate microspheres	56.26	25.11	9.59	1.35	2.35	0.83	2.9	1.19		0.28
	Initial sample of light ash fraction	56.28	25.06	8.44	1.32	2.22	0.73	2.86	1.2		0.28
	(both from fly ash of TPS[a])										
Bibby[55]	Pulverised fuel ash in a power station	60.88	29.20	0.70	2.60	0.57	1.94	1.52	2.02		

Table 2-2 (continued).

Vassilev et al[56]	CCC1 (domestic Spanish coals)	53.7	31.5	5.5	2.0	2.6	0.8	2.4	0.7
	CCC2 (domestic Spanish coals)	53.5	29.9	3.2	6.3	2.4	0.6	3.0	0.7
	CCC3 (imported Gondwana coals)	50.1	30.8	2.2	10.9	1.6	0.6	2.7	0.7
	CCC4 (domestic Spanish coals)	56.4	31.6	3.4	0.7	2.5	1.0	2.7	0.7
	CCC5 (domestic Spanish coals)	52.9	33.4	5.1	1.5	2.4	0.8	2.3	0.8
	CCCS (collected from riverbank)	51.0	29.8	4.7	6.6	3.2	0.8	2.3	0.7
	CCCV (pond depository)	55.6	25.4	7.2	3.4	3.6	1.1	1.7	0.8
CHAVEZ ALCALA et al[57]	Coal combustion in a pilot plant unit	54.9	11.9	4.6	5.3			5.7	

[a]TPS: Thermo-electrical power station.
[b]TPP: Thermal power plant.

Thermal Properties. Various methods were used to investigate the thermal behaviour of ash cenospheres from solid fuel combustion, such as TGA/DTA analysis,[22, 50] DTA/DTG analysis[58] and a Leitz heating microscope.[20] Decrepitation of ash cenospheres was observed to take place at 230 – 330 °C, due to the release of water dissolved in the silicate glass[20, 22, 50] and/or some gases escaped from the hollow ash cenospheres,[22] as suspected. Therefore, ash cenospheres should be finely ground for thermal analysis to avoid the samples loss due to the decrepitation. Additionally, an exothermic effect may also take place at 260 – 600 °C and cause weight loss,[22, 58] due to the oxidation of residual unburnt carbon materials in the ash particles. This fact also suggests that ash cenospheres harvested from ash lagoons are necessary to be heat-treated under oxidizing atmosphere to remove possible unburnt carbon materials for further analyses.[19, 52] Thermal analysis on several ash cenosphere samples by Raask[20] also indicated that the sintering of ash cenospheres commenced at 1200 °C – a temperature higher than the sintering temperature of dense fly ash. For other ash cenosphere samples, Vassilev and co-authors[22] found that the sintering and softening started at 1010 – 1330 °C while complete fusion was reached at 1315 – 1450 °C.

2.2.2 Advantages and Applications of Ash Cenospheres

Ash cenospheres have unique properties such as being spherical, lightweight, heat resistant, enhanced insulation, good thermal stability and chemical inertness etc. These materials have a wide variety of applications on the area of industry, agriculture, recreation and others. Figure 2-3 (adopted from the literature) summarized the various applications of ash cenospheres considering their unique advantages. Ash cenospheres can be used in manufacturing value-added products such as lightweight materials.

Lightweight Construction Products. Lightweight construction products have many benefits including low density, excellent mechanical strength and reasonable cost. Ash cenospheres can be used as fine aggregate in the manufacture of lightweight concrete[26, 29, 41, 51] and as additive for producing lightweight cements.[58]

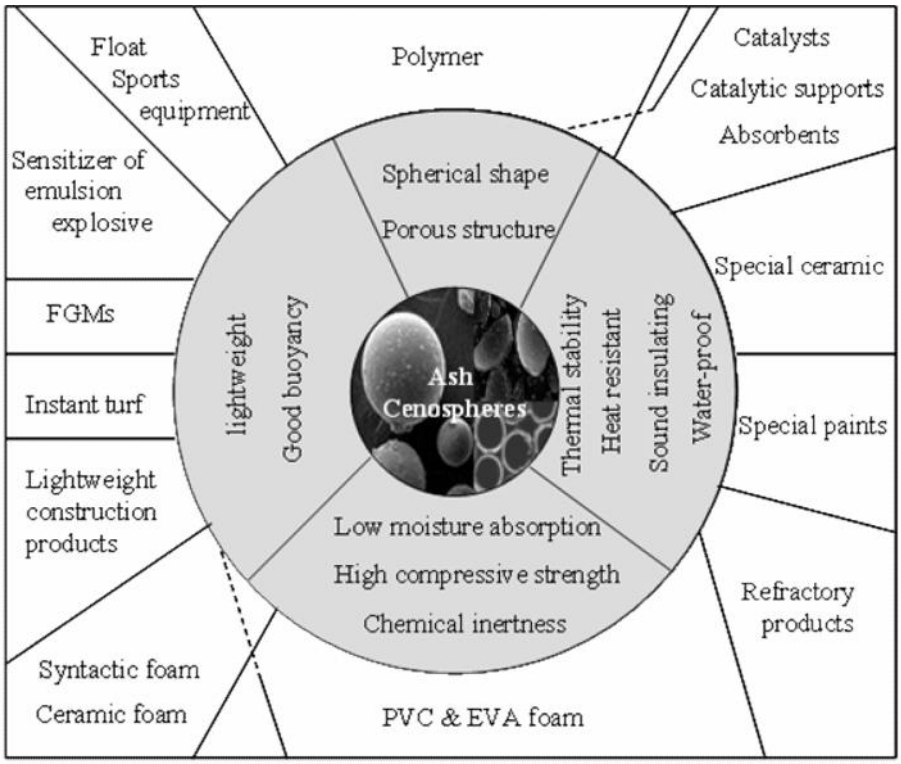

Figure 2-3: Summary of various applications of ash cenospheres considering their unique advantages.[17, 22, 24, 26, 27, 29-31, 40-43, 45, 46, 51, 52, 58-75]

Cenospheres can be used as aggregate to produce lightweight concrete,[41] resulting in significantly-improved thermal conductivity of the lightweight concrete and significantly decreased weight of products. It was also suggested that ash cenosphere additives can improve the crystallization of hydration products. The acoustic behaviour of the product also does not deteriorate compared with the lightweight concrete manufactured with other aggregate.[41] As additives of lightweight cement, ash cenosphere also leads to the changes in the structure of lightweight cement and raises hardening temperature.[58] However, the addition of ash cenosphere does lead to some strength loss.[29, 41] Fortunately, such strength loss can be recovered by improving the interfacial strength between the cenospheres and the cement.[29] It should be noted that special consideration needs to be given to the excessive moisture uptake/loss by cenospheres (hence the water uptake/loss in cenosphere-concrete products) when ash cenospheres are used to replace fine sand to be the aggregates in concrete. The work of Barbare et al[26] showed that the equilibrium moisture content of cenospheres is ~18

times higher than that of sand, suggesting that substantially more water should be added prior to curing the concrete.

Composites.

- **Polymer Composites.** As results of unique properties such as spherical shape, controlled particle size, porous structure, low density, good insulation and low cost, ash cenospheres are extensively introduced as lightweight fillers into various polymer composites.[17, 24, 27, 30, 42, 45, 46, 59] For example, ash cenosphere particles coated with Cu could be utilised for manufacturing conducting polymers for EMI shielding applications.[59] While the use of cenospheres in polypropylene and polyethylene is limited due to high-shear conditions in extrusion and injection moulding, new manufacturing techniques may be employed to address this aspect by controlling cenosphere particle size.[24] Lightweight, high strength polyester materials can also be produced by the incorporation of a controlled size, surface modified cenospheres into a polyester matrix.[27] Comparison of the mechanical properties of both epoxy resin and high density polyethylene shows the similarity with the two fillers.[17] It is known that significant advantage could be achieved by filling ash cenospheres into the high density polyethylene since the wider variety of colours and more importantly, less pigment required.

- **Syntactic Foams.** Syntactic foams are made by mixing hollow cenosphere particles in a matrix material, achieving various advantages including excellent buoyancy, low moisture absorption, high compressive strength, high energy absorption during deformation, and high damage tolerance.[51, 61-64] Such materials are extensively applied in automotive industries,[66] in marine and aerospace industries for core material in sandwich structured composites,[65] and as underwater buoyant structures which can withstand high hydrostatic pressures of deep ocean.[63] It was found that the density and mechanical properties of syntactic foam can be affected by ash cenosphere sizes and specimen aspect ratio.[61] An increase in compressive strength and modulus can be achieved as the internal radius of cenospheres decreases.

- **Ceramic Foams.** Ceramic foam has advantages including lightweight, high compressive strength, and good resistant towards gas erosion. It can be easily shaped, making this material desirable for producing high performance products, including

sensors, heat dissipaters, thermal insulators etc.[67] Russak and co-authors[52] demonstrated that a ceramic closed cell foam insulation material made from ash cenospheres could meet all the requirements for developing a fully reusable ceramic heat shield of space shuttle to protect the vehicle prime structure during the reentry maneuver.

- **Polyvinyl Chloride (PVC) and Ethylene Vinyl Acetate (EVA) Foams.** PVC foam is an insulation material with various characteristics of light, fire-proof, water-proof, heat-resistant, sound-insulating, non-flammable and non-toxic.[48] EVA foam has unique properties of lightweight, elasticity and insulation and is mainly used to make sports shoe bottoms. For manufacturing PVC foams, $CaCO_3$ and talc are the two major constituents. For manufacturing EVA foams, a rather high proportion of $CaCO_3$ is added as the filler. Considering the vast economic benefit, ash cenospheres can be added to replace the talc present in 5% of the mixture to make PVC foams. For EVA foams, ash cenospheres can be used to completely replace $CaCO_3$ present in the mixture. It was found that such replacement resulted in excellent strength and insulation properties compared to the original products.[48]

- **Functionally Gradient Materials.** Functionally gradient materials are composites made of varied material compositions to optimize the performance so as to achieve specific applications. These materials are extensively used in applications such as internal combustion engines, insulating and thermal coatings for turbine blades, military armor and other engineering applications.[69] Parameswaran and Shukla[68] developed a technique to prepare a model functionally gradient material using polyester resin and ash cenospheres. The results showed that increasing cenosphere volume fraction can reduce the density of the functionally gradient material by 20%.

- **Metal-matrix Composites.** Ash cenospheres have desired characteristics to be used as fillers or reinforcement in aluminium, lead, magnesium and several other nonferrous metal matrices, e.g. spherical shape, low density, especially the high melting point.[30, 31, 70] It was found that the aluminum composites with 50-60 vol.% of ash cenosphere exhibit sound microstructure except near the regions of contacting particles.[70]

Other Applications. Ash cenospheres can also find applications in making catalytic supports, absorbents and catalysts,[22, 40, 71, 72] as results of their spherical shape, chemical inertness, and thermal stability. For example, catalysts were developed based on ash cenospheres for deep methane oxidation.

Ash cenospheres are also used to manufacture special ceramics such as fire-, heat-, and sound-insulating materials, taking advantage of their heat-resistant, thermally-stable, and sound-insulation features.[22] Ash cenospheres can also be incorporated into mortars as binders to produce ceramic products such as man-made marble and insulation/refractory ceramics.[24]

Another application of ash cenospheres is for manufacturing anti-corrosive paint and wear resistant coating due to their excellent mechanical properties and chemical inertness.[73, 74] Ash cenosphere is also a good option for producing fire retardant and insulation paints as these hollow particles are non flammable and high temperature resistant.

The gas trapped within enclosed ash cenospheres becomes an excellent insulating medium, which makes cenospheres having excellent heat insulation properties. Therefore, cenospheres are ideal materials for heat-insulating refractory products.[17, 24, 43] Test has shown that the mixture of ash cenospheres and clays can be used to produce various refractories for metallurgical industry.[17]

Pearlite microspheres with low density were found as the sensitizer of emulsion explosives after investigations of the physical-chemical and explosive properties of emulsion compositions contained pearlite microspheres.[75]

Apart from the various industrial applications, ash cenospheres can also be used to manufacture materials used in recreation and home. For example, ash cenospheres could be used for the manufacture of sports equipments such as kayaks, surfing boards and other floaters due to their low density and excellent buoyancy properties. [46] Interestingly, ash cenospheres combined with other floating materials are helpful to grow a special instant turf.[51] This type of turf is thinner and therefore lighter than natural turf, and has an intact root system. Such instant turf also has a long duration of keeping moist and thus saves water and costs.

2.2.3 Formation of Ash Cenospheres

2.2.3.1 Separation of Cenospheres from Fly Ash and the Typical Yields

The most common method for separating ash cenospheres from fly ash is the sink-float method that uses water as the medium for density separation because ash cenospheres have bulk density lower than that of water (1 g cm^{-3}).[18-20, 22, 24, 48, 54, 55, 57, 76-78] Briefly, the method involves dispersing the dry fly ash samples collected from the power plants in water (distilled water and/or tap water) at room temperature. After continuous stirring and settling for 24 hours, the float ash samples above water are collected via decantation followed by filtration. The float samples are then heated to 800-900 °C in a furnace with air continuously flowing through for 2 hours in order to remove unburnt carbon. The yields of ash cenospheres using this separation procedure vary strongly with the sources of fly ash, up to 35.6 % wt, with the most common values are 0.1 - 5.0 % wt.[11, 19-22, 25, 26, 48, 49, 53, 57, 63, 77, 78] It should be noted that, apart from using water as medium, other solvent liquids were also used for separating ash cenospheres from ash, such as ethanol and hexane,[55, 71, 72] acetone containing 1% triethanol amine lauryl sulphate [46] and n-heptane. [52]

The other method is centrifugal separation that can be used to determine the amount of ash cenospheres in fly ash. Various liquid medium may be considered, including water,[50] distilled water and lithium metatungstate solutions of density 1.5 and 2.0 g cm^{-3}, and liquid of density 2.2 g cm^{-3} prepared by mixing carbon tetrachloride, dibromomethane and di-iodomethane in appropriate proportions.[79, 80] However, it is obvious that the ash cenospheres separated with the last two liquids have density greater than that of water.

Lastly, a combination of hydro- and aerodynamic separation can also be employed to isolate the concentrates of magnetic microspheres and cenospheres.[13] It was also reported that an integrated method combining dry fluid bed gravity separation technology and carefree cyclone technology can be used to separate ash cenospheres.[81]

2.2.3.2 Formation Mechanisms of Ash Cenospheres

It is generally accepted that during pulverised-coal combustion, the formation of molten precursor ash droplets and a source of gas generation inside the droplet are two essential requirements for ash cenosphere formation.[14, 17-22, 50-52, 54, 79, 80, 82, 83] It is also known that the shell of ash cenosphere contains various mineral phases including aluminosilicate, mica, feldspar, quartz, sulphide and so on.

The constituents of gas enclosed within ash cenospheres are generally CO_2 and N_2, with traces of O_2 and CO.[15, 20, 21, 84] There are still debate on the source of these gases, with two main possibilities being speculated. One is that the flue gas in the boiler is trapped in silicate melts, forming submicron bubbles enclosed inside the droplets.[54] As temperature increases, volume of gas increases and bubbles expand to form hollow spheres. The other is that the gas products are generated within the molten ash droplets, due to decomposition of carbonates, dehydration/ dehydroxylation of clay minerals, evaporation of pore water, and/or fusion of silicates.[14, 18-22, 24, 35, 52, 79, 82, 83]

To form ash cenosphere, it is reasonable to say that there should not be too much gas trapped inside the molten ash droplets as it leads to the burst of the ash cenosphere particles. The molten ash droplets should have relatively high viscosity so as to being capable of sustaining the internal pressure from trapped gas within the droplets. While the precursor ash particles travels along the furnace in which temperature decreases, the droplets resolidify as a result of fast quenching at the later stage of combustion. These particles follow the gas stream and eventually exist as ash cenospheres so that its temperature-time history (particularly cooling rate) may also be an important consideration.

Ash cenospheres were also observed during the combustion of pyrite at high temperature (>1100 °C).[32, 33] It was speculated that the gaseous sulphur oxides formed by oxidation inside the droplets are responsible for cenosphere formation. The other mineral which was observed could contribute towards the formation of cenospheres is illite.[85, 86] It was believed the fluxing action of K_2O in the illite coupled with synchronous evolution of CO_2 gas being responsible for the cenosphere glass froth.

2.2.3.3 Key Factors Influencing the Formation of Ash Cenospheres

The formation of ash cenospheres during pulverised coal combustion can be governed by a number of important factors, as summarized below.

Coal Properties. These include three aspects: particle size, properties of coal organic matter and properties of coal inorganic matter. *Coal particle size* was reported to be an important factor in the formation[20, 22] and size[14, 37] of ash cenosphere. According to Raask,[20] mineral particles smaller than 10 μm are incapable of expanding to stable cenospheres. The speculated reason is that carbonaceous matter is completely separated from ash particles due to extensive milling, or as results of excessively vigorous gas evolution and expansion inside small ash droplets, resulting in their bursting to form dense particles.

The properties of coal organic matter are also believed to be critical in ash cenospheres formation. Vitrain, clarain and durain have very different organic properties, resulting in substantial difference in their devolatilisation behavior. This includes the swelling characteristics of coal particles, thus influencing the combustion condition hence ash cenospheres formation.

The properties of mineral matter in coal, including the content and mineralogy of mineral matter play important roles in the formation of ash cenospheres. Ghosal and Self [79] showed that ash cenosphere yield appears to be positively correlated with the total ash content of coal. In addition, it was also indicated by the studies that the mineral type present in coal, such as clay mineral, mica, zeolite, feldspar and anauxite, will favor the cenosphere formation.[17, 22, 25, 55, 79, 83, 85, 86] Furthermore, Kruger and Toit [17] claimed that alkalis in the mineral matter can act as precursors for the generation of cenospheres at the prevailing combustion.

Characteristics of Ash Droplets. Generally speaking, these include three factors, i.e. carbon in ash droplets, iron content of ash droplets and viscosity and surface tension of ash droplets.

Carbon in Ash Droplets was considered to be one of the favorable conditions for cenosphere formation by Raask. [20, 21] Via a Leitz heating microscope, it was found that

a minimum of 1 % by weight of carbon should be incorporated or attached to fused silicate particles as one of the conditions for cenosphere formation.

*Iron Content in Ash Droplets***.** As summarized in the Section 2.2.3.2, the gases locked inside the ash cenospheres were found to be CO_2 and N_2 with traces of O_2 and CO. Based on ash cenosphere chemistry and the possible formation routes, Raask ruled out the possibility of dissociation of carbonates and combustion of carbonaceous matter being the origin of CO_2. Via experiments on gas evolution by heating various minerals in the Leitz heating microscope, Raask[20, 21] originally suggested that the presence of iron can catalyse the reactions to produce CO_2 and CO inside the fused ash particles via the following possible reactions:

$$2Fe_2O_3 + C = 4FeO + CO_2 \quad (2.1)$$

$$2Fe_3C + SiO_2 = Fe_3Si + 3Fe + 2CO \quad (2.2)$$

Rassk's estimation based on his experiments results suggested that generally, a minimal ~5% wt of iron oxide is required for the formation of substantial quantities of ash cenospheres. More than 7 % iron oxide is required for the formation of a large amount of ash cenospheres from bituminous coal combustion, while for some sub-bituminous coal, 3-4% iron oxide is sufficient.

While the requirement of high iron oxide contents for the formation of substantial ash cenospheres is generally supported by the published experimental data, there have been various exceptions, as evidenced in the data listed in Table 2-2. For example, Ngu and co-authors[19] reported the high ash cenosphere yield from an Australian power station which burns coals with negligible iron contents in ash (~0.6 wt % on average). Else, some studies[18, 51] also suggested that high iron contents do not always lead to high ash cenospheres yield. As shown in Morrison's survey,[51] there were even cases that have Fe_2O_3 contents up to 25% but do not produce a large quantity of floaters. Similar phenomenon was also reported by Lauf[18] when the content of Fe_2O_3 in ash is > 20%.

*Viscosity and Surface Tension of Ash Droplets***.** Viscosity and surface tension of molten ash droplets control the expansion of the precursor ash droplet and determine

the survival of ash cenospheres.[14, 17, 18, 20-22, 33, 54, 79] The change rate of a hollow sphere radius is governed by viscous relaxation as following:[20, 21]

$$\frac{dr}{dt} = \frac{1}{4\mu(r - r_1)}\left(\frac{Kr^2}{r_1^3} - P_a r^2 - 2\sigma\frac{r}{r_1}(r + r_1)\right) \quad (2.3)$$

where μ is the viscosity, σ is the surface tension, r is the external radius, r_1 is the internal radius, P_a is the external pressure, and K is a constant. The equation clearly indicates that viscosity and surface tension of the precursor ash droplets determine the final size of ash cenospheres. In order to sustain the high intrinsic pressure of expanding gas bubble within the precursor ash droplet, the precursor droplets should have relatively high viscosity. The cenosphere precursor will collapse if the force as results of surface tension is too low to maintain the equilibrium pressure between the internal and external gas. This was supported by the work of Lauf[18] who investigated ash cenospheres produced by melts with relatively high viscosities from ash samples of seven different locations. Calculations also suggest that only those molten droplets that are sufficiently viscous can survive long enough to be resolidified into ash cenospheres. Unfortunately, there are few published data in terms of the value of viscosity and surface tension of molten precursors responsible for ash cenosphere formation.

Combustion Conditions. These mainly include three key parameters, i.e. furnace temperature, residence time and cooling rate. *Furnace Temperature* is considered to be a critical factor in ash cenosphere formation during pulverised-coal combustion.[14, 17, 19, 22, 37, 38, 87] It affects not only the rate of gas released from the ash particle, but also the formation of molten ash droplets (hence the viscosity and surface tension of these ash droplets). There is still debate on the effect of furnace temperature. For example, it was reported that the yield of ash cenospheres increased with combustion temperature and reached the highest at 1600 °C.[87] However, Vassilev and co-authors[22] suggested that the suitable furnace temperature for ash cenosphere formation is 1315 – 1500 °C. Considering the viscosity and surface tension of fused silicate glass, as well as the rate of gas production, Raask[20] estimated that the optimal temperature for ash cenosphere formation is 1400 °C.

Residence Time. According to Equation 2.3, a proper residence time is required for the formation of ash cenospheres with different sizes, governed by the rate of gas evolution and viscous relaxation of the molten ash droplets. Sufficiently long residence time of ash particles in the boiler during combustion is required to enable the molten ash droplets formation and trapping an appropriate amount of expanding gas to form ash cenospheres. However, it should not be excessive as further expansion of gas inside the melts would lead to bursting before solidifying of the precursors to form ash cenospheres.

Cooling Rate. During cooling stage, ash precursor droplets of cenospheres solidify and ash cenospheres survive eventually. Upon cooling, the molten ash droplets will contract due to a reduction in gas pressure within the cenospheric particle. The viscosity and surface tension will change upon cooling. Therefore, the net balance between the internal pressure and the strength of the shell of molten droplets may lead to the breakage of the particles hence reduce ash cenosphere formation.[88] Rapid cooling of molten ash droplets is critical for ash cenospheres formation.[22, 51] However, cooling should not be too rapid. It is logic to reason that due to the thin wall thickness of cenosphere precursor, the high internal pressure will cause the rupture of the cenospheres. Another opinion based on calculation suggested that there is no significant contraction of cenospheres taken place upon rapid cooling about 1000 °C in boiler flue gas.[20] After this rapid cooling in high-temperature flue gas, the pressure inside the frozen cenospheres will reduce steeply, causing the possible breakage of ash cenospheres, although there is no experimental evidence to support so.

2.2.4 Conclusions of the Review on Ash Cenospheres from Pulverised Fuel Combustion

Ash cenospheres can be widely used in manufacturing various value-added products due to their unique advantages. Substantial research have been devoted to characterize ash cenospheres but largely based on bulk, applying for further concerns on the difference in the properties of ash cenospheres of different size fractions. The formation of ash cenospheres has also been widely investigated to understand their formation mechanisms and keys factor influencing the ash cenosphere formation were suggested. However, understanding on the mechanism of ash cenosphere

formation is still largely unclear. In addition, to evidence the key factors necessitates further systematical experimental work.

Therefore, a systematical experimental program is desirable to investigate the formation and behaviour of ash cenospheres. While coal has been the principal fuel for the formation of ash cenosphere, its complex ingredients restrict understanding the formation and behaviour of ash cenospheres. Pyrite (FeS_2) appears to be a good option due to its simple constituent and wide presence in coal. The up-to-date progress on pyrite combustion is therefore reviewed in Section 2.3.

2.3 Transformation of Pyrite under Combustion Conditions

In this PhD study, pyrite is used as a model fuel to study ash cenosphere formation during solid fuel combustion. A brief review was then conducted on the occurrence of pyrite in coal and the transformation of pyrite during combustion.

Pyrite (FeS_2) is a common mineral in coal and has been recognized as a major source of ash deposition and SO_2 emission.[21, 89] Based on carbon-pyrite association, pyrite in coal can be generally classified as *included (inherent)* or *excluded (extraneous)* pyrite, as shown in Figure 2-4:

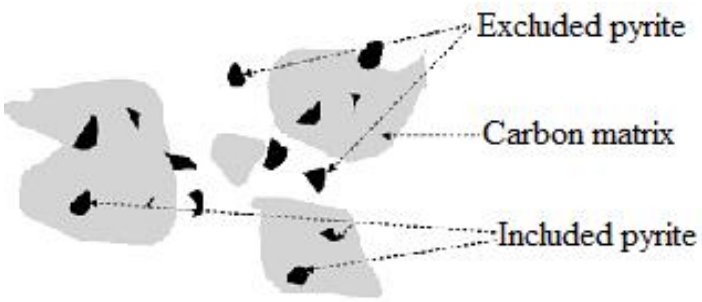

Figure 2-4: Included and excluded pyrite in coal.

- **Included pyrite** is discrete pyrite particle intimately associated with the carbonaceous portion of coal and other mineral particles within the same coal particle, which cannot be readily separated from coal by common physical methods.

- **Excluded pyrite** is liberated particle that is not included closely in the carbonaceous matrix of coal and can be separated from coal through beneficiation.

The transformation of included pyrite during pulverized coal combustion is complex due to its intimate association with the carbonaceous matrix of coal and other minerals within the same coal particle. Included pyrite, as other included minerals, may experience a higher particle temperature, local reducing environment, and coalescence with other included minerals in the same coal particle.[21, 89, 90] Included pyrite can therefore undergo a variety of processes during pulverized coal combustion, including decomposition, fragmentation, fusion, and coalescence etc. The complicated physical and chemical transformation of included pyrite during coal combustion has been well documented.[33, 90-97] However, present study only utilizes excluded pyrite as the model fuel in the experimental program for cenosphere formation investigation. Therefore, the detailed information regarding included pyrite transformation is not introduced in this review.

Excluded pyrite undergoes either direct oxidation or two-step transformation during combustion. Direct oxidation[98-102] of excluded pyrite refers to a process that excluded pyrite is directly oxidized to form hematite and/or sulphate simultaneously. Two-step transformation[103] refers to that excluded pyrite decomposes initially to produce an intermediate product pyrrhotite FeS_x ($1 \leq x < 2$) that is absent in the direct oxidation process, followed by the oxidation of pyrrhotite to magnetite and/or hematite.[32, 33, 99, 101, 104-107] During the two-step transformation of pyrite, Fragmentation of decomposition product pyrrhotite may take place and the formation of a Fe-S-O melt from the pyrrhotite intermediate is also observed.[32, 105-107] The two pathways during pyrite combustion are therefore reviewed and discussed in Sections 2.3.1 and 2.3.2, respectively.

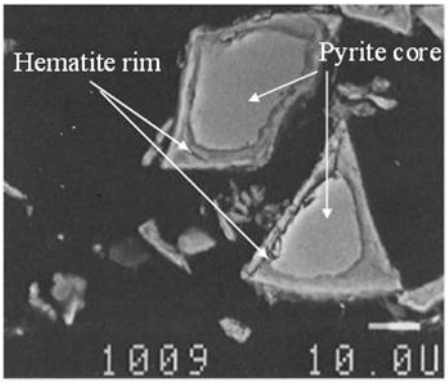

Figure 2-5: A cross-sectional SEM image of pyrite particles (< 45 μm) after heat treatment in air from 30 to 470 °C at 2.5 °C min^{-1} in a TG-DTA.[100]

2.3.1 Direct Oxidation of Excluded Pyrite

Direct oxidation of pyrite takes place when oxygen is in direct contact with pyrite, which can then be directly oxidized to form hematite. As observed,[98-102] the direct oxidation of pyrite follows an 'unreacted core model'[103] and produces a oxidation product as shown in Figure 2-5. Briefly, under the 'unreacted core model', oxidation commences and always exists at the surface of the reacting pyrite particle, while the reaction front gradually moves towards the centre of pyrite particle.[99-101] Therefore, there always exists an unreacted pyrite core during pyrite oxidation, surrounded by a rim which is the oxidation product hematite (see Figure 2-5).

The reaction of direct oxidation of pyrite can be represented by:[98, 102, 103]

$$2\ FeS_2\ (s) + 5.5\ O_2\ (g) \rightarrow Fe_2O_3\ (s) + 4\ SO_2\ (g) \qquad (2.4)$$

It was hypothesized that this reaction in air atmosphere is controlled by oxygen diffusion through the product layer.[99, 100, 102] It should be noted that during pyrite direct oxidation in air, a small amount of ferric sulfate may be formed simultaneously via the following reaction:[99, 100, 102]

$$2\ FeS_2(s) + 7\ O_2(g) \rightarrow Fe_2(SO4)_3(s) + SO_2\ (g) \qquad (2.6)$$

If this is the case, the formed sulfate may lead to the closing of pores within the product layer due to its larger molar volume compared to iron oxides. This will inhibit oxygen inward diffusion hence influence the transformation of pyrite particle.

The reaction route of direct oxidation of pyrite and its oxidation products in practice are determined by the combustion conditions. As suggested in literature, direct oxidation of pyrite was evidenced only at temperatures <~530 °C during transformation in an air atmosphere.[98-102] In addition, small pyrite particle size, faster heating rate, and air atmosphere favour the direct oxidation of pyrite to form hematite, while slow heating rate and/or an oxygen atmosphere support the formation of sulphate as the simultaneous oxidation product.[99, 100, 102]

2.3.2 Two-step Transformation of Excluded Pyrite

Under the conditions which do not support direct oxidation of excluded pyrite during combustion, the two-step transformation is suggested to be responsible for the combustion of pyrite. The two-step transformation of excluded pyrite during combustion involves mainly thermal decomposition of pyrite and the successive oxidation of the decomposition product pyrrhotite. Figure 2-6 graphically generalizes the two-step reaction pathway (adopted from the literature).

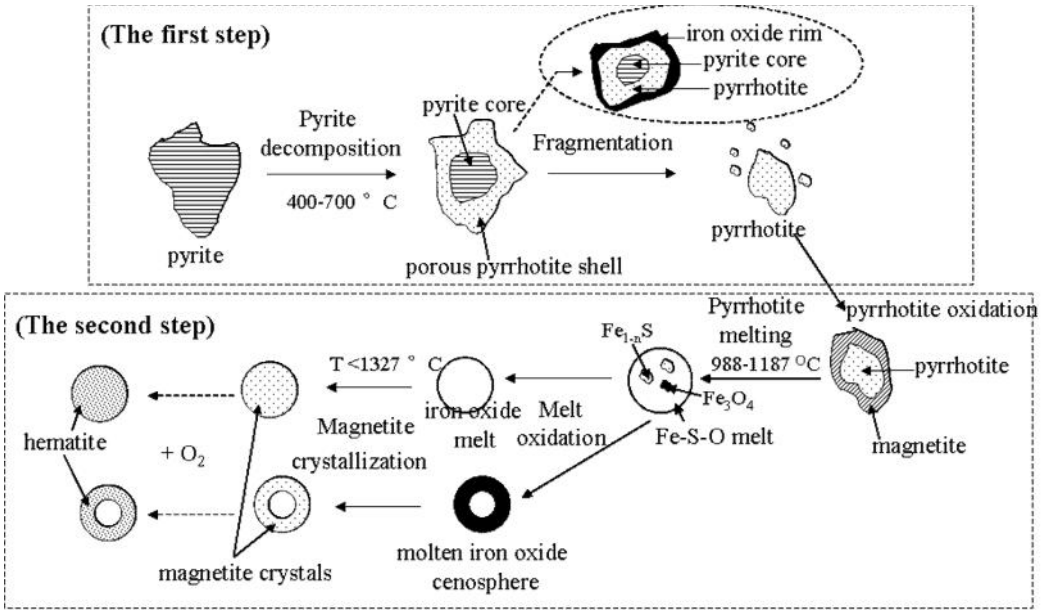

Figure 2-6: Schematic diagram illustrating the two-step transformation of excluded pyrite during combustion.[93, 94, 99-101, 104-106]

The first step is the thermal decomposition of pyrite once the temperature of pyrite particle reaches its decomposition temperature (400 − 700 °C).[105, 106, 108] This leads to the production of pyrrhotite as the intermediate product, accompanied with the release of sulphur gas via the following reaction:

$$FeS_2\,(s) \rightarrow 1.14\,Fe_{0.877}S\,(s) + 0.43\,S_2\,(g) \qquad (2.7)$$

This reaction is endothermic and generally limited by the rate of heat transfer (ΔH = 916.67 kJ/kg_FeS_2).[105, 106] The gaseous decomposition product S_2 in Reaction 2.7 will react with oxygen in the particle boundary via

$$S_2\,(g) + O_2\,(g) = 2\,SO\,(g) \qquad (2.8)$$

or

$S_2(g) + 2\ O_2(g) = 2\ SO_2\ (g)$ (2.9).

Reactions 2.8 and 2.9 are exothermic, which can in turn generate heat to enhance the endothermic pyrite decomposition reaction. This can result in an increased temperature gradient inside the reacting pyrite particle hence increase sulphur release rate. Due to the fast release of sulphur gas and the porous structure of pyrrhotite, fragmentation of pyrrhotite has been widely suggested,[21, 89, 90, 105, 106, 109, 110] as shown in Figure 2-6. Among the studies, simulation estimated that the fragmentation would lead to the generation of 4 pieces of fragments per pyrite particle.[110] Increasing oxygen concentration enhances the fragmentation of pyrite particles.[109] Also, it was speculated that fragmentation during pyrite decomposition may contribute to the formation of submicron particulate matter (PM_1).[89, 90]

Similar with direct oxidation of pyrite, Figure 2-6 indicates that the decomposition of pyrite also follows the 'unreacted core model'. Differently, the unreacted dense pyrite core is surrounded by porous pyrrhotite shell,[33, 99-101, 104-106, 109] as shown in Figure 2-7. Furthermore, in this process, the existence of oxygen in the gaseous phase enables part of the intermediate product pyrrhotite being possibly oxidized simultaneously along with pyrite decomposition, producing the partially reacted pyrite particles with hematite rim surrounding the porous pyrrhotite shell, as shown in Figure 2-8.[99-101, 104] It can then be deduced that the formation of such a dense rim around the reacting particle may restrict the fragmentation of the partially reacted pyrite particle during combustion.

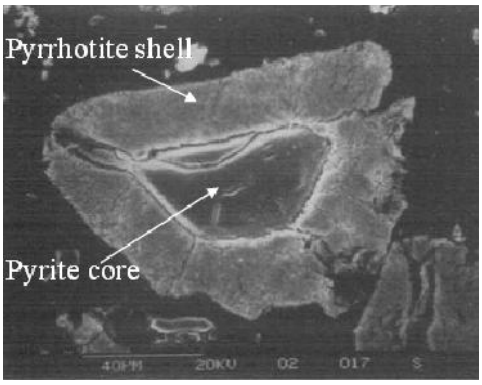

Figure 2-7: A cross-sectional SEM image of a decomposed pyrite particle sampled from an experiment in a drop-tube furnace extracted (particle size: 53-63 µm; T_{gas}: 1217 °C; oxygen mole %: 3.0; residence time: < 0.6 s), illustrating the presence of a pyrite core and pyrrhotite shell.[106]

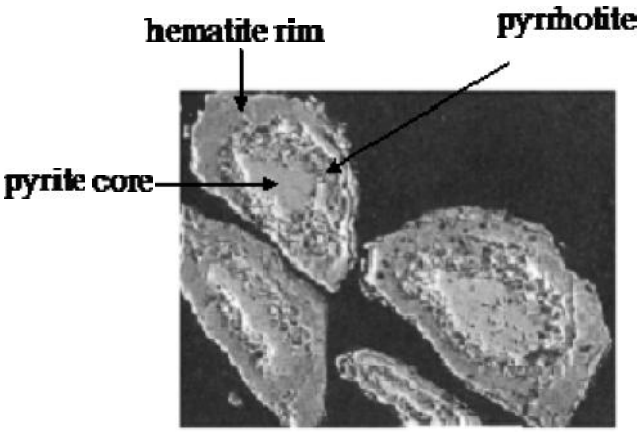

Figure 2-8: A SEM image of pyrite particles (90-125 µm) after heat treatment in air from 30 to 520 °C at 2.5 °C min^{-1} in a TG-DTA. [99]

The second step is the successive oxidation of pyrrhotite to produce magnetite (Fe_3O_4) via the following reaction:[32, 93, 105, 106]

$$1.14\ Fe_{0.877}S\ (s) + 1.2367\ O_2 \rightarrow 0.33\ Fe_3O_4\ (s) + 1.14\ SO\ (g) \qquad (2.10)$$

This reaction is exothermic (ΔH = -201.24 kJ/mol_O_2),[105] leading to the particle temperature higher than the surrounding gas temperature. Once the particle temperature reaches the melting point of pyrrhotite (988 − 1187 °C),[103, 105, 106] the

pyrrhotite will melt and form a liquid phase. The oxidation product magnetite may then dissolve in the melt and result in an iron oxysulphide (Fe-S-O) melt, as presented in Figure 2-6. It is worthy to note that after the production of Fe_3O_4 within the second step, even the particle temperature does not reach the melting point of pyrrhotite but is higher than the eutectic temperature of the Fe-S-O tertiary system (915 °C at an Fe:S:O molar ratio of 1.22:0.76:0.45[111]), the intermediate product of Fe-S-O melt will also be produced.

This was clearly evidenced in previous studies, which were mainly concerned with pyrite combustion at temperatures > 1100 °C.[32, 33] Depending on residence time, the sulphur in the molten Fe-S-O droplet would continue to be oxidised with the oxygen diffused from the gaseous phase. The completion of sulphur oxidation would then leave behind a fully-molten product of iron oxides (magnetite) (see Figure 2-6). These subsequent reactions were suggested to be controlled by the oxygen diffusion inside the molten droplets.[105] The viscosity of the molten droplets and consequently the particle temperature were also believed to play significant roles in the reaction of the molten particle.[33] It was also observed that cenosphere might be formed during the process,[32, 33] although there was little work done on investigating the formation mechanism of such particles.

As the melt of iron oxides (magnetite) cools down to < 1327 °C following the flue gas stream during combustion, magnetite crystallizes out of the melt and the pyrite transformation process will be completed. However, an increasing particle residence time and oxygen concentration in the gas stream may promote the oxidation of magnetite into hematite under kinetic control.[21, 33, 90, 105, 106, 108]

2.3.3 Conclusions of the Review on Pyrite Transformation

The literature suggests that there have been substantial research on understanding the reaction pathways and transformation of pyrite during oxidation. There has also been considerable research on the transformation of pyrite during coal combustion although the work is generally concerned with conditions at temperatures > 1100 °C. The formation of cenosphere was observed during pyrite combustion (at T > 1100 °C), however, little work was done on investigating the mechanism of ash cenosphere formation.

Therefore, it is feasible to use pyrite as a simple fuel for designing an experimental program so as to systematically investigate the formation mechanism and behaviour of ash cenospheres. This offers significant advantages because a) pyrite is a very simple fuel; and b) the chemical reactions during pyrite combustion is well documented. In addition, it has been long speculated that fragmentation of ash cenosphere may contribute to the formation particulate matter during coal combustion, although there have been no direct experimental support to such a claim. Using pyrite as a fuel also offers the opportunity to investigate this important aspect. From this point of view, this thesis also provides a concise review on formation mechanisms of PM_{10} formation during pulverised fuel combustion in Section 2.4.

2.4 PM_{10} Formation during Pulverised Fuel Combustion

Particulate matter (PM) is originated from mineral matters in solid fuels (e.g. coal and/or biomass) during combustion, leading to adverse impact on equipment operation efficiency, environment and human health.[35, 112] The particulate matter with aerodynamic diameter less than 10 µm (PM_{10}) is of important considerations due to the poor capture efficiency of conventional electrostatic precipitator for these particles. Especially, the submicron particulate matter with aerodynamic diameter less than 1µm (PM_1) is of great concerns as submicron ash particles can be deposited in the pulmonary region of the respiratory system and ultimately enter into the bloodstream, resulting in serious health risks.[113] PM_1 also generally has highest enrichment of many toxic heavy elements.[35, 36, 112, 114-119] Compared to other coarser particulates, PM_1 has considerably longer lifetimes in the atmosphere, causing long-lasting adverse effect.[120] Therefore, this section reviews the current understanding on PM_{10} from pulverised-fuel combustion, including the characteristics and formation mechanisms as well as key factors influencing PM_{10} formation.

2.4.1 Characteristics of PM_{10}

2.4.1.1 Particle Size Distribution

It is generally accepted that PM_{10} is of a bimodal mass size distribution during the combustion of coal[87, 116, 121-126] and biomass[118, 127], as shown in Figure 2-9. One is a fine mode (also referred to as submicron mode or vaporization mode) in the

submicron region (< 1 µm), centered at ~ 0.05 − 0.1 µm. The other is a coarse mode (also referred to as supermicron mode or residual mode) in the supermicron region (1−10 µm). The two modes represent particulate matter formed via different mechanisms, which are discussed in the following sections.

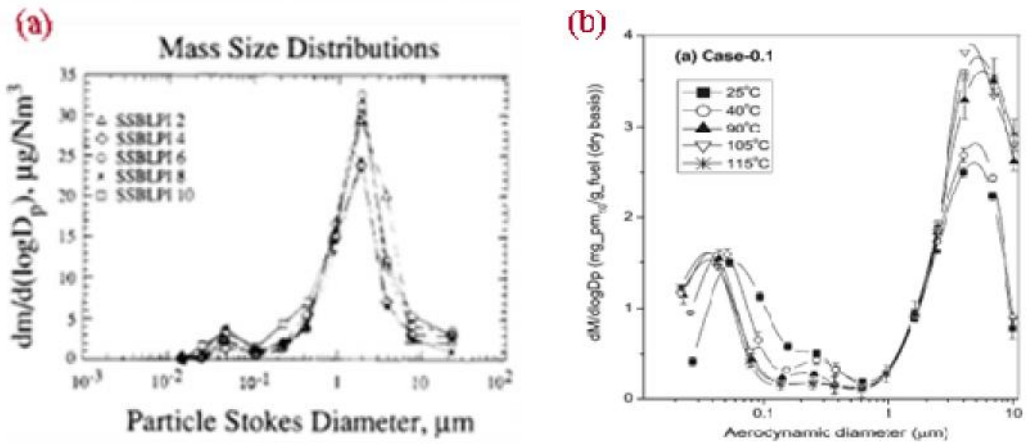

Figure 2-9: Mass size distributions of particulate matter from (a) coal combustion in a boiler collected by BLPI;[116] (b) biomass (mallee bark) combustion in a DTF collected by DLPI.[127]

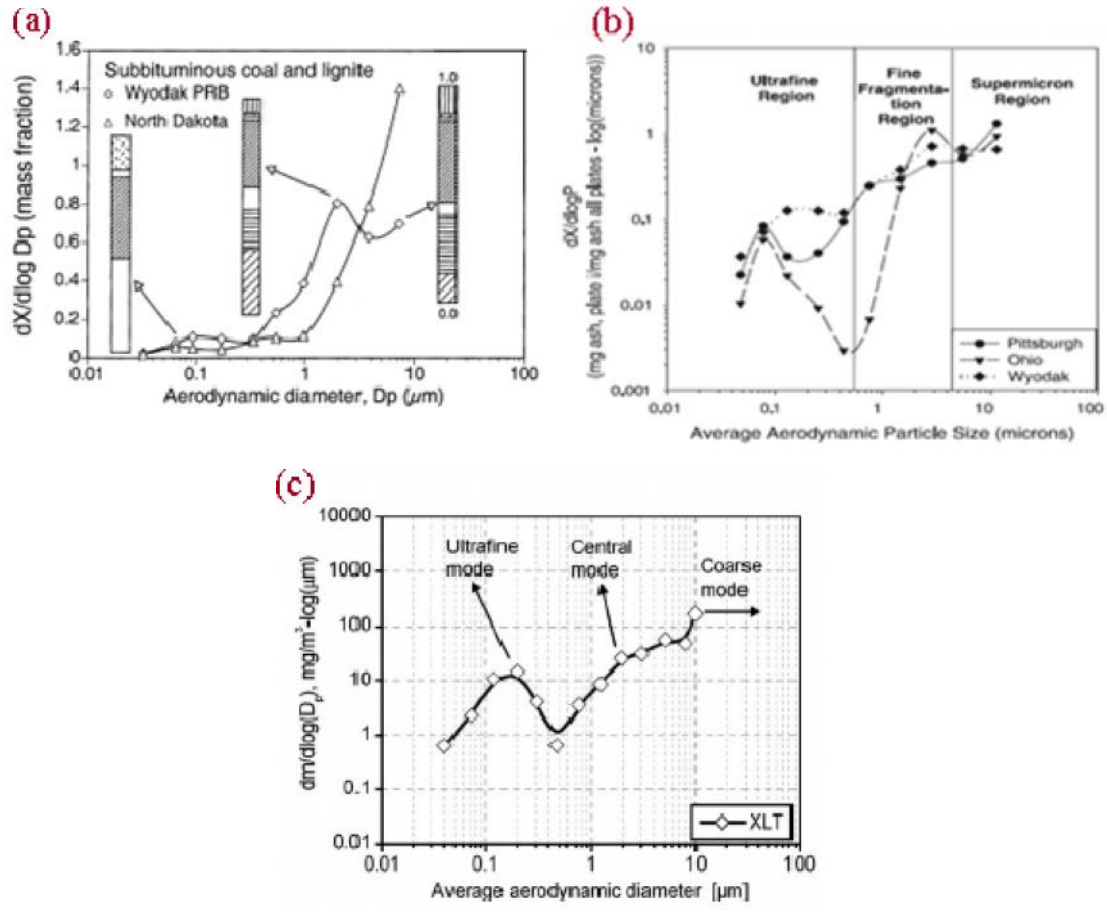

Figure 2-10: Mass size distributions of fly ash from coal combustion (a) in a UA combustor collected by DLPI[128]; (b) in a laboratory combustor collected by BLPI[129]; (c) in a DTF collected by DLPI[130].

It was also proposed that PM_{10} derived from pulverised coal combustion may be of a trimodal size distribution. Apart from the fine and coarse modes, a central particle mode (i.e. the so-called fine fragmentation mode) was suggested in the supermicron region, centered at ~ 4μm as initially proposed by Kang.[131] Followed-up studies[128, 129] also argued the existence of the central mode at ~ 1−2 μm in fly ash, as shown in Figures 2-10 (panels a and b). So did a recent study on coal fly ash produced from the combustion of pulverised coal in a drop-tube furnace (see Figure 2-10c).[130]

2.4.1.2 Morphology

Figure 2-11 presents typical SEM images of ash particles in supermicron region formed during pulverised coal combustion. The supermicron ash particles generally have either a s*pherical or near-spherical shape* with either a smooth surface or a surface sintered with discrete submicron particles[128-130, 132, 133] (see figure 2-11a), or an *irregular shape*, including individual ash particles due to incomplete melting[124, 128, 129] (see Figure 2-11b), or ash particle agglomerates[124, 129] (see Figure 2-11c).

Figure 2-12 shows the typical morphology of ash particles in the fine fragmentation region (generally with aerodynamic diameter of 1-2 µm). The spherical particles generally have smooth surfaces (see Figure 2-12a[130]).[128, 130] For irregular ash particles (see Figure 2-12 b-d), some are sintered spherical ash particles (Figure 2-12b[129]) while others appear to be broken ash particles (Figure 2-12 c[129] and d[130]). The agglomerate of fine ash particles are also evidenced (see Figure 2-12e[134] and Figure 2-12f[130]).

The typical morphology of submicron ash particles are illustrated in Figure 2-13. The submicron particles can be individual spherical ash particles[124, 128-130, 134-136] (see Figure 2-13a[130]) and agglomerates of fine particulates[121, 128, 134, 136] (see Figure 2-13b[136]) while the ultrafine ash particles are generally chain/cluster aggregates of fine particulates[132, 133, 136] (see Figure 2-13c[133]).

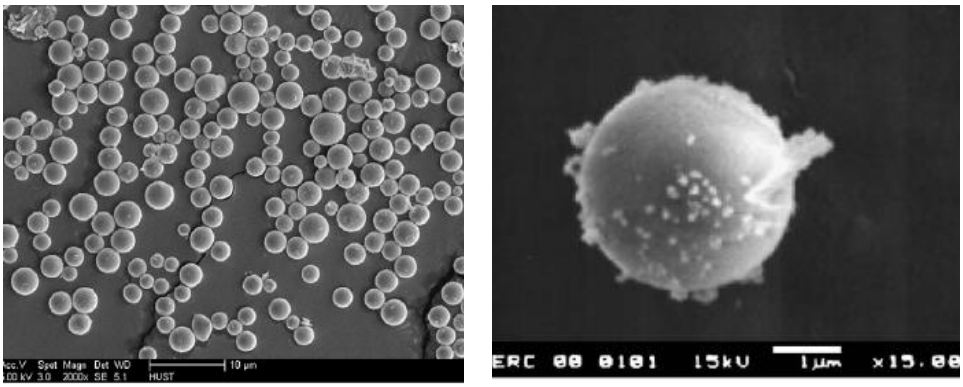

(a) Spherical or near-spherical shape

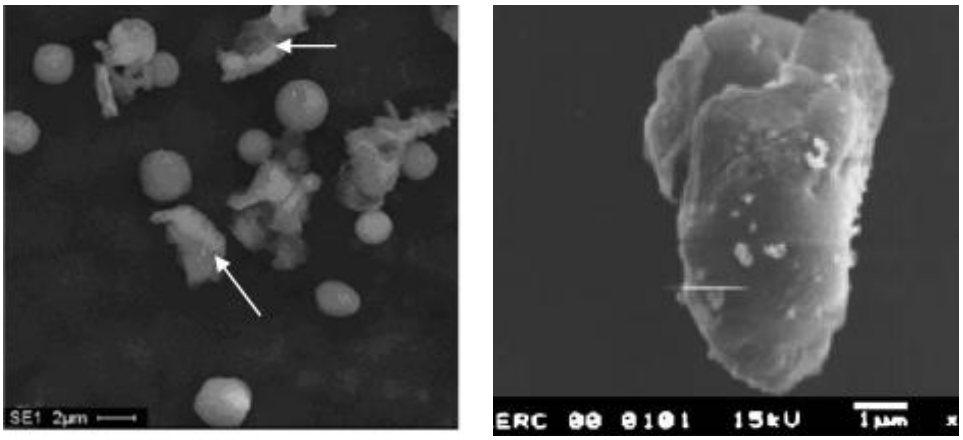

(b) Irregular shape

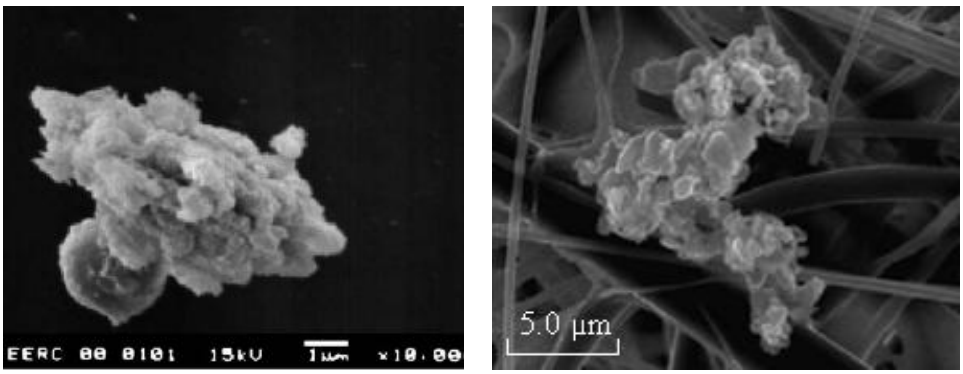

(c) Agglomerate shape

Figure 2-11: Typical SEM images of ash particles in supermicron region produced from pulverised coal combustion.[124, 129, 130, 134]

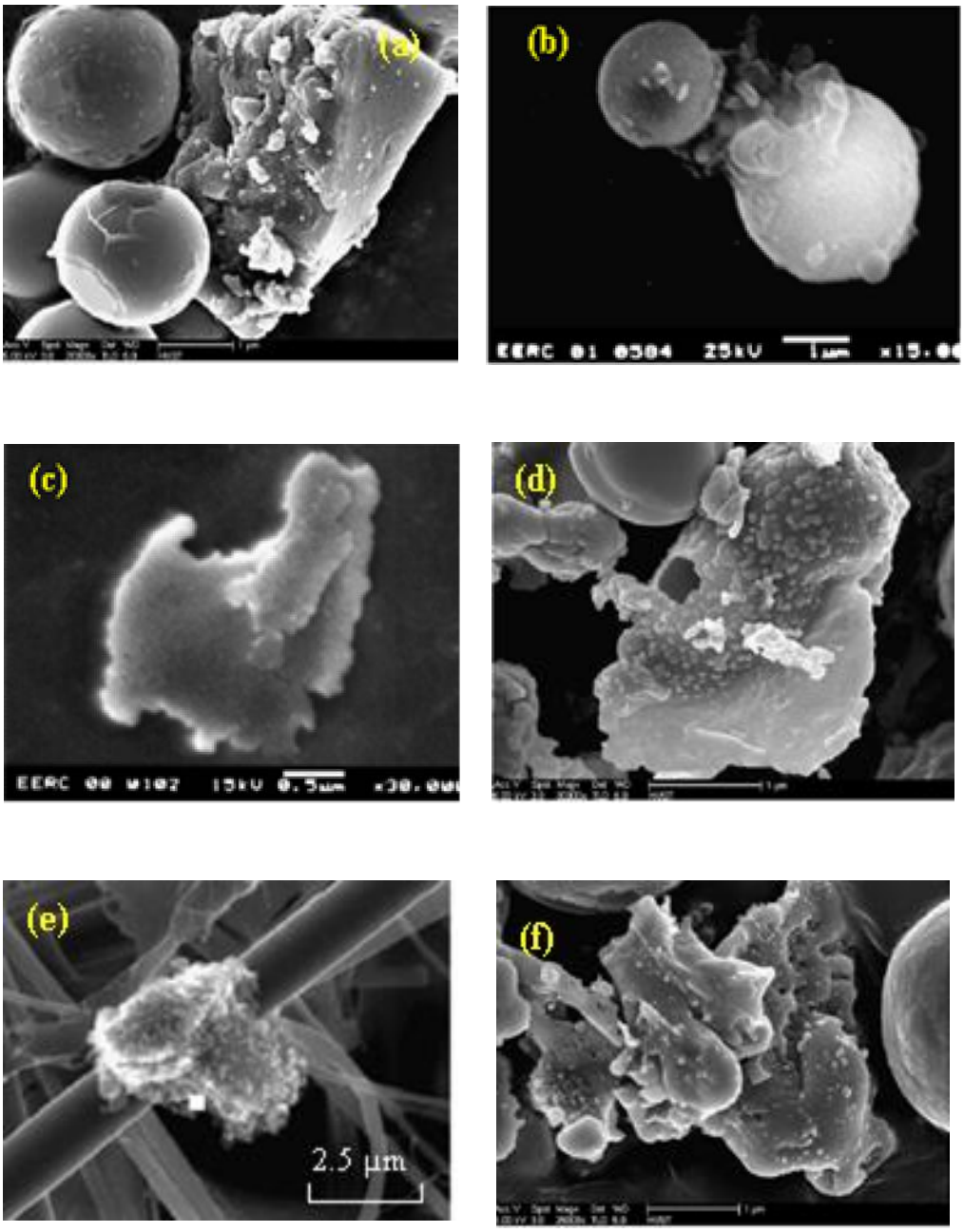

Figure 2-12: Typical SEM images of ash particles in fine fragmentation region from coal combustion.[129, 130, 134]

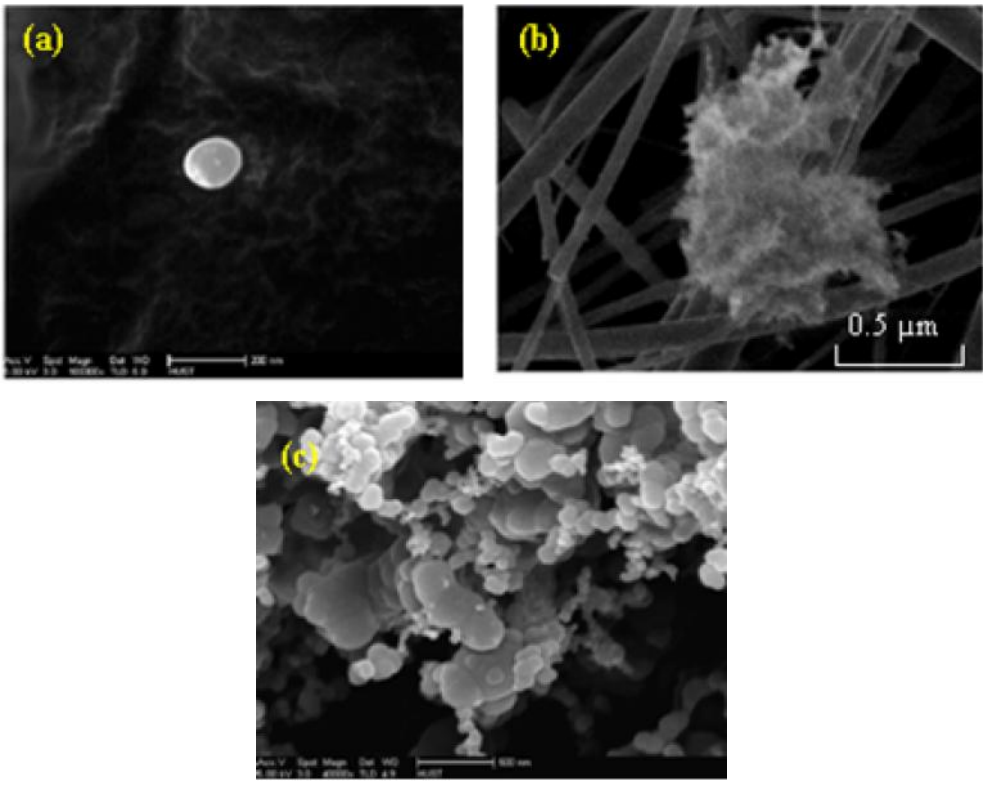

Figure 2-13: Typical SEM images of submicron ash particles from coal combustion.[113, 115, 118]

2.4.2 Formation Mechanisms of PM_{10}

Substantial research efforts were devoted to investigate the formation mechanisms of particulate matter during solid fuels combustion. An overview on these aspects can be found in a recent review,[137] as illustrated in Figure 2-14. There are two categories of pathway for PM formation. One is solid-to-particle processes, producing $PM_{1\text{-}10}$ typically via coalescence of included mineral particles within the same burning coal/char particles and fragmentation of mineral and/char particles. The other is solid-vapour-particle processes, producing both PM_1 and $PM_{1\text{-}10}$ via possible pathways involving homogeneous nucleation, coagulation and agglomeration.

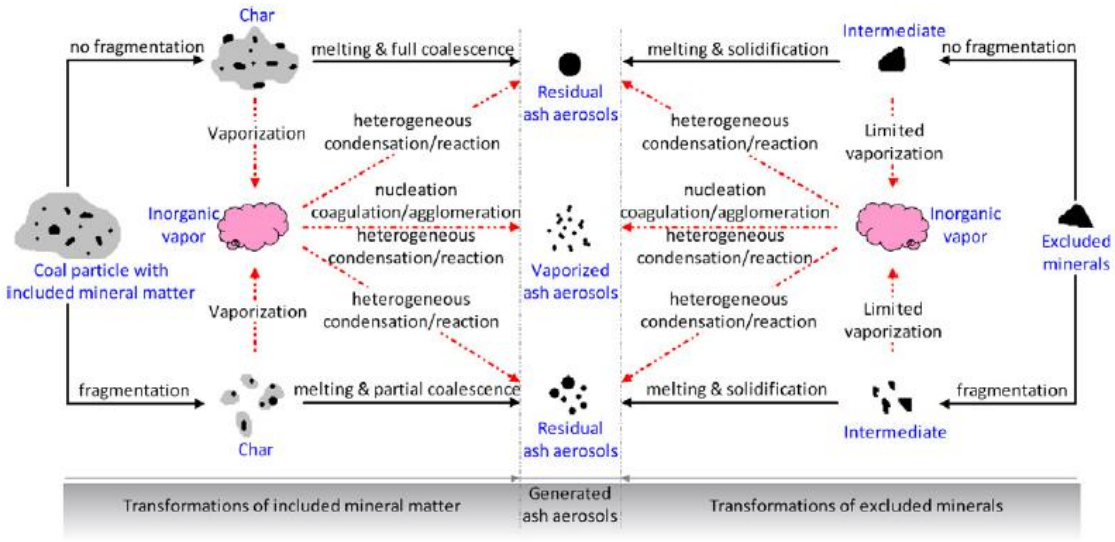

Figure 2-14: Formation mechanisms of particulate matter during coal combustion, solid arrows indicate solid-to-particle processes while dotted arrows indicate solid-vapor-particle processes.[137]

Formation Mechanisms of PM_{1-10}

There are three key mechanisms responsible for PM_{1-10} formation during coal combustion, including coalescence of included minerals, char fragmentation and the fragmentation of excluded minerals.

Coalescence of Included Minerals is a solid-to-particle process and well accepted as a key mechanism responsible for the formation of PM_{1-10}.[87, 114, 119, 121, 130, 133, 137] After initial devolatilisation and combustion of the volatiles, the remaining char particle will continue to combust, leading to the char particle temperature being considerably higher than the gas temperature. Melting of the included mineral particles within the burning coal/char particle may take place. As the char particle recedes, the molten included minerals would be exposed to the surface of burning char particle and coalesce to form larger ash particles.[34, 138, 139] This process is referred to as coalescence of included minerals. It takes place under the following conditions:[114, 131, 140] (1) more than one mineral grain present in the char particle; (2) the temperature of the burning char particle is sufficiently high, leading to ash melting; and (3) the sintering/melting individual ash particles contact each other to coalescence during combustion.

Coalescence of included minerals depends on various factors, including the particle size distribution, content, mineralogy and chemical compositions of included minerals within the reacting coal particle[141] and the temperature of the burning coal/char particle.[87, 114, 131, 140] Additionally, coalescence of included minerals also depends on char fragmentation (discussed in the following subsection) that is a competition process reducing mineral coalescence.[119, 142, 143]

Char Fragmentation. Char fragmentation generally takes place after coal devolatilisation as the resultant char particles become porous. Two mechanisms are proposed to be responsible for char fragmentation. One is the burn-off of bridges connecting regions of a char particle of irregular shape.[144] The other is percolative fragmentation,[143, 145] which is referred to the disintegration of particle structure due to pore enlargement and coalescence during char combustion. Therefore, char structure (especially the macrostructure and macroporosity) of char is considered to be a key factor for char fragmentation.[143, 146, 147] A higher macroporosity induces more extensive fragmentation.[143, 147] It is known that the structure of char after coal devolatilisation strongly depends on coal rank, particle size and pyrolysis conditions.[143, 147] Therefore devolatilisation would in turn affect char fragmentation and hence particle ash distribution of fly ash. A cenospheric char particle is expected to fragment extensively during combustion due to its highly porous structure with a thin wall.[37-39, 140, 142, 147]

Char fragmentation is an important mechanism for PM_{1-10} formation from coal combustion.[87, 124, 130, 132, 140, 148, 149] Helble et al.[148] indicated that, 200-500 ash particles with sizes of 1−4 μm might be produced by each individual coal particle during combustion due to the combined consequences of char fragmentation and shedding of fused ash inclusions from the receding char surface. Char fragmentation was suggested to contribute to the formation of ash particles with 1−5 μm (via perimeter fragmentation) by Helble and Sarofim,[149] the formation of fly ash particles with sizes > 5μm by Wibberley and Wall[87] and the formation of the fine fragmentation mode and $PM_{2.5}$ by Sheng et al.[124] and Buhre et al.[140] The contribution of char fragmentation to the formation of supermicron ash particle was also reported in other literature.[124, 130, 132]

Fragmentation of Excluded Minerals. Excluded minerals as discrete particles have limited collision with other mineral matter or coal particles during combustion. Excluded mineral transformation may involve fragmentation, attributed to thermal shock and rapid gas release from inside the particle depending on the chemical reactions experienced by excluded mineral particles. Raask[21] showed that little fragmentation was found for the silicate minerals, quartz, illite, and muscovite during thermochemical processing. Pyrite is known to fragment due to the vigorous evolution of gaseous products under combustion conditions. [21, 88, 90, 105, 106, 109, 110] So are carbonates including siderite, ankerite and calcite which fragment extensively on rapid heating because of the release of carbon dioxide.[21, 110] Fragmentation of excluded minerals is also dependent on the particle size distribution of mineral particles. [149] Excluded mineral fragmentation generally produces supermicron ash particles,[110, 125, 140] although it was also speculated that it may also possibly produce PM_1.[21, 89, 90, 150, 151]

Formation Mechanisms of PM_1

Generally, it is believed that formation of PM_1 follows a vaporization-condensation process. However, it was also speculated that PM_1 may be formed via other possible mechanisms, including direct carryover of fine mineral particles in coal, surface ash shedding, and cenosphere fragmentation.

Vaporization and Condensation. This mechanism is regarded as the dominant mechanism of PM_1 formation during coal combustion. During coal combustion at high temperatures, a small portion of ash components (typically 0.2-3%) may vaporize into the gaseous phase as inorganic vapors.[89, 138, 141, 148-150, 152] Diffused away from the char particle, the inorganic vapors may experience two pathways.[89, 112, 116, 138, 149, 150, 152]

One is that outside the flame zone that is of reducing atmosphere, the inorganic vapors are re-oxidized and becoming supersaturated and homogeneously nucleating to form substantial amounts of fumes (<0.01 μm [138]). The newly-formed nuclei may collide with each other due to Brownian motion, followed by coagulation to form larger particulate matter in the submicron size range. This formation mechanism will

result in the composition size distribution of PM_1 independent of particle size − one of most reasonable criteria for distinguishing such mechanism of PM_1 formation.

The other is heterogeneous condensation/reaction, referring to the condensation of inorganic vapors on the surface of existing super fine ash particles. This mechanism results in the composition size distribution of ash particles to be proportional to d_p^{-1} (free molecular regime) or d_p^{-2} (continuum regime),[112, 116] where d_p is the particle diameter.

The growth of ash particles continues till the gas temperature decreases, consequently agglomerating into chain or cluster aggregates of < 1 μm.[149] Homogeneous nucleation, heterogeneous condensation and growth by coagulation are competition processes, depending on various parameters such as coal properties and combustion conditions.

Generally speaking, PM_1 formed via vaporization/condensation is attributed to the vaporization of volatile elements such as Na, K, and S, which are usually enriched in PM_1.[116, 117, 122, 124, 125, 128, 130, 134, 136, 140, 153] However, refractory components including Si, Al, Fe, Ca, and Mg were also observed in PM_1.[116, 117, 130, 133, 136, 150, 153, 154] The mechanism responsible for the vaporisation of the oxides of these refractory elements is the reduction of these oxides to more volatile reduced species (SiO, Al_2O and AlO) and metals (Fe, Ca and Mg).[114, 119, 150] Therefore, the reducing atmosphere within burning char particles is an important factor, favouring the vaporization of these refractory components. It was also found that coal particle size, mode of minerals occurrence in coal, and particle temperature are also key factors influencing the volatility of the inorganic elements during coal combustion.[114, 117, 126, 128, 136, 150, 155]

Carryover of Fine Mineral Particles. The submicron mineral particles originally presented in pulverised-coal samples may also be carried over to form particulate matter after combustion. Holve[156] firstly speculated that, not the popular vaporization-condensation mechanism but this carryover process most possibly hold the responsibility for much of the submicron fly ash formed during pulverised coal combustion. In the experimental study on the formation of submicron fly ash > 0.1μm by Sadakata and co-authors,[135] it was suspected that approximately half of the submicron fly ash was carried over from the submicron coal particles originally

present in the raw coal particles. Baxter[92] also hypothesized that fine non-volatile inorganic particles in coal matrix may also be carried over along with the rapid release of volatiles during coal devolatilization. Zhang et al[157] also suggested the possible mechanism for the formation of PM_1 due to the presence of major ash-forming inorganic elements in the condensed volatile matter < 1μm during coal pyrolysis. However, there was no direct experimental evidence to support these speculations.

Surface Ash Shedding. The shedding of ash particle from the surface of burning char particles may be caused by the particle rotation due to gas evolution. [114, 158] Some studies claimed the important process of ash shedding also contributing to the formation of fine ash particles. [114, 150, 158, 159] However, this is debatable as mathematical calculation suggests that ash shedding may not take place for the molten ash on the surface of burning char particles. [143]

Cenosphere Bubble Bursting. It has been long speculated that fragmentation of ash cenospheres may contribute to the formation of particulate matter. For example, Ramsden[34] postulated that the bursting of gases inside the molten ash droplets may produce small droplets of 0.1μm, consequently producing submicron fly ash after the successive solidification. Smith et al[35, 36] deduced that the bursting of larger hollow spheres by rapid gas release and the subsequent coagulation are also likely to produce submicron particles. However, there has been no direct experimental proof to support these hypotheses.

2.4.3 Key Factors Influencing the Formation of PM_{10}

Above review suggests that the formation of PM_{10} during coal combustion is a consequence of the combination of various possible mechanisms. Therefore, the parameters such as coal properties and combustion conditions may play significant roles in the formation and properties of PM_{10}. Figure 2-15 presents the typical factors influencing the formation and characteristics of PM_{10} during coal combustion as summarized from the literature.

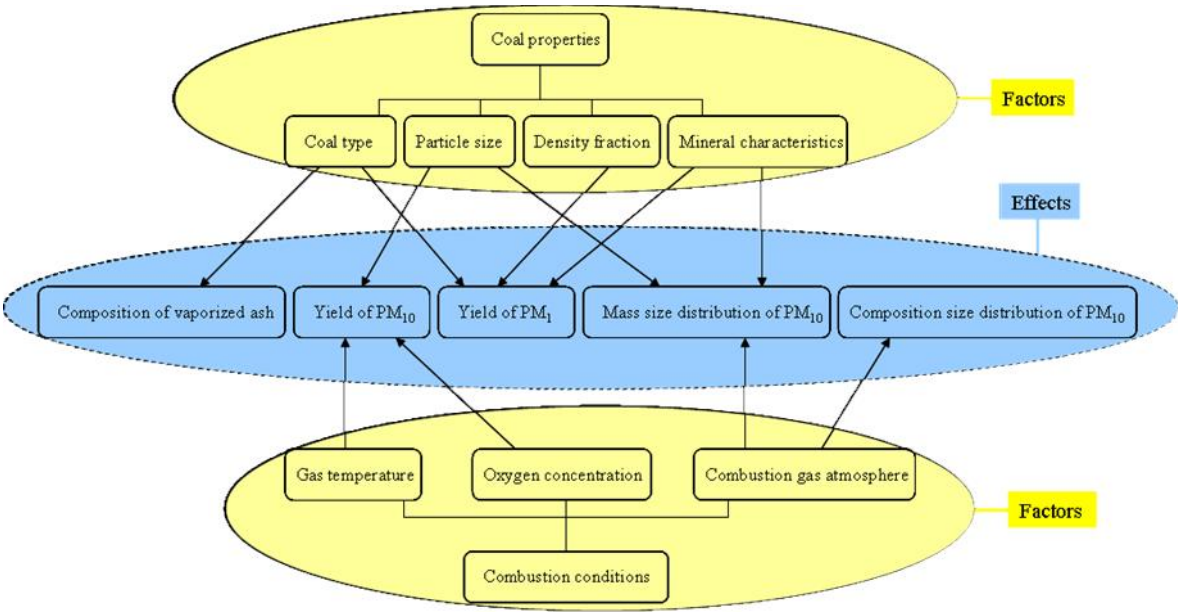

Figure 2-15: Typical factors influencing the formation of PM_{10} during coal combustion.

Coal Properties. Generally speaking, these included four aspects: coal type, particle size, density fraction of coal, and characteristics of mineral matter in coal.

Coal Type was believed to be an important factor in the amount of composition of the vaporized ash mainly due to different rank of coals contain different concentrations of organically bound alkaline earth metals.[150] It was also proposed that combustion of bituminous coals produced more PM_1 than the anthracite coals did.[136]

Coal Particle Size was also considered to be a significant factor in the emission of PM_{10} during coal combustion.[134, 152] According to the studies,[134, 152] decreasing coal particle size produced more PM_1 and PM_{1-10}. However, Dunn et al claimed the proportion of PM_{10} independent with coal particle size.[87] In addition, mass size distribution of fly ash was proposed to be approximately proportional correlated with coal particle size.[87]

Density Fraction of Coal. Liu et al[154] combusted a Chinese bituminous coal with three density fractions, i.e. heavy (> 2.0 g cm^{-3}), medium (1.4-2.0 g cm^{-3}) and light (< 1.4 g cm^{-3}), to investigate the formation and emission of PM_{10}. It was found that,

compared with the combustion of medium and light fractions of coal, less PM_{10} was produced from the combustion of the heavy fraction, mainly owing to excluded minerals dominated the coal with heavy density fraction while included mineral principally in the other two fractions.

Characteristics of Mineral Matter in Coal, including mode of occurrence of minerals in coal, minerals particle size, and the composition play important roles in the formation of PM_{10} during pulverised coal combustion. The *mode of occurrence of minerals in coal* i.e. included or excluded minerals generally have different reaction pathways during coal combustion, resulting in fly ash with different size distributions. For example, some studies[126,160] proposed that the interactions between included and excluded minerals combined with the interactions amongst included minerals significantly influenced the formation of PM_1 and PM_{1-10} during coal combustion. In addition, *mineral particle size* may affect the formation of PM_1 supposing that carryover of the fine fuel particles is the formation mechanism of PM_1. *Composition of minerals in coal* was considered to be critical in the formation of PM_{10}.[36, 90, 125, 140, 149, 152] The reason is mineral composition in coal determines ash fusion temperature, and higher ash fusion temperature restricts the coalescence of inherent minerals, resulting in elevated PM_{10} yields.[140]

Combustion Conditions. These include three key parameters proposed to influence the formation of PM_{10}: gas temperature,[36, 87, 122, 136, 149, 150] oxygen concentration in combustion gas,[122, 124, 140, 153] and combustion gas atmosphere[124]. Generally, increasing *gas temperature* increases the amount of PM_{10} increases during coal combustion, as results of intensified inorganic elements vaporization and extensive char fragmentation coupled with increased liberation of fine included minerals from the burning char surface at high temperatures. However, Wibberley and Wall[87] pointed out the mass size distribution of fly ash was independent of combustion temperature. Similarly, increasing *oxygen concentration* in combustion gas generally increases gas temperature, favoring the formation of PM_{10}. Additionally, *combustion gas atmosphere* is another important factor influencing the formation of PM_{10} during coal combustion. According to Sheng et al[124], compared to air combustion, O_2/CO_2 combustion significantly affected the mass and composition size distributions of both PM_1 and PM_{1-10}.

2.5 Conclusions and Research Gaps

The main conclusions based on the above review of the literatures are as follows:

(1) Ash cenospheres can be widely used in manufacturing various value-added products. The properties of ash cenospheres formed from pulverised fuel combustion have been extensively studied based largely on bulk samples.

(2) The formation mechanisms of ash cenospheres during pulverised fuel combustion have been proposed. Key factors influencing ash cenospheres formation include coal properties, characteristics of ash droplets and combustion conditions.

(3) The transformation behaviours of excluded pyrite under combustion conditions have been well documented. Fragmentation is known to take place during pyrite combustion.

(4) The formation of ash cenosphere was observed during pyrite combustion at gas temperatures > 1100 °C.

(5) The characteristics and formation mechanisms of PM_{10} during solid fuels combustion have been extensively investigated. Fragmentation of excluded minerals was suggested to produce mainly $PM_{1\text{-}10}$ but also possibly PM_1. There have also been speculations that ash cenosphere fragmentation during pulverised coal combustion may contribute to the formation of PM_{10}.

(6) Formation and/or emission of PM_{10} are influenced by key parameters including coal properties and combustion conditions.

However, further R&D is needed to bridge the several research gaps identified, which are summarised below:

(1) It is still largely unclear on the mechanisms responsible for ash cenospheres formation during pulverised fuel combustion.

(2) While various factors are proposed to determine the formation of ash cenosphere, there has been no systematic research to investigate how each factor or a combination of these factors influence ash cenosphere formation.

(3) There is a strong need to investigate ash cenosphere formation from solid fuels using a simple fuel. This review identifies that pyrite is a good model fuel for such purpose due to its simple component and well-documented chemistry during combustion.

(4) While the formation of ash cenosphere from pyrite combustion was observed at temperatures > 1100 °C, there is no systematic work focusing on investigating the mechanism of ash cenosphere formation during pyrite combustion.

(5) There is also no experimental evidence to support the claim that ash cenosphere fragmentation may lead to substantial formation of particulate during solid fuels combustion.

2.6 Objectives of the Present Study

During a period of 3.5-year for a PhD study, it is impossible to carry out extensive research to fill research gaps identified. Therefore, this thesis will focus on fundamental investigation on the ash cenosphere formation, fragmentation behaviour and its contribution to particulate matter emission during pulverised fuels combustion.

The specific objectives of the present study are:

(1) To understand formation mechanism of ash cenospheres during solid fuels combustion through characterising thermal behaviours, ash chemistry and properties of gas locked in various size-fractioned ash cenosphere collected from an Australian power station.

(2) To design a systematic program for fundamentally investigating the formation mechanisms of ash cenospheres during solid fuels combustion under various conditions using pulverised pyrite as a model fuel.

(3) To investigate the significant role of ash cenosphere fragmentation in the formation of ash and particulate matter during pulverised pyrite combustion.

CHAPTER 3 METHODOLOGY AND ANALYTICAL TECHNIQUES

3.1 Introduction

This chapter firstly describes the overall research methodology employed to achieve the thesis objectives which were outlined in Chapter 2. Experimental and analytical techniques used in this thesis are then followed in details.

3.2 Methodology

In present study, ash cenospheres from two different sources were characterized to understand its formation and behaviour. One is ash cenosphere in fly ash from a coal-fired power station. Ash cenosphere samples were firstly prepared by a series of methods such as sink-float separation, sieving, etc. Then, the ash cenospheres were characterised by a number of analytical techniques including X-Ray fluorescence (XRF), thermomechanical analysis (TMA), gas chromatography (GC), and scanning electron microscope equipped with energy dispersive spectroscopy (SEM-EDS).

The other is ash cenosphere produced in a laboratory-scale drop-tube furnace system using pyrite (FeS_2) as a model fuel. The experiments of pyrite combustion were conducted under various designed conditions. The collected samples, including fly ash in the cyclone and PM_{10} (particulate matter with aerodynamic diameter less than 10μm) in a Dekati low pressure impactor (DLPI), were mainly characterised by sieving, gravimetric determination, morphology observation, quantification of chemical compositions, mineralogical analysis. Experiments and analyses were repeated to ensure the reproducibility of the results.

The overall research methodology to achieve the objectives outlined in Chapter 2 is shown in Figure 3-1, which will be explained in the following sections in details.

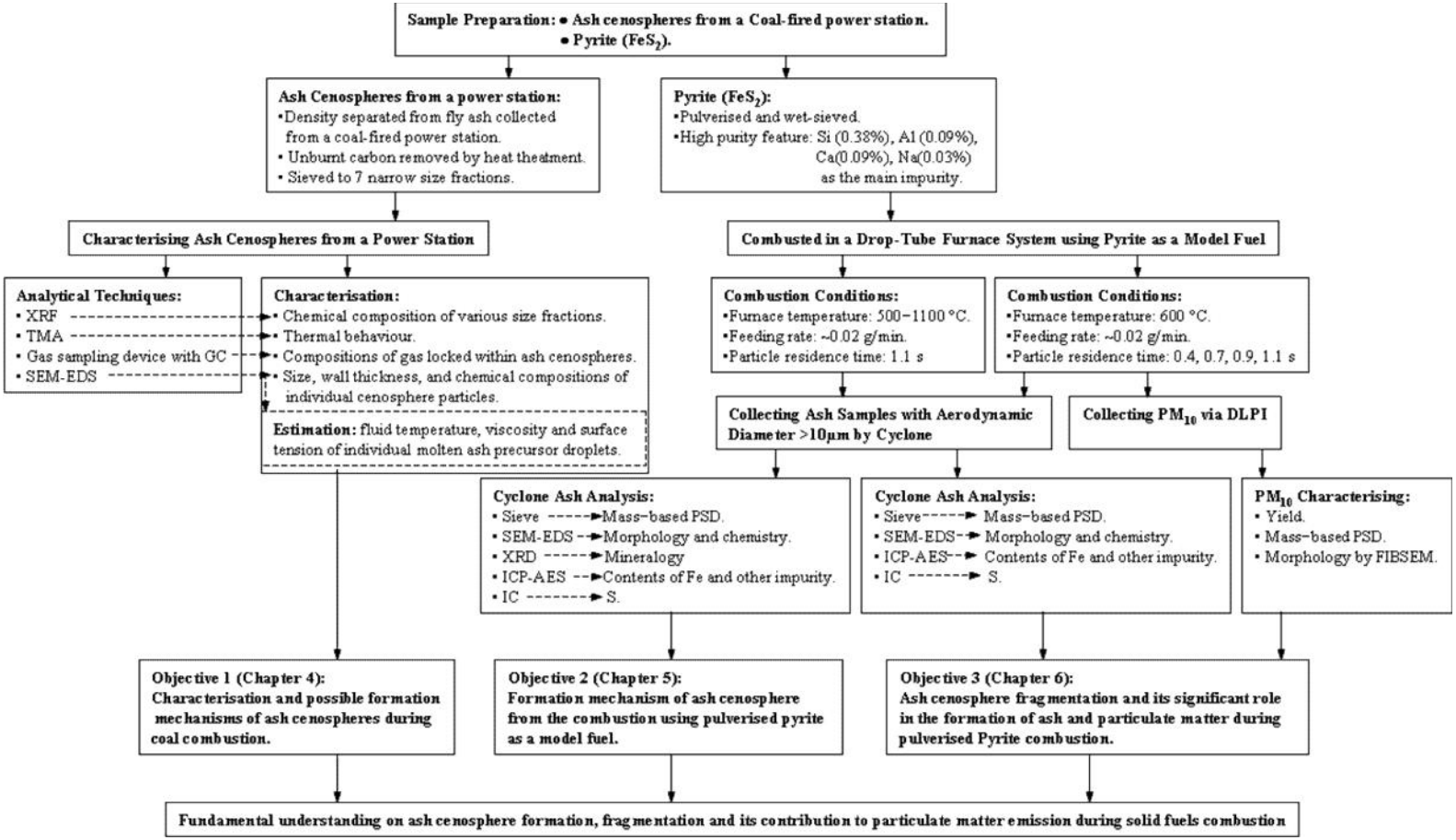

Figure 3- 1: Research methodology

- **Possible Formation Mechanisms of Ash Cenospheres from a Coal-fired Power Station**

To achieve the first research objective outlined in Section 2.6 of Chapter 2, ash cenospheres in fly ash from a coal-fired power station were characterised. Firstly, a series of ash cenosphere samples were prepared by density separation, heat treatment, and sieving (see Section 3.3.1). The prepared ash cenosphere samples were then analysed by XRF to determine the chemical compositions of ash cenospheres (see Section 3.4.1). In order to investigate the thermal behaviour of ash cenospheres and the compositions of gas locked in ash cenosphere samples, TMA and GC were employed, respectively (see Section 3.4.2 and 3.4.3). SEM-EDS analysis was then utilized to quantify the chemical compositions of individual ash cenosphere particles to derived correlations for individual cenosphere particles of various sizes (see Section 3.4.4). Based on the chemistry of ash cenospheres, the fluid temperature, viscosity and surface tension of ash cenospheres were then estimated (see Section 3.4.5). The detailed results and discussion are presented in Chapter 4.

- **Formation Mechanism of Ash Cenosphere from the Combustion using Pulverized Pyrite as a Model Fuel**

A systematic experimental program was designed in this study to achieve the rest objectives outlined in Section 2.6 of Chapter 2, using pyrite as a model fuel. Pyrite was firstly sieved into a nominal size fraction of 38 – 45 µm after pulverisation (see Section 3.3.1). The pyrite sample was then combusted in a laboratory-scale drop-tube furnace system (see Section 3.3.2) at furnace temperatures of 530 – 1100 °C (see Section 3.3.3). In order to achieve the second objective outlined in Section 2.6 of Chapter 2, ash particles with aerodynamic diameters > 10 µm were collected in a cyclone to investigate ash cenosphere formation. The ash samples collected from the cyclone were firstly sieved into 7 size fractions for studying mass-based particle size distribution (see Section 3.4.6). The size-fractioned ash samples were then characterised by a series of analytical techniques including SEM-EDS, X-ray diffractometer (XRD), inductively coupled plasma-atomic emission spectroscopy (ICP-AES), and ion chromatography (IC). The results and discussion are reported in Chapter 5.

- **Ash Cenosphere Fragmentation and its Significant Role in the Formation of Ash and Particulate Matter during Pulverised Pyrite Combustion**

To investigate the fragmentation behaviour of ash cenosphere and its role in the formation of ash and PM_{10}, pyrite with particle size of 38 – 45 µm was used again as a model fuel. The pyrite sample was combusted in the laboratory-scale drop tube furnace system (see Section 3.3.2) at furnace temperature 600 °C but different residence times (0.4, 0.7, 0.9, and 1.1 s) (Section 3.3.3). In order to achieve the third objective outlined in Section 2.6 of Chapter 2, both ash particles with aerodynamic diameters > 10 µm and PM_{10} were collected via cyclone and DLPI (see Section 3.3.2 and Section 3.3.4) for characterisation. The collected samples were then subjected to various analyses including mass-based particle size distribution, morphology, and chemical composition. The detailed results and discussion are presented in Chapter 6.

3.3 Experimental

3.3.1 Sample Preparations

Ash cenospheres formed from coal combustion. Fly ash was collected from an Australian coal-fired power station. The ash sample was **t**hen dispersed in distilled water at an ash/distilled water ratio of 1:20 at room temperature, followed by continuous stirring and settling for 24 hours. The float ash samples were then collected as ash cenospheres, which were further heated to 850 °C under an oxidizing atmosphere in a muffle furnace to remove unburnt carbon. The ash cenospheres after heat treatment were sieved into 7 size fractions (45-63, 63-75, 75-90, 90-106, 106-125, 125-150, and 150-250 µm) as the samples for the characterization in Chapter 4.

Pyrite (FeS_2). Raw pyrite was pulverised using a laboratory-scale ball mill. The pulverised pyrite sample was then wet-sieved, i.e. using ethanol to keep flowing through the top sieve during sieving, to collect the nominal size fraction of 38-45 µm as pyrite sample for all experiments in Chapters 5 and 6. To analyse the chemical compositions of the pyrite sample, a procedure [161] that was developed on the basis of a method used for brown coals[162] was used after the preliminary analyses (quantification of Fe, Al, and Si via ICP-AES, and that of Na, K, Ca, and Mg via IC). The results are listed in Table 3-1. The purity of the size-fractioned pyrite sample is

high, containing only low concentrations of Si (0.38%), Al (0.09%), Ca (0.09%), and Na (0.03%) and trace amounts of Ti, Mg, and K.

Table 3- 1: Ash compositions (wt %) of pulverised pyrite sample (38-45 µm)

Fe[a]	S[b]	Si[a]	Al[a]	Ti[a]	Na[b]	K[b]	Mg[b]	Ca[b]
45.85	53.52	0.38	0.09	0.01	0.03	0.01	0.01	0.09

[a]Analyzed by ICP-AES. [b]Analyzed by IC.

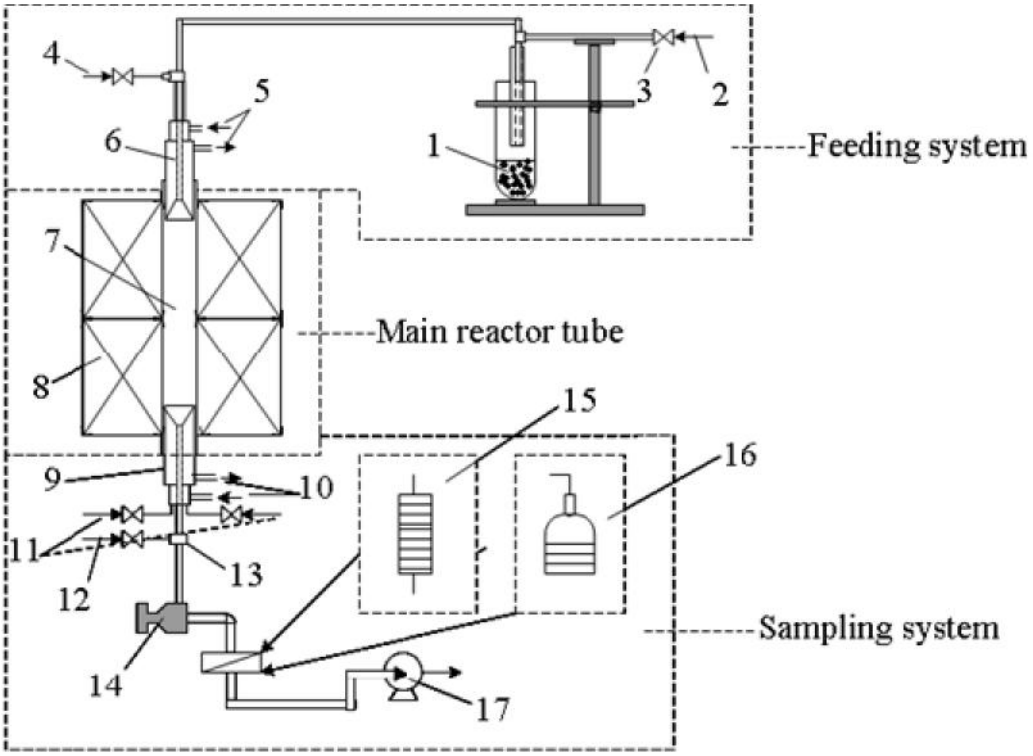

Figure 3- 2: Schematic diagram of DTF system: (1) Feeder, (2) Primary air, (3) Mass flow controller, (4) Secondary air, (5) Cooling water of feeding probe, (6) Feeding probe, (7) Dense mullite reactor tube, (8) Two heating-zone furnace, (9) Sampling probe, (10) Cooling water of sampling probe, (11) Quench helium, (12) Makeup and dilution air, (13) Diluter, (14) Cyclone, (15) DLPI, (16) Cascade impactor, (17) Vacuum pump.

3.3.2 Drop-Tube Furnace System

The experimental apparatus used for the experiments of pulverised pyrite combustion in this study was a laboratory-scale drop-tube furnace (DTF) system. The schematic diagram of the DTF system is shown in Figure 3-2, which is similar with the one employed in recent studies.[127, 163, 164] The DTF system consists of a feeding system, a main reactor tube, and the subsequent sampling system. The DTF system is described in details as following.

Feeding system. As shown in Figure 3-2, the feeding system consists of an entrained flow feeder, an inlet of primary gas, an inlet of secondary gas, and the attached mass flow controllers, followed by a water-cooled feeding probe. The entrained flow feeder includes mainly a 1/4'' stainless steel tubing which is inserted into a 3/8'' stainless steal tubing being placed inside a glass tube. During feeding, a stream of primary air (instrumental grade) flows through a mass flow controller via the annular space between the 1/4'' and 3/8'' stainless steal tubing. Fuel samples preloaded into the glass tube are then entrained by the primary air through the 1/4'' stainless steal tubing and then fed into the reactor tube via a water-cooled feeding probe inserted into the top of the furnace. A stream of secondary air (instrumental grade) is introduced into the furnace to achieve complete combustion.

Main reactor tube. The main reactor tube is made up of dense mullite with inner diameter of 54 mm and length of 1280 mm. It is vertically placed and electrically heated. There are 2 heating zones in the furnace, with temperatures being controlled and monitored by thermocouples. The gas temperature profile of the DTF is shown in Figure 3-3 which indicates an isothermal zone of around 600 mm.

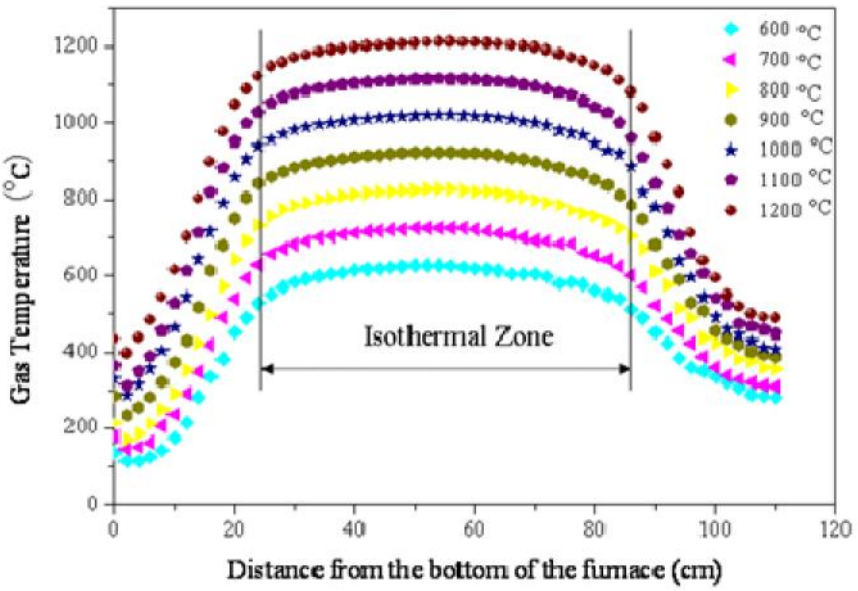

Figure 3- 3: Gas temperature profiles in the DTF

Sampling system. The sampling system consists of a water-cooled quench sampling probe, a diluter, followed by the collecting system. The collecting system includes a Dekati cyclone (Model SAC-65) with a nominal cut-off size of ~ 10 µm, a cascade impactor with a backup filter (for experiments in Chapter 5) or a Dekati low pressure impactor (DLPI) with backup filter (for experiments in Chapters 6), and a vacuum pump (Leybold Sogevac SV25). After combustion, the flue gas that contains ash particles is directed into a water-cooled quench sampling probe, which is designed for quick quenching and diluting the particle stream with quench medium (high-purity helium). This minimizes the interaction among ash particles. It also forces the nucleation of vaporized materials. The cyclone collects the coarse ash particles with aerodynamic diameter > 10 µm, while the ash particles with aerodynamic diameter < 10 µm are collected by the subsequent cascade impactor or DLPI as samples of interests for characterisation.

DLPI Stages	D50% [um]
1	0.03
2	0.06
3	0.108
4	0.17
5	0.26
6	0.4
7	0.65
8	1
9	1.6
10	2.5
11	4.4
12	6.8
13	10

(a) (b)

Figure 3- 4: DLPI (a) and its nominal cut-off size calibrated at 21.5 °C with gas flow rate of 10.01 L/m (b).

The DLPI used is composed of 13 collection stages and a backup filter stage, as shown in Figure 3-4 (a). It was calibrated by the manufacturer before delivery and the nominal values are presented in Figure 3-4 (b). When ash particles entrained by the flue gas are going through the DLPL, those particles larger than stage cut diameter are impacted on the substrate of collection plate, while the rest are going through the subsequent impactor stages for further size classification and collection. During experiments, the gas flow is controlled by the bottom stage of the DLPI as a sonic orifice at a nominal flow rate of ~ 10 L/m. The inlet and outlet pressure of the DLPI is controlled at 1013.3 mbar and 100 mbar, respectively. When there is insufficient flue gas flow (< the nominal value of 10 L/m) during a combustion run, additional air (instrumental grade) is then introduced as makeup gas.

Table 3- 2: Experimental conditions during pulverised pyrite combustion in DTF

Parameter	Details of combustion for the objectives of	
	Chapter 5	Chapter 6
Feeding sample	Pyrite particle: 38−45 µm	
Feeding Rate (g min^{-1})	~ 0.02	
Furnace Temperature (°C)	530 − 1100	600
Residence Time (s)	1.1	0.4 0.7 0.9 1.1

3.3.3 Combustion of Pulverised Pyrite

All the combustion experiments were performed in the DTF system described in the above section 3.3.2 using pyrite as the model fuel (detailed in Section 3.3.1). There are two different batches of combustion experiments, with results being presented in Chapters 5 and 6, respectively. The details of experimental conditions are listed in Table 3-2.

In an experimental run, the DTF system is preheated to a desired temperature. Via the feeding system, pulverised pyrite particles are entrained by the primary air and fed into the furnace through the entrained flow feeder. The feeding rate for all of the combustion experiments is ~ 0.02 g/min. A stream of secondary air is also fed into the main reactor. The residence time of pulverised pyrite particle in the isothermal zone is adjusted via the total air (primary and secondary air) introduced into the main reactor. The value for each batch of experiments can be seen in Table 3-2. The total combustion air flow rate is 3.2 – 6.9 L/min. The value of λ (expressed as the ratio of the actual air/fuel ratio to the stoichiometric air/fuel ratio) is from ~ 22 to ~ 52, so that there is excessive oxygen available for pyrite combustion.

3.3.4 Sampling of Particulate Matter (PM)

After the pulverised pyrite combustion in the main reactor under the well-controlled conditions, flue gas contained particulate matter is directed through the water-cooled helium quench sampling probe into the cyclone firstly to remove the coarse ash particles with aerodynamic diameter > 10µm. For the experiments in Chapter 5, a cascade impactor is followed the cyclone to collect the rest ash particles. But only the coarse ash particles with aerodynamic diameter > 10µm collected in cyclone are the samples of interests to ash cenosphere formation in Chapter 5.

For combustion experiments in Chapters 6, the flue gas with particulate matter with aerodynamic diameter < 10 µm (PM_{10}) is further directed into the DLPI for size-segregated collection (0.0275 – 10 µm). The ultrafine ash particles (< 0.0275 µm) are collected by the backup filter. During PM_{10} sampling, aluminium foils are used as collection substrates, which are covered by Apiezon-H vacuum grease to prevent particle bounce. Before used for collection, the greased aluminium foils are dried at 115 °C for 12 hours to avoid any possible mass losses during sampling. In addition, during experiments, the sampling system, including diluter, cyclone, DLPI, and the stainless steel sampling lines, is heated and insulated at 115 °C, same as the flue gas temperature at the exit of quench sampling probe. This is to avoid any possible acid gas condensation and suppress particle coagulation during sampling.

3.4 Instruments and Analytical Techniques

3.4.1 X-ray Fluorescence (XRF) Spectroscopy

XRF was employed to determine the chemical composition of the different size fractions of ash cenospheres from the coal-fired power station. Prior to analysis, the samples were heat treated in a muffle furnace at 850 °C under an oxidizing atmosphere to remove unburnt carbon, as detailed in Section 3.3.1.

3.4.2 Thermomechanical Analysis (TMA)

TMA measurement was carried out in a SETARAM TMA92 Thermo Mechanical Analyser at the University of Newcastle for several different narrow size fractions of ash cenospheres. This is to evaluate their thermal behaviour. Prior to measurements, the ash cenospheres were heat treated to remove unburnt carbon and then grounded

into fine ash fragments. In a TMA measurement, ~50 mg fine powder of an ash cenosphere sample was put into the sample assembly with a molybdenum crucible, and then heated from ambient temperature to 1600 °C at 5 °C /min in argon.

3.4.3 Quantification of Gas Compositions within Ash Cenosphere

A gas sampling system was designed and fabricated to collect and analyse the gas products enclosed inside the ash cenosphere samples. Figure 3-5 presents the schematic diagram of the gas sampling system.

The gas sampling system includes a gas tight chamber made from stainless steel, a vacuum pump, a gas cylinder with argon, two Perkin-Elmer gas chromatography (GCs) installed with dual columns (molecular sieve column and Porapak-N column), a mass flow controller, and the tubing following control system (e.g. valves, connectors etc). A steel ball was preloaded into the steel chamber and the chamber is fixed on a bench. Prior to a measurement run, a known amount (~ 1 g) of an ash cenosphere sample (size-fractioned) was loaded into the chamber. The chamber is then vacuumed followed by the purge of argon gas into the system to refill the chamber. The vacuum-purging process was done for three times in order to eliminate the residual air in the chamber. A stream of argon (1 L min^{-1}) then continued to purge through the chamber. The flow through gas was also collected after purging and then subjected to GC analysis. The purge process is considered to be completed when the GCs doesn't detect any gas. Then, the chamber was isolated by closing both inlet and outlet valves, followed by vigorously shaking the chamber for 5 minutes to force the steel ball inside break all the ash cenosphere particles. The mixed gas inside the chamber, including argon and the gas released from ash cenosphere samples, was introduced into the GCs for composition analysis.

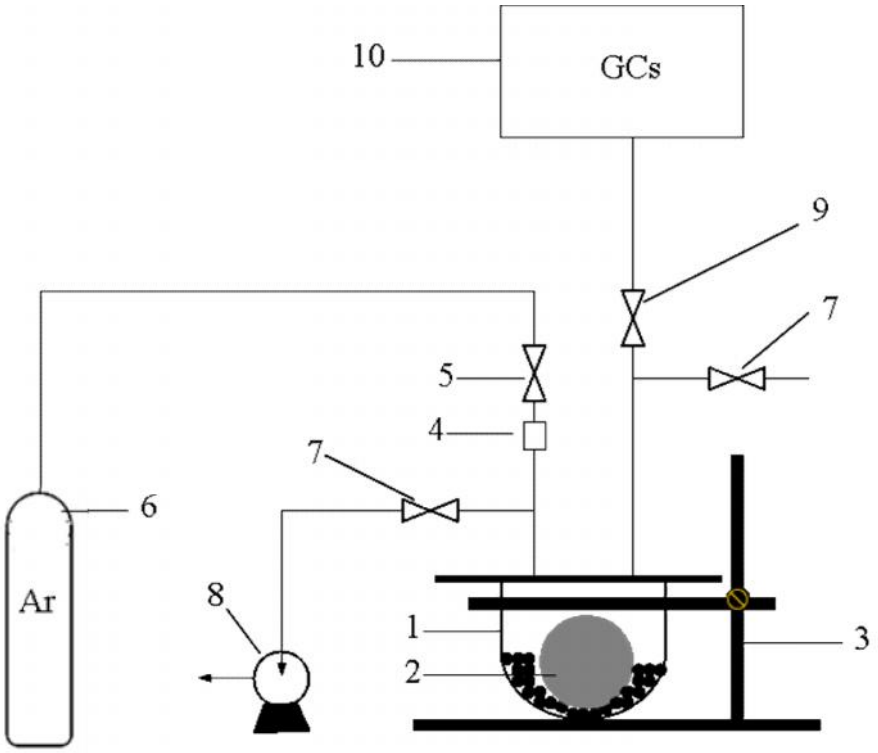

Figure 3- 5: Schematic diagram of gas sampling system used to collect and analyse the gas locked inside ash cenosphere particles: (1) Steel chamber, (2) Steel ball, (3) Bench, (4) Mass flow controller, (5) Inlet valve, (6) Argon gas cylinder, (7) Bypass valve, (8) Vacuum pump, (9) Outlet valve, (10) Two Perkin-Elmer gas chromatography (GCs).

3.4.4 Scanning Electron Microscopy Equipped with Energy Dispersive Spectroscopy (SEM-EDS)

A JEOL 6400 SEM was used to image the cross-sections of various size fractions of ash cenospheres from coal combustion. The ash cenosphere samples were fine polished using the method in a recent work from our research group.[19] ImageTool software was applied to examine the diameter and wall thickness of individual ash cenosphere particles presented in the SEM images. An Oxford EDS detector equipped with SEM was employed to quantify the chemical compositions of individual ash cenosphere particles with a single-ring structure (operation conditions: accelerating potential: 15 KV; sample current: 5 nA). To well represent the properties of ash cenosphere particles in each size fractions, ~100 cenosphere particles from each size fractions were analysed point-by-point. For each cenosphere

particles, approximate 3 individual dot analyses were conducted to reveal the homogeneity of ash cenosphere particles.

A Zeiss Evo 40XVP SEM was employed to examine the morphology of ash particles collected in the cyclone from pyrite combustion, including bulk ash samples and their various size fractions. Additionally, ash particles were also cross-sectioned for SEM examination of morphology and structure. The equipped EDS X-ray detector also analysed chemical compositions of cross-sectioned ash particles quantitatively and size-fractioned ash particles qualitatively.

For PM_{10} samples collected from pyrite combustion, a Zeiss Neon 40EsB focused ion beam scanning electron microscope (FIBSEM) was used to image the selected PM samples. This FIBSEM has a field emission electron gun providing high brightness and high resolution (0.8 nm achieved) therefore being suitable for imaging PM.

3.4.5 Estimation of Fluid Temperature, Viscosity and Surface Tension of Ash Cenosphere Precursors

Based on the chemical compositions of individual ash cenospheres detected by EDS (see Section 3.4.4), fluid temperature of individual ash cenospheres was calculated by the empirical formulas developed by Winegartner and Rhodes[165], as shown below:

$$T\left(^{o}\mathrm{C}\right)=\left[\begin{array}{c} 2449.3-42.35*Na_2O+405.28*Na_2O*0.3+0.1378*\left(CaO\right)^2 \\ -420.63*\left(\left(Na_2O*0.3\right)^2\right)-0.1076*SiO_2*FeO \\ +0.1248*SiO_2*Al_2O_3-0.1355*SiO_2*CaO \\ +0.4348*FeO*Al_2O_3-21.45*\left(\%Base\right)+0.9046*\left(\%Base\right)^2 \\ -1695.21*\left(Base/Acid\right)+96.69*\left(Base/Acid-1\right)^2 \\ +36.36*\left(Base/Acid\right)*Na_2O+296.13*ABS\left(Base/Acid-1\right) \\ +238.55*Dolomiteratio \end{array}\right]/1.8 \quad (3.1)$$

The calculation is based on mole% of the stated oxides shown in the equation.

Where: $\left(\%Base\right)=K_2O+Na_2O+MgO+CaO+FeO$ (mole%)

$$(\%Base) = 100 - (\%Acid)$$

$$Dolomiteratio = (MgO + CaO)/(MgO + FeO + CaO + Na_2O + K_2O) \quad (\text{wt\%})$$

Surface tension ($\pm$) of individual molten cenosphere precursor was estimated according to the following expression:[166]

$$\pm(at\,1400^oC) = 3.24 * SiO_2 + 5.85 * Al_2O_3 + 4.4 * Fe_2O_3 + 4.92 * CaO + 5.49MgO + 1.12 * Na_2O - 0.75 * K_2O \quad (\text{dyne/cm}) \qquad (3.2)$$

A temperature coefficient of -0.017 dyne/cm (°C) is applicable for the calculation.

Viscosity (η) of individual molten cenosphere precursor was determined using a so-called 'modified Urbain Model'[167] due to this model was found to be suitable for ash melts with higher SiO_2 and lower Fe as present samples. The calculation follows the equation below at a given temperature T in degrees K:

$$\ln[\eta] = \ln[A] + \ln[T] + (1000 * B/T) \quad (\text{poise}) \qquad (3.3)$$

As suggested in the literature[166], the calculation steps include:

- Determining the mole fraction of all components based on chemical oxide composition. Fe_2O_3 is converted to equivalent FeO.
- $M = CaO + MgO + Na_2O + K_2O + FeO + 2 * TiO_2$ (mole fractions)
- $\sim = M/(M + Al_2O_3)$ (mole fractions)
- $B = B0 + B1 * SiO_2 + B2 * (SiO_2)^2 + B3 * (SiO_2)^3$

  Where: $B0 = 13.8 + 39.9355 * \sim - 44.049 * (\sim^2)$

  $B1 = 30.481 - 117.1505 * \sim + 129.9978 * (\sim^2)$

  $B2 = -40.9429 + 234.0486 * \sim - 300.04 * (\sim^2)$

  $B3 = 60.7619 - 153.9276 * \sim + 211.1616 * (\sim^2)$
- $\ln[A] = -(0.2812 * B + 11.8279)$

3.4.6 Mass-based Size Distribution of Ash Particles in the Cyclone

Ash particles collected in the cyclone during all the experiments of pyrite combustion were sieved into 7 different size fractions (<45, 45−53, 53−75, 75−90, 90−106, 106−125, and >125 μm). The size-fractioned ash cenosphere samples were then weighed using a balance with accuracy 1 mg to obtain the mass-based particle size distribution of ash cenospheres in the cyclone.

3.4.7 Mass-based Size Distribution of PM_{10}

PM_{10} samples from each DLPI stage were weighed using a microbalance (Mettler MX5, accuracy: 0.001 mg) to obtain the mass-based size distribution of PM_{10}.

3.4.8 Quantification of Fe and Minor Impurity Species

Quantification of inorganic species (dominantly Fe and minor impurities) in various narrow size fractions of ash samples collected in the cyclone during pyrite combustion follows a method used previously[161]. This method was based on Australian Standard AS 1038.14.1-2003, including procedures of borate fusion and acid digestion. Briefly, 1-3 mg of ash samples were fused with the X-ray flux (50% lithium tetraborate and 50% lithium metraborate) at an ash/flux ratio of 1:30 in a muffle furnace at 950 °C for 2 hours. The fusion bead was then dissolved in dilute nitric acid (10% V/V) to prepare a solution for subsequent quantification of inorganic species via a Varian Vista Axial CCD Simultaneous ICP-AES.

3.4.9 Quantification of S

Quantification of S in various narrow size fractions of ash samples collected in the cyclone during pyrite combustion follows the Eschka method as detailed in Australian Standard AS 1038.6.3.1-1997.

In brief, 0.5−1 mg of ash was mixed intimately with the Eschka mixture at an ash/Eschka mixture ratio of 1:30 in a Pt crucible, followed by a layer of ~50 mg of the Eschka mixture covered on the top of the ash mixture. The sample was then left in a muffle furnace at 800 °C for 8 hours under an oxidizing atmosphere to convert all sulphur to sulphate. The sulphate was then completely dissolved into Milli-Q water for sulphur quantification using Dionex ICS-1100 IC, which is equipped with

an AS22 analytical column and uses 2.25 mM Na_2CO_3/0.7 mM $NaHCO_3$ solution as an eluent.

In separate analyses, ash samples were also directly extracted by Milli-Q water to leach sulphate ions (if any) into the solutions. The resultant solutions were then analysed via the same procedure using IC to check whether sulphate is possibly formed during pyrite combustion under the various conditions.

3.4.10 X-ray Diffraction Spectroscopy (XRD)

A Bruker-AXS D8 advance type XRD spectroscopy was employed to characterise the mineralogy of ashes collected in the cyclone during pyrite combustion. The analyses were performed via Cu radiation and a LynxEye position sensitive detector in a 2θ range from 5° to 70°. Analytical software Jade 6 was used to identify the mineral phases of the ash cenospheres.

3.5 Summary

Ash cenospheres from a coal-fired power station were sieved into various narrow size fractions for characterisation to understand the possible formation mechanisms of ash cenospheres. Analytical and instrumental analyses were employed on the ash cenospheres of various size fractions, including thermal behaviour analysis by TMA, examining gas composition locked inside cenosphere particles by GCs, and structure and chemical composition analysis by SEM-EDS. Based on these data, fluid temperature, viscosity and surface tension of ash cenospheres were also calculated to investigate the formation of ash cenospheres during coal combustion.

A systematic experimental program was also designed in present study to understand the formation and behaviour of ash cenospheres during solid fuels combustion using high-purity pyrite as the model fuel. The raw pyrite was wet-sieved to a nominal size fraction of 38–45 µm as the pyrite sample for the combustion experiments in DTF under various well-designed conditions. Ash particles with aerodynamic diameter > 10 µm collected by cyclone were sieved into seven size fractions for characterisation. Ash particles with aerodynamic diameter < 10 µm (PM_{10}) were size-segregated and collected by DLPI. The bulk ash particles collected in cyclone and their different size fractions, and PM_{10} were characterised via various analytical techniques and

instrumental analyses, including SEM-EDS, XRD, PSDs, and quantification of Fe, S and other minor impurities via fusion procedure and ICP-AES/IC analysis.

CHAPTER 4 POSSIBLE FORMATION MECHANISMS OF ASH CENOSPHERES FROM A COAL-FIRED POWER STATION

4.1 Introduction

As shown in literature review, the fundamental mechanism of ash cenosphere formation it still largely unclear. The formation of ash cenosphere requires a source of gas trapped inside molten ash droplets which expand and resolidify to form the hollow particles. There are still debates on the sources of gas enclosed within the molten ash droplets. One possibility is that the flue gas in the boiler is trapped by the molten ash droplets in the high temperature zone.[54] The other is the gas products generated within the molten ash droplets, which are unable to escape out of the highly viscous droplets and inflate the droplets to be hollow spheres.[14, 15, 18-22, 24, 52, 79, 82, 83] The formation of an ash cenosphere is also largely dependent on the melting properties of the precursor ash particle and the viscosity and surface tension of molten ash droplets formed.

Continuing the previous work of the same group,[19] this chapter is focused on the characterization of ash cenospheres collected from coal-fired power stations using a series of analytical methods. An ash cenosphere sample was collected from an Australian power station that is known to produce high yield of ash cenospheres. The ash cenosphere sample was sieved into a series of narrow size fractions (45−63, 63−75, 75−90, 90−106, 106−125, 125−150, and 150−250 μm).

The size-fractioned ash cenosphere samples were ground into powder and then subject to thermomechanical analysis (TMA) analysis. To understand the gas locked inside ash cenosphere samples of various size fractions, a device was designed and fabricated to enable the release of the gas for composition analysis via a gas chromatography (GC). Based on a novel characterization technique developed by the same group[19], the true cenosphere size and wall thickness were then determined for

ash cenospheres on a particle-by-particle basis. Additionally, the quantification of chemical compositions of individual cenosphere particles was achieved, via scanning electron microscope equipped with quantitative energy dispersive X-ray analyzer (SEM-EDS).

Based on these detailed info for a single particle, it is therefore possible to estimate the fluid temperature, viscosity and surface tension of individual molten ash precursor droplets. Considering the gas compositions and pressure measured, this chapter aims to provide an insightful understanding the characteristics of ash cenosphere samples and the possible formation mechanisms of these ash cenospheres.

4.2 Chemistry of Ash Cenospheres of Various Size Fractions

The previous study[19] of the same group studied the chemistry of three different size fractions (<25 μm, 63–75 μm and 125–150 μm) of ash cenosphere separated from the fly ash via sink-float method using water as the media. The fly ash was dry collected after the electric-static-precipitator (ESP) of an Australian power station. It was found that the smaller ash cenospheres have a high SiO_2/Al_2O_3 ratio.

This study continues our previous work and carries out a detailed study. In this case, a batch of ash cenosphere sample was collected from the ash lagoon. To remove any non-cenosphere particles mistakenly collected, in the laboratory, the ash cenosphere sample was then dispersed in distilled water at an ash/distilled water ratio of 1:20 at room temperature, followed by continuous stirring and settling for 24 hours. The float ash samples were then collected as ash cenospheres, which were further heated to 850 °C under an oxidizing atmosphere in a muffle furnace to remove unburnt carbon.

The ash cenospheres after heat treatment were sieved into 7 continuous size fractions (45-63, 63-75, 75-90, 90-106, 106-125, 125-150, and 150-250 μm) as the samples for the characterization in Chapter 4. The chemical compositions of these size-fractioned ash cenospheres were then analysed by XRF. The data are presented in Table 4-1. There are several important observations can be made from the data:

(a) In agree with the previous study,[19] the SiO_2/Al_2O_3 ratio indeed decreases with increasing ash cenosphere size, from 1.96 for 45-63 µm to 1.64 for 150-250 µm, as shown in Figure 4-1a.

(b) For every size fraction of ash cenospheres, the ash chemistry is dominantly SiO_2, Al_2O_3, TiO_2 and Fe_2O_3, which make up >99.3 wt% of the total ash chemical compositions. While the Fe_2O_3 contents are generally low (<0.5%), the contents of TiO_2 are generally high (1.25 – 1.45%) for all size fractions.

(c) Furthermore, it is also interesting to see that the sum of TiO_2 and Fe_2O_3 increases with ash cenosphere size, from 1.70% for 45–63 µm to 1.95% for 150–250 µm, as shown in Figure 4-1b.

The previous work by Raask[20] suggested that sufficient amount of (>5%) ferric oxide (Fe_2O_3) is essential to ash cenosphere formation, as it provides the required source of oxygen for gas generation inside the molten silicate particles for expansion. For ash cenospheres in Table 4-1, the content of iron oxide in the bulk ash cenosphere chemistry is very low (<0.5%). The results appear to suggest that TiO_2 may play an important role in ash cenosphere formation in this case.

Table 4-1: Chemical compositions of different size fractions of ash cenospheres (wt%)

	size fractions (µm)						
	45-63	63-75	75-90	90-106	106-125	125-150	150-250
SiO_2	64.66	64.11	63.51	62.49	61.45	61.19	60.44
Al_2O_3	33.03	33.53	34.04	35.06	36.05	36.23	36.88
TiO_2	1.25	1.28	1.33	1.38	1.45	1.43	1.42
Fe_2O_3	0.45	0.46	0.47	0.46	0.46	0.51	0.53
CaO	0.06	0.06	0.06	0.05	0.05	0.05	0.06
MgO	0.14	0.15	0.19	0.15	0.15	0.16	0.16
Na_2O	0.05	0.05	0.05	0.05	0.04	0.04	0.06
K_2O	0.36	0.36	0.35	0.35	0.35	0.38	0.47
$SiO_2+Al_2O_3+TiO_2+Fe_2O_3$	99.39	99.38	99.35	99.39	99.42	99.36	99.27

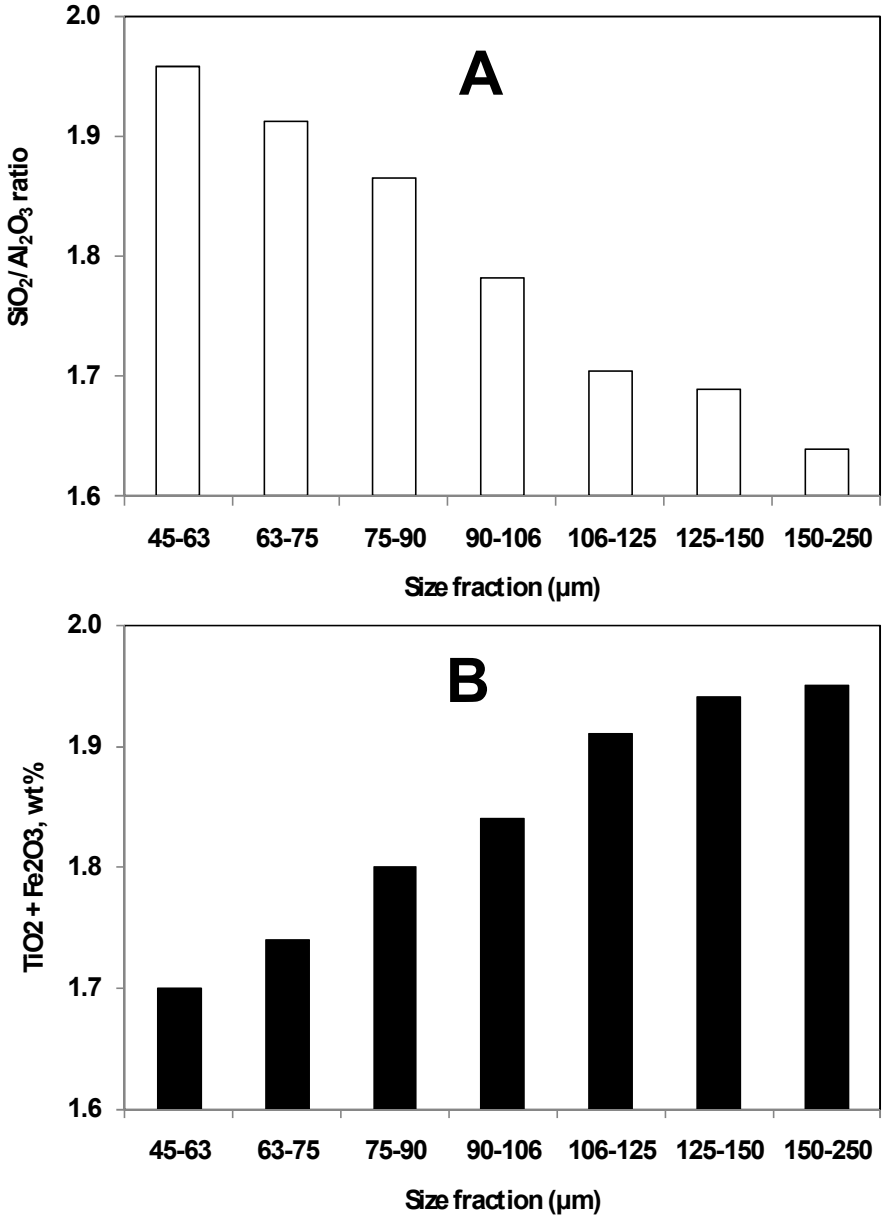

Figure 4-1: SiO_2/Al_2O_3 ratio and (TiO_2+Al_2O_3) content of ash cenospheres as a function of size fraction

4.3 Gas Locked in Ash Cenosphere of Various Size Fractions

Previous studies[15, 20, 21, 84] investigated the compositions of gas products locked in ash cenosphere samples, however focusing on only the bulk ash cenosphere. In this work, using the device designed in this study (see Section 3.4.3 of Chapter 3), a series of work was carried out to study the compositions of gas within ash cenospheres of various size fractions. Briefly, an ash cenosphere sample (of a particular size fraction) was loaded in the chamber of the device, which was then vacuumed for three times

with argon purging to remove all residue air in the chamber. The ash cenosphere sample was then crushed to release the gases locked inside these ash cenospheres. The released gas products were then collected and analysed using two GCs.

The results are presented in Table 4-2 for the composition of gas locked within ash cenosphere particles of different size fractions. As narrow size fractions are used, the data in Table 4-2 also enable the estimation of the volume of gas locked in an average individual ash cenosphere particle in a particular size fraction, and the calculation of the average gas pressure inside the individual cenosphere particle following the Ideal Gas Law. Several interesting observations can be made from the data in Table 4-2.

(a) The results indicate that gases trapped inside the ash cenosphere particles are mainly CO_2 and N_2, with trace amount of CO (the concentrations were very low but appreciable in the GC chromatograms). This is in agreement with the observations in previous studies.[15, 20, 21, 84] In this case, typically, above 75 % of the gases locked inside ash cenospheres are CO_2.

(b) For various size fractions of ash cenospheres, the average internal pressure of ash cenosphere particles is between 0.17 and 0.24 atm. This is also broadly in agreement with previous studies on bulk ash cenospheres,[20, 21] indicating that the survival of ash cenospheres needs to overcome the significant pressure force exerting on the shell during rapid cooling process.

(c) Most importantly, the data in Table 4-2 clearly show that the pressure and volume of CO_2 and N_2 are strongly dependent on ash cenosphere size. The volume (at NTP) of gas products (CO_2 and N_2, total and individual) increases significantly with ash cenosphere size. Overall, the average internal gas pressure gradually decreases with ash cenosphere size. The results are interesting as it clearly indicate that more gaseous products are required for the formation of larger ash cenospheres. This is obvious and expected.

Table 4-2: Compositions, internal pressure and average volume of gas inside individual cenosphere particle of different size fractions

Size Fraction (µm)	Pressure at 20 °C (atm)	Volume of gas at NTP ($1*10^{-11}$ mol/particle)	
		CO_2	N_2
63-75	0.227	0.086	0.002
75-90	0.239	0.139	0.017
90-106	0.217	0.209	0.033
106-125	0.222	0.333	0.071
125-150	0.183	0.461	0.100
150-250	0.172	1.067	0.349

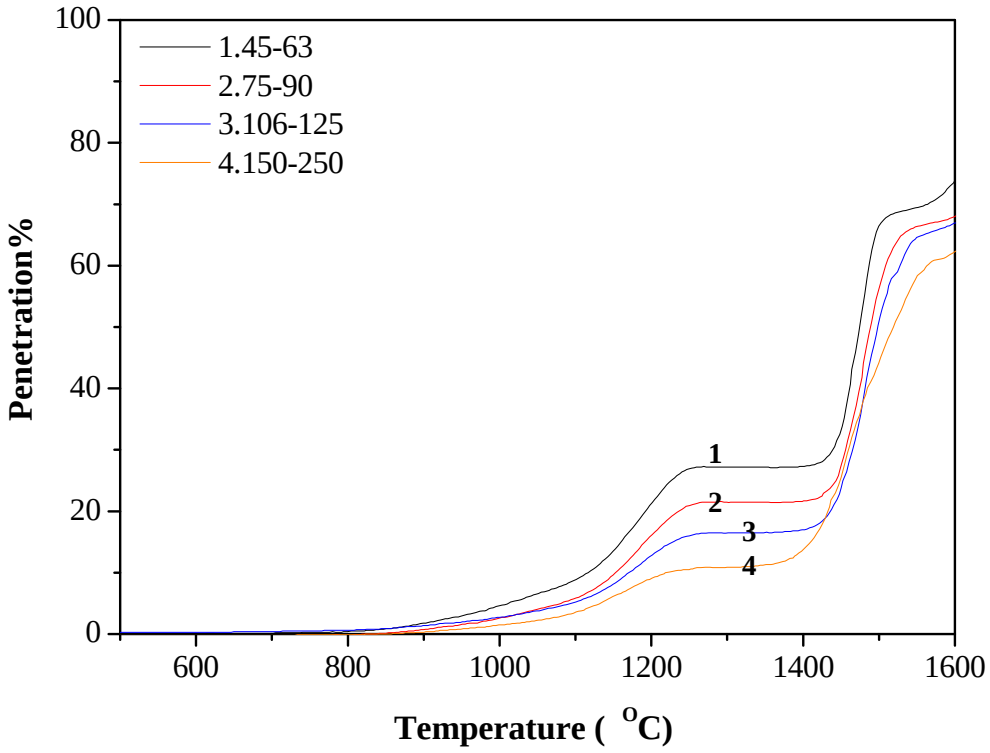

Figure 4-2: TMA results of various size fractions of ash cenospheres.

Table 4-3: Fusibility temperatures (°C) derived from TMA analysis on ash cenospheres with different size fractions.

Size Fraction (μm)	T25	T50	T75
45-63	1223	1473	1545
75-90	1439	1487	1545
106-125	1452	1496	1544
150-250	1446	1519	1545

4.4 Fusion Characteristics of Ash Cenosphere Size Fractions

Further work was then done to investigate the fusion behaviour of four different size fractions of ash cenospheres (45-63, 75-90, 106-125, and 125-150 μm) using a TMA. The detailed procedure for the TMA measurement can be seen in Section 3.4.2 of Chapter 3. During TMA analysis, the ash cenospheres would experience sintering and melting process. To minimise the effect of ash cenosphere collapse on TMA measurement, the ash cenosphere samples were finely ground before subject to TMA measurement. Therefore, the TMA results represent the true fusion behaviour of the ash materials forming the ash cenospheres.

The results are presented in Figure 4-2, as the ram penetration into samples (Penetration%) expressed as a function of temperature. In addition, the penetration levels (denoted as T (P%)) of 25%, 50%, 75%, and 90% can indicate the characteristic temperatures of the onset of melting T25, intermediate melting T50, complete melting T75, and slag flow T90, respectively. To help understand the thermal behaviours of ash cenospheres, these characteristic temperatures represented the fusibility properties of ash cenospheres with different size fractions are presented in Table 4-3. The results in Figure 4-2 and Table 4-3 lead to several important observations:

(a) First, as shown in Figure 4-2, there is no obvious penetration observed at temperatures below 800 °C. It should also be noted that the proposed exothermic effect at temperatures between 260 and 600 °C in the previous studies[22, 58] did not take place in present study, because the ash cenosphere samples used in this study

were already treated in a furnace for removing unburnt carbon before TMA measurement.

(b) Generally, the TMA traces of ash cenospheres with different narrow size fractions follow the same trend and show two major thermal events. One is the gradual penetration observed at lower temperatures of 800 – 1250 °C. The published analytical results indicated that the phase-mineral compositions of ash cenospheres from coal-fired power stations generally include aluminosilicate glass, mullite and quartz.[17, 20, 41, 44, 46, 50, 55] Therefore, it is believed that the low temperature penetration of ash cenospheres may be attributed to the agglomeration, softening, and/or sintering of the silicate/aluminosilicate glass. The other thermal event is the extremely rapid displacement of ram penetration at temperatures above ~ 1410 °C after a stable stage of the traces. It is related to the melting of the amorphous phases of the ash cenospheres during TMA measurement.

(c) The fusion characteristics of ash cenospheres are obviously dependent on particle size of ash cenosphere. The samples of smaller ash cenosphere fractions favour higher percentages of penetration at a given temperature. For example, at the end of the first thermal events at ~1250 °C, the percentage of penetration is ~ 27 % for the ash cenospheres of size fraction 45-63 µm, which decreases to ~10 % for ash cenospheres of size fraction 150-250 µm.

(d) The differences in the fusion characteristics of various size-fractioned ash cenospheres are clearly reflected in the characteristic temperatures of different size-fractioned ash cenospheres (see Table 4-3). For example, the smallest ash cenospheres start melting at ~1223 °C, considerably lower than those of larger ash cenospheres (1452 °C and 1446 °C for the size fractions of 106-125 µm and 150–250 µm, respectively). Similar observations can also be made for the intermediate melting temperatures. However, it is noteworthy that the temperature interval between the initial and intermediate melting temperatures is 250 °C for the size fraction 45-63 µm, much higher than those (only ~ 44-73 °C) for other size fractions. While there are differences in the thermal behaviour of various size fractions, all ash cenosphere samples complete melting at a similar temperature (1545 °C). The fusion behaviours of ash cenospheres with different size fractions are supported by the

chemistry data in Table 4-1, which clearly indicates that SiO_2/Al_2O_3 ratio of ash cenospheres decreases with the increase of ash cenospheres size.

(e) Figure 4-2 shows that all the ash cenosphere samples with different size fractions cannot achieve 100 % penetration even at 1600 °C, which is the end temperature limited by the TMA instrument. It is clear that the ash cenosphere samples are not completely molten at 1600 °C, therefore impossible to be produced at temperatures below 1600 °C.

4.5 Chemistry, Size and Wall Thickness of Individual Ash Cenosphere Particles

Chemical compositions of individual ash cenospheres with a single-ring structure were quantified by SEM-EDS. Generally, the results show that SiO_2, Al_2O_3 , TiO_2 and Fe_2O_3 dominate the ash chemistry of individual cenospheres in all size fractions. On the basis of chemical compositions of individual ash cenospheres, the significant parameters, including fluid temperature, viscosity and surface tension, of the cenosphere precursors are estimated by empirical correlations.[165-167] The details of these empirical correlations used are given in Section 3.4.5.

The results are presented in Figure 4-3 and Figure 4-4. As shown in Figure 4-3, the individual ash cenospheres with various diameters and wall thickness have a wide range of fluid temperatures. However, the fluid temperature is generally higher than ~1640 °C and limited to ~ 1800 °C. The results are in good agreement with the TMA results which indicate the ash cenosphere samples could not reach completely molten at 1600 °C. The calculated fluid temperature of individual ash cenospheres clearly shows that the particle temperature needs to be > ~1640 °C in order to enabling the formation of ash cenosphere samples. The results also clearly suggest that each ash particles may experience different temperature-time history during coal combustion, which would consequently influence the formation of ash cenospheres hence the sizes and structures of ash cenospheres formed.

Figure 4−4 presents the viscosity and surface tension of cenosphere precursors at the lowest fluid temperature 1640 °C. It is known that, if gas evolution is very rapid during molten ash droplets expansion, the growth of molten ash cenosphere precursor will be controlled by the viscous relaxation according to the relationship shown in Equation 2.3 of Chapter 2. It is clear that, the viscosity ¦ and surface

tension ± of the molten ash droplets determine the growth of ash droplets and thus the survival of ash cenospheres. Literature generally proposed that the molten ash droplets should have relatively high viscosity and surface tension. The result from Figure 4-4 shows that the individual molten ash droplets even with similar sizes present a variety of fluid properties. The viscosity of molten ash droplets widely ranges from ~ 1 to 3.5 (log10 poise) while surface tension from ~ 350 to 450 dyne/cm. The vast variations existed in the fluid properties of molten ash droplets will inevitably induce their different growth processes, accordingly resulting in the formation of ash cenospheres with various wall thicknesses. Figure 4-4 also indicates that, the viscosity of molten ash droplets is generally inversely proportional to the surface tension. It was generally suggested in the literature that during ash cenosphere formation, the precursor droplets should have relatively high viscosity. However, the present results clearly demonstrates that the molten ash droplets may have relatively low viscosity during ash cenospheres formation, as long as the force of surface tension of the precursor is high enough to be able to hold the high intrinsic pressure caused by the rapid expanding gas bubble.

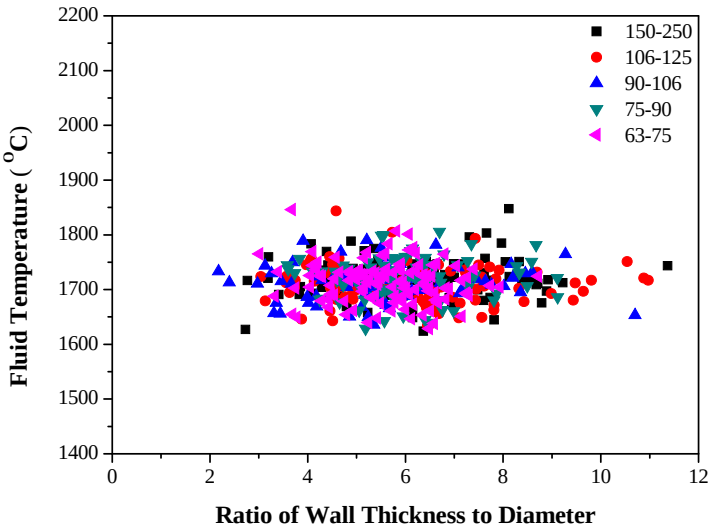

Figure 4-3: Fluid temperature of individual cenosphere particles with a function of wall thickness to diameter ratio.

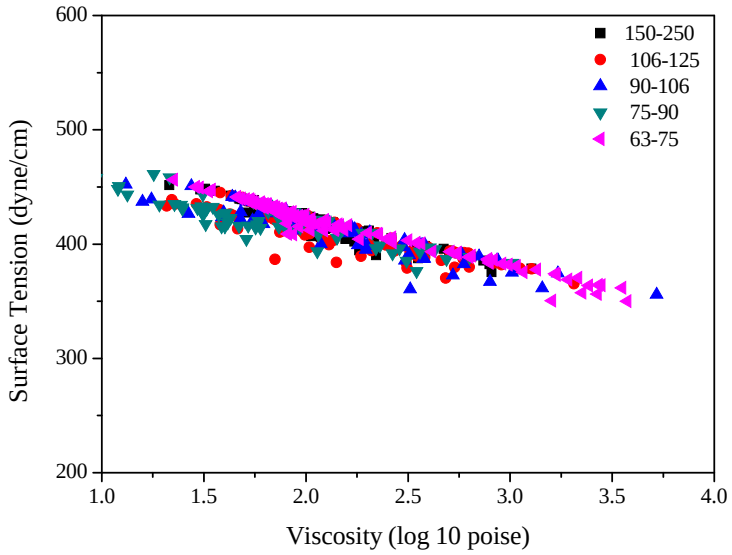

Figure 4-4: Correlation of viscosity with surface tension of ash cenosphere precursors at fluid temperature of 1640 °C.

4.6 Mechanisms of Ash Cenosphere Formation

In the literature, there have been two possibilities speculated for the sources of gases enclosed inside the ash cenospheres, as summarized in the Subsection 2.2.3.2 of Chapter 2. The first is the flue gas in the boiler and the second is gas products produced within molten ash droplets. The data in this study provide important insights into the source of gas responsible for ash cenosphere formation. If flue gas is the one as the expanding medium for ash cenosphere formation, N_2 should be the dominant gas locked in ash cenospheres. However, this is in contradictory to the data in Table 4-2 which clearly show that CO_2 is the major gas in the ash cenosphere samples. Therefore, the first possibility is not the dominant mechanism.

However, there are appreciable N_2 in the gas products locked in ash cenospheres of large sizes (e.g. 150–250 µm) (see Table 4-2). The mechanisms for the origin of N_2 inside ash cenospheres are largely unknown, although Raask[20] suggested that N_2 might be formed due to silicon nitride reacted with ferric oxide. Regarding to the possible origin of gases generated within molten ash droplets, Raask[20] proposed the possible reactions responsible for CO_2 generation as following:

$$2\ Fe_2O_3 + C = 4\ FeO + CO_2 \quad (4.1)$$

This hypothesis is reasonable when there is sufficient Fe in the composition. Such reactions are also likely to proceed because as aforementioned, the formation temperature for the ash cenosphere samples is >1640 °C. Also, while it is difficult to directly provide experimental evidence on the presence of dispersed carbon in the precursor particles, the presence of CO_2 does indicate that there must be a source of carbon to enable the process. However, Table 4-1 shows that there are < 0.53 % of iron oxides in the chemical compositions of ash cenosphere. Such a low amount of iron oxides is not likely to be sufficient to generate required amount of CO_2 for ash cenosphere formation.

The other possible explanation for CO_2 generation inside molten ash droplets is that titanium dioxide provides the oxygen source and could be reduced by the dispersed carbon at temperature >1550 °C to release CO_2 by the following reaction:

$$4TiO_2 + C = 2Ti_2O_3 + CO_2 \quad (4.2)$$

This is possible because each different size fraction of ash cenosphere samples contains average TiO_2 contents of 1.25 – 1.42 wt%. A combination of Fe_2O_3 and TiO_2 is more likely to generate sufficient amount of gas inside the molten ash droplets for ash cenosphere formation. There may also possibly be other mechanisms governing the ash cenosphere formation and clearly further investigation is required.

4.7 Conclusions

This chapter is to further understand the formation mechanism of ash cenospheres formed from pulverized-coal combustion. Ash cenospheres in the fly ash from an Australian power station were sieved into a series of narrow size fractions and characterized by various analytical methods. The main conclusions are drawn as follows:

(1) Thermomechanical analysis shows that ash cenospheres of different size fractions do not melt at 1600 °C, suggesting that these ash cenospheres from coal-fired power station are impossible to be formed at temperatures <1600 °C.

(2) The chemistry of ash cenospheres of various size fractions indicate that SiO_2/Al_2O_3 ratio decreases with increasing ash cenosphere size, accompanied with an increase in the sum of TiO_2 and Fe_2O_3 contents (i.e. $TiO_2+Fe_2O_3$).

(3) The gas products locked inside ash cenospheres of all size fractions are dominantly CO_2 and some N_2. The average gas pressure decreases from 0.227 atm to 0.172 atm (NTP) as particle size increases from 63-75 µm to 150-250 µm.

(4) The characteristics of molten ash cenosphere precursors derived from the ash chemistry of individual cenospheres indicate that the optimum particle temperature for cenosphere formation is from ~ 1640 to 1800 °C. Under these conditions, molten ash droplets can be formed and trap a certain amount of gas generated within the ash droplets.

(5) The wide range of viscosity of molten cenosphere precursors together with the force of surface tension, which is demonstrated to be inversely proportional to the viscosity of molten droplets, governs the growth of cenosphere precursors and producing ash cenospheres with various wall thicknesses.

(6) In addition to Fe_2O_3, the data also appear to suggest that TiO_2 may play a role in ash cenosphere formation.

CHAPTER 5 FORMATION MECHANISM OF ASH CENOSPHERE FROM THE COMBUSTION USING PULVERISED PYRITE AS A MODEL FUEL

5.1 Introduction

Chapter 4 characterises the properties of ash cenospheres collected from a coal-fired power station for the understanding of possible formation mechanisms of ash cenospheres during coal combustion. The results suggest that SiO_2/Al_2O_3 ratios of the cenosphere samples of various size fractions decrease with the increase of ash cenosphere size, accompanied with an increase in the sum of TiO_2 and Fe_2O_3 contents. The data of thermomechanical analysis indicate that these ash cenospheres from the coal-fired power station are impossible to be formed at temperatures < 1600 °C. Indeed, the optimum particle temperature for the formation of these ash cenospheres is from ~ 1640 to 1800 °C, as indicated by the characteristics of molten cenosphere precursors.

The results in Chapter 4 also present that the gas products locked inside the ash cenospheres of all size fractions are dominantly CO_2 and some N_2, originated from thermochemical processing within molten ash droplets formed during coal combustion. The molten ash droplets can trap a certain amount of the gas products generated within the droplets as cenosphere precursors and grow in the governance of wide range of viscosity of molten cenosphere precursors together with the force of surface tension, producing ash cenospheres with various wall thicknesses. However, the origin of gas inside the ash cenospheres is not completely clear, leading to the fundamental formation mechanism of ash cenospheres unclear, mainly due to the difficulty of linking the formation (and properties) of ash cenospheres with the individual minerals in parent coal. This therefore necessitates further and systematic investigation on the formation of ash cenospheres during solid fuels combustion.

Clearly, it is desirable to design an experimental program to fundamentally investigate the formation mechanism and behaviour of ash cenosphere during

combustion using a fuel, which should only contain simple mineral and can produce ash cenospheres during combustion. A good fuel option is pyrite (FeS_2), which is an iron-bearing mineral widely present in coal. Previous research efforts were mainly focused on chemical reactions, kinetics and modelling of pyrite transformation during combustion,[21, 32, 33, 91, 105, 106, 168] some of which[32, 33] reported the observation of ash cenosphere formation. Unfortunately, those studies[32, 33] were not focused on ash cenosphere formation mechanism and only concerned with pyrite combustions at temperatures > 1100 °C. From the point view of ash cenosphere formation, it is unknown under which conditions ash cenospheres can be formed during pulverised pyrite combustion. Most importantly, it is still not well understood on the fundamental mechanism responsible for the formation of ash cenospheres and the behaviour of ash cenosphere during combustion.

Therefore, it is the objective of this chapter to conduct a set of systematic experiments to investigate ash cenosphere formation during the combustion of pulverised pyrite using a laboratory-scale drop-tube furnace under various combustion conditions at temperatures ranging from 530 to 1100 °C. It should be noted that in this study, pyrite is used as a model fuel for studying the fundamental mechanism of ash cenosphere formation during solid fuels combustion. The coarse ash particles with aerodynamic diameter > 10 μm collected by cyclone during pulverized pyrite combustion under the various conditions are the samples of interests to be characterized by a series of analytical methods, corresponding to the second objective outlined in Chapter 2.

5.2 Conditions Required for Ash Cenosphere Formation during Pulverised Pyrite Combustion

Figure 5-1 presents the surface and internal morphology/structure of ash particles produced from pulverised pyrite combustion at furnace temperatures from 530-1100 °C. Ash particles produced at furnace temperatures of 530 °C and 560 °C are of irregular shapes, as shown in panels a-d of Figures 5-1. No melting of ash particles is evidenced, suggesting that under the combustion conditions, the temperature of an oxidising pyrite particle is below its melting point so that softening and/or melting transformation of the oxidising pyrite particle did not take place. The ash samples contain substantial amount of small ash particles, suggesting that pyrite particles

experienced fragmentation during combustion/oxidation under the conditions. There are two possible mechanisms, one is fragmentation as a result of thermal shock when pyrite particles are introduced into hot zone,[169] and the other is fragmentation of the reacting pyrite/pyrrhotite particles as a result of thermal decomposition with sulphur release[106].

As shown in panels e and f of Figures 5-1, as the furnace temperature increases to 580 °C, the morphology of ash particles produced from pyrite combustion is significantly different from that of ash particles produced at lower temperatures. The ash samples contain a mixture of irregular and round (or partially-round) ash particles, suggesting that at least a proportion of the reacting particles experienced softening or partial (even complete) melting during combustion/oxidation under the conditions. In Figure 5-1f, the cross-section of the ash particles clearly shows the presence of scattered hollow ash cenosphere particles in the ash samples, demonstrating that ash cenospheres can indeed possibly be formed at this furnace temperature (580 °C). These hollow ash cenospheres typically have small sizes (20-45 µm in diameter), with shells of thickness 2- 10 µm.

As the furnace temperature further increases to 600 °C, the ash samples contain large round ash particles and ash cenosphere fragments of various sizes (see Figures 5-1g). There are substantial quantities of ash cenospheres produced (see panels g and h of Figures 5-1) with fragments of ash particles that appear to stick to the surface of these large ash cenosphere particles. These ash cenospheres also have rough surfaces, large sizes (up to 130 µm in diameter) and thin shells (1-3 µm).

At furnace temperatures > 600 °C, large ash cenospheres and their fragments are also dominantly present in the ash products collected from pulverised pyrite combustion. Some small cenospheric particles can be also found in the sample. Using the case at 900 °C as an example, panels i and j of Figures 5-1 show that the ash samples contain mainly large ash cenospheres and thin-shell fragments. Compared to ash cenospheres formed from pulverised pyrite combustion at 600 °C, the surface of these large ash cenospheres appear to be smooth.

The formation of ash cenospheres requires that the precursor ash particles must be fully molten during combustion. Figure 5-1 suggests that no such molten precursor

ash particles can be formed during pyrite combustion at temperatures < 580 °C so that no ash cenospheres can be produced. Therefore, 580 °C is the minimal temperature at which molten precursor ash particles can be possibly formed. At 600 °C, most of precursor ash particles are fully molten, leading to the formation of abundant ash cenosphere particles under the conditions.

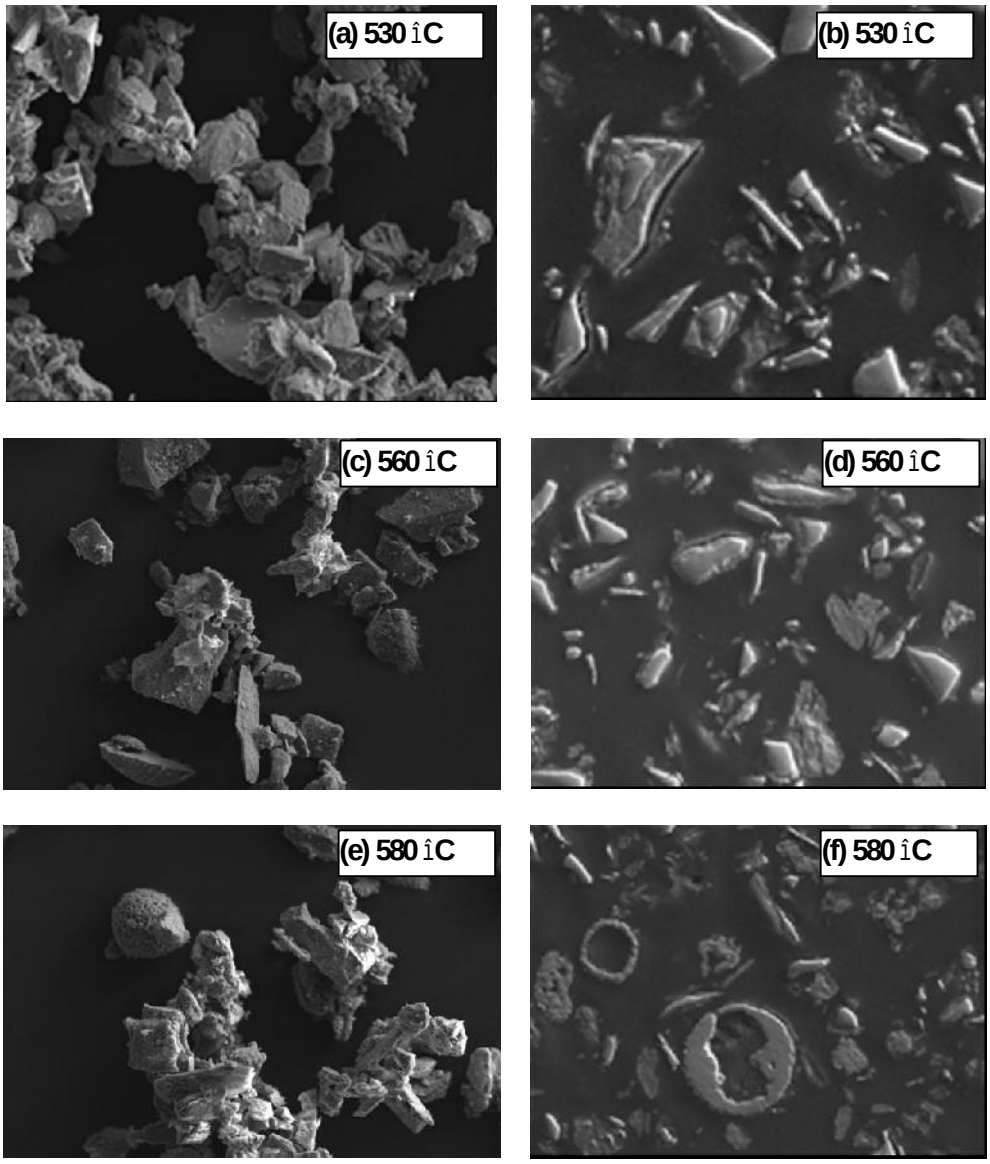

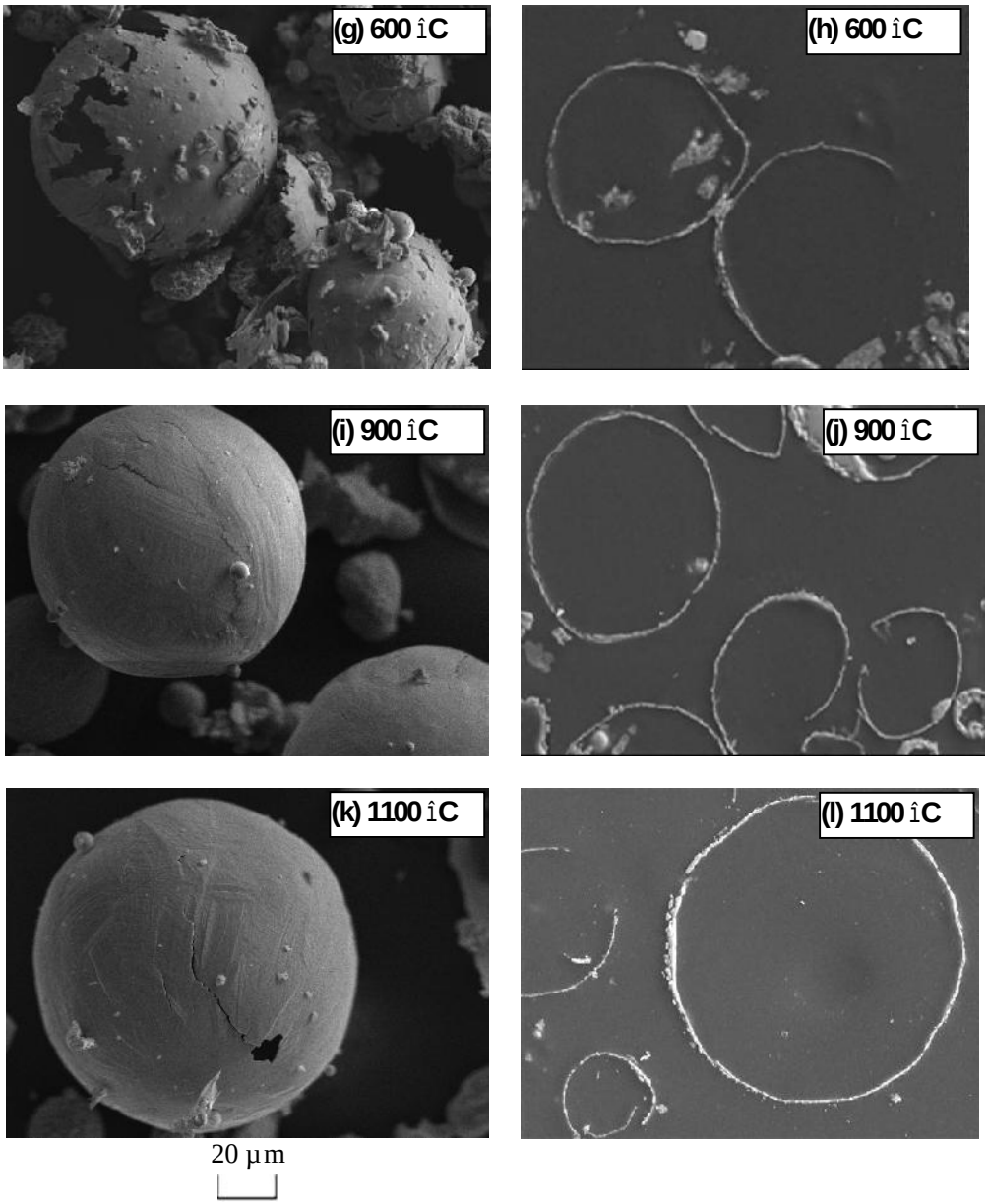

Figure 5-1: SEM images of general morphology and cross-sections of ash particles during pyrite combustion from 530 °C - 1100 °C. The scale bar applies for all the images.

5.3 Mineralogy of Ash and Ash Cenospheres Produced from Pulverised Pyrite Combustion

To further understand the formation mechanism of ash cenospheres during pyrite combustion, the mineralogy of ash particles formed at 530-1100 °C were investigated using XRD. As shown in Figure 5-2a, at 530 °C, the mineral phases in

ash particles are mainly pyrite and iron sulphide (FeS_x). Such observations have two implications. One is that pyrite decomposition has already commenced at 530 °C, leading to the formation of FeS_x. This is in consistence with the conclusion that thermal decomposition of pyrite takes place under the conditions.[103] The other is that such transformation is only partial decomposition and at least part of parent pyrite remains intact without significant thermal decomposition and oxidation. As the sample was collected from combustion conditions, oxidation reactions must have taken place and under the prevailing combustion conditions, pyrite is known to be oxidised to produce iron oxides or iron sulphates.[99, 100, 103] However, only pyrite and iron sulphide peaks are present in the XRD diffractogram in Figure 5-2. Further efforts were then taken to extract the ash samples using Milli-Q water. The IC analysis of the solutions (data not shown) clearly indicates the presence of some iron sulphates in the ash products. It is known that iron sulphates can be formed at temperatures up to 600 °C during pyrite oxidation. Therefore, the absence of iron oxides and sulphates in the XRD diffractogram suggests that these products seem to be amorphous in the samples.

As the furnace temperature increases to 560 °C, magnetite starts to appear in the XRD diffractogram of the ash as shown in Figure 5-2b, although the intensity is low. At 580 °C, the mineral phases in the ash produced are similar. However, the intensity of magnetite in the XRD diffractogram of the ash particles is increased (see Figure 5-2c), accompanying with a significant reduction in the intensity of pyrite and iron sulphide. Therefore, besides extensive decomposition, pyrite and the decomposition products FeS_x were also oxidized to magnetite. As temperature further increases to 600 °C (see Figure 5-2d), pyrite and iron sulphide disappear completely and the dominant mineral phases are iron oxides including magnetite and hematite, indicating that at least part of magnetite was further oxidized to hematite under the combustion conditions. At higher temperatures (e.g. 900 and 1100 °C), the mineralogical phases are dominantly hematite although there is still appreciable magnetite. This suggests that deep oxidation of magnetite did take place but was incomplete, most likely due to the short residence time (~1.1s) of the particles in the DTF.

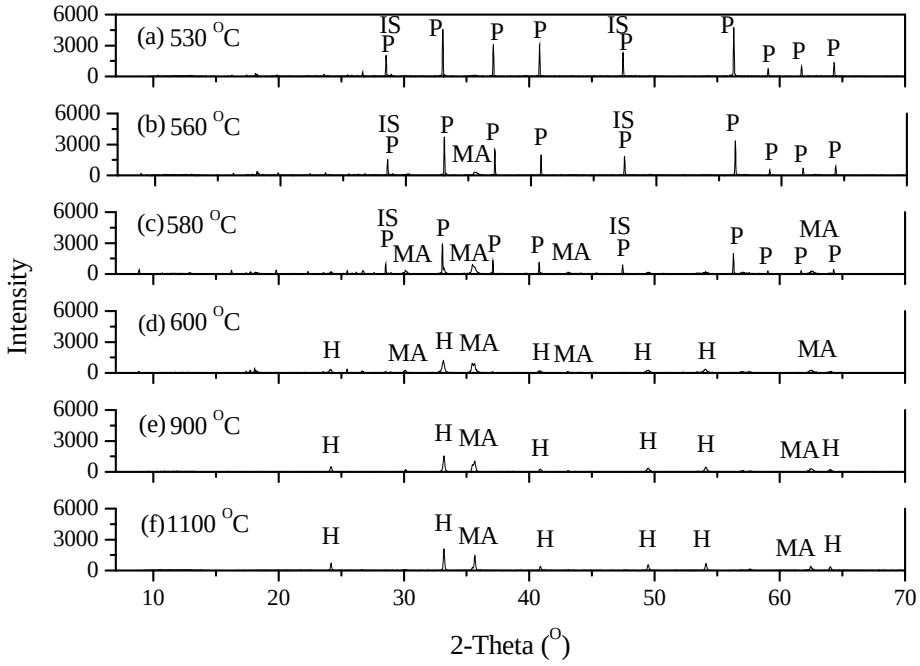

Figure 5-2: XRD patterns of ash particles during pyrite combustion under various temperatures of (a) 530 °C, (b) 560 °C, (c) 580 °C, (d) 600 °C, (e) 900 °C and (f) 1100 °C. Present are peaks for P – Pyrite (FeS_2); IS – iron sulphide (FeSx); MA – magnetite (Fe_3O_4); H – hematite (Fe_2O_3).

5.4 Ash Chemistry of Ash Cenosphere Particles Produced from Pulverised Pyrite Combustion

Figure 5-3 presents the ash chemistry of individual ash particles (including ash cenospheres) produced from pulverised pyrite combustion at various furnace temperatures (530 – 1100 °C) to provide more insights into ash cenosphere formation mechanism. A typical ash particle produced from pyrite combustion at 530 °C is shown in Figure 5-3a. Based on EDS analysis, it can be seen that the pyrite particle is partially-reacted, including a sightly-oxidised pyrite core (Fe:S:O = 1:1.93:0.08, molar ratio) and a porous layer which is partially oxidised. It appears that at 530 °C, pyrite particles decompose to form iron sulphide (FeS_x, $1<x<2$), following the so-called 'unreacted core model',[103] accompanying with slight oxidation under the conditions.

At 560 °C, the slightly-oxidised pyrite core still exists (see Figure 5-3b), having an Fe:S:O molar ratio of 1:1.85:0.11 (see position 1). The particle core near the interface (see position 3) is largely slightly-oxidised pyrite (Fe:S:O = 1:1.83:0.12) while the porous layer near the interface (see position 4) experienced substantial oxidation (Fe:S:O = 1:0.71:0.54), although sulphur has not been completely oxidised. Near the particle surface (see position 2 and position 5), it is evident that sulphur has been almost all oxidised, resulting in Fe:S:O molar ratios of 1:0.06:1.33 and 1:0.09:1.19, close to that of magnetite (Fe:S:O = 1:0.00:1.33). This is consistent with the results reported previously[170] and in agreement with the appearance of magnetite peak in XRD diffractogram (see Figure 5-2b). It however should be noted that although pyrite particles experienced decomposition and oxidation, melting is not evident during combustion under the conditions.

At 580 °C, ash cenosphere particles are typically small (see panels c and d of Figure 5-3). Three important observations can be made from the ash chemistry of these ash cenospheres. Firstly, abundant Fe, S and O are in ash chemistry, suggesting that the ash precursor particle for ash cenosphere formation was fully molten Fe-S-O melt. Secondly, the ash chemistry varies substantially across the shell. Sulphur depletes from the inner to outer surfaces of the shell. For example, for the ash cenosphere with thick shells in Figure 5-3c, the sulphur in the Fe:S:O molar ratio decreases from position 1 (1:0.29:0.78) and position 2 (1:0.38:0.62) near the inner surface of the shell to position 3 (1:0.13:0.73) and position 4 (1:0.07:1.30) near the outer surface of the shell, respectively. For the ash cenosphere with thin shells, the sulphur in the Fe:S:O molar ratio decreases from position 1 (1:1.19:0.81) near the inner surface of the shell to position 2 (1:0.14:1.22) near the outer surface of the shell. It appears that oxidation reactions proceed as oxygen diffuses into the molten Fe-S-O droplets from the outer surface where oxygen is supplied. The ash chemistry of position 4 in Figure 5-3c and position 2 in Figure 5-3d suggests that near the outer surface of shells, sulphur is depleted by oxidation reactions to produce magnetite (Fe:S:O = 1:0.00:1.33). Third, the precursor Fe-S-O melt is already in cenospheric forms, while oxidation reactions have not completely consumed all the sulphur in the precursor particles that solidified to form cenospheres containing abundant sulphur in the shell.

At 600 °C, ash chemistry analysis shows that the large ash cenospheres with thin shells (~1 µm) contain predominantly iron oxides (see Figure 5-3e). However, the ash cenospheres with relative thicker shells (~3 µm) still consist of appreciable sulphur (see Figure 5-3f). The data in panels e and f of Figures 5-3 also show the presence of magnetite (Fe:S:O = 1:0.00:1.33) and/or hematite (Fe:S:O = 1:0.00:1.50). At higher temperatures (e.g. 900 and 1100°C), both large (see panels g and i of Figure 5-3) and small (see panels h and j of Figure 5-3) ash cenospheres consist of mainly hematite.

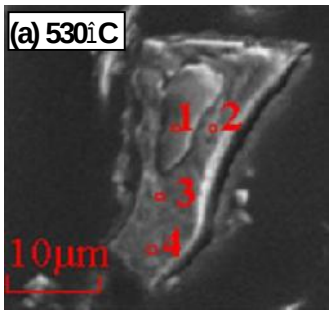

Pos#	Fe:S:O
1	1:1.93:0.8
2	1:1.39:0.54
3	1:1.55:0.21
4	1:1.63:0.35

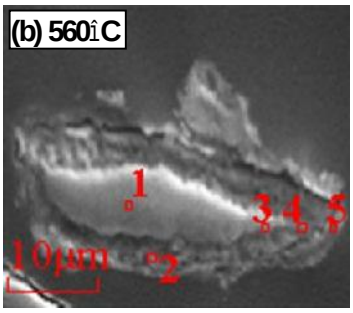

Pos #	Fe:S:O
1	1:1.85:0.11
2	1:0.06:1.33
3	1:1.83:0.12
4	1:0.71:0.54
5	1:0.09:1.19

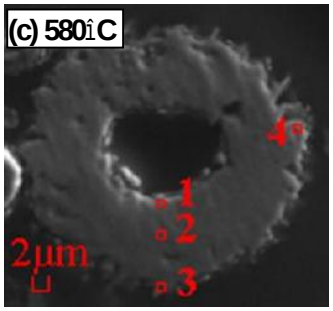

Pos #	Fe:S:O
1	1:0.29:0.78
2	1:0.38:0.62
3	1:0.13:0.73
4	1:0.07:1.30

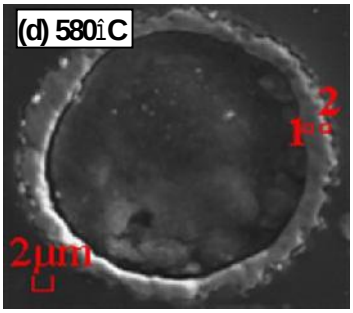

Pos #	Fe:S:O
1	1:1.19:0.81
2	1:0.14:1.22

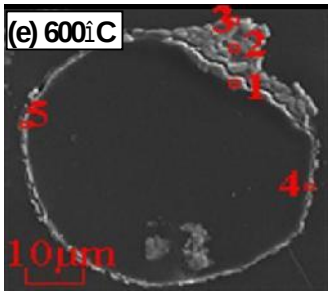

Pos #	Fe:S:O
1	1:0.00:1.27
2	1:0.00:1.00
3	1:0.00:1.55
4	1:0.00:1.56
5	1:0.00:1.51

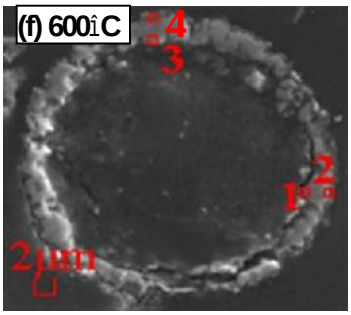

Pos #	Fe:S:O
1	1:0.06:1.23
2	1:0.19:1.15
3	1:0.13:1.13
4	1:0.10:1.42

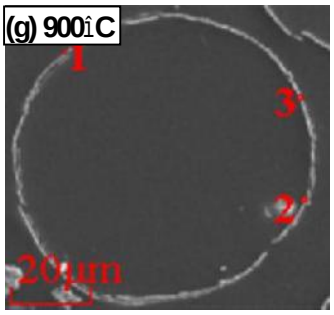

Pos #	Fe:S:O
1	1:0.00:1.47
2	1:0.00:1.52
3	1:0.00:1.52

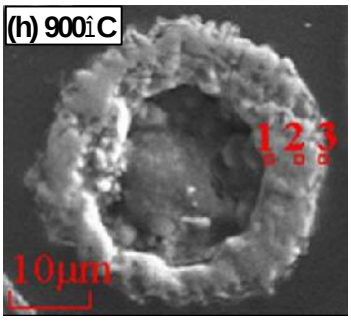

Pos #	Fe:S:O
1	1:0.00:1.50
2	1:0.00:1.51
3	1:0.00:1.56

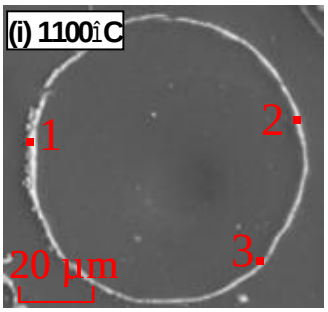

Pos #	Fe:S:O
1	1:0.00:1.51
2	1:0.00:1.50
3	1:0.00:1.50

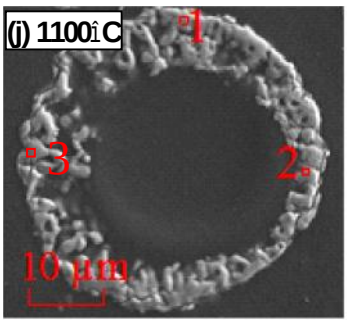

Pos #	Fe:S:O
1	1:0.00:1.53
2	1:0.00:1.50
3	1:0.00:1.51

Figure 5-3: Chemical compositions of typical particles in ash samples produced from pulverized pyrite combustion at furnace temperatures of 600 – 1100 °C.

5.5 Temperature-Dependent Properties of Ash Cenospheres Produced during Pyrite Combustion

The results in this study show that at temperatures ≥ 600 °C, ash cenospheres are the dominant particles in the ash samples produced from the combustion of pulverised pyrite. Efforts were then taken to investigate the effect of temperature on the properties of ash cenospheres. The results are presented in Figure 5-4 for the PSDs of ash collected at furnace temperatures 600 - 1100 °C, Figure 5-5 for typical SEM images of ash particles in different size fractions (using that produced at 900 °C as an example) and Table 5-1 for Fe:S molar ratios of different size fractions of ash samples produced at 600, 900 and 1100 °C.

There are three important observations can be made based on the results in Figure 5-4, Figure 5-5 and Table 5-1. Firstly, the ash samples indeed consist of dominantly ash cenospheres and cenosphere fragments. For example, at 900 °C, ~60% of ash particles are large ash particles > 45 µm (see Figure 5-4). Complete spherical ash cenospheres are present in the size fractions of >125 µm and 106-125 µm (see SEM images in panels a and b of Figure 5-5, respectively). However, ash particles in smaller size fractions, including 90-106, 75-90 and 53-75 µm (see panels c-e of

Figures 5-5), are mostly the fragments of ash cenospheres which have thin shells (~1 µm). Even in the size fractions of 45-53 µm (see Figure 5-5f) and < 45 µm (see Figure 5-5g), a substantial proportion of the ash particles are small ash cenospheres and/or cenosphere fragments.

Secondly, the temperature has significant influence on the size distributions of ash cenospheres. A higher temperature appears to produce more small ash particles. For example, the percentage of small ash particles (<45 µm) increases from ~23 % at 600 °C to ~45 % at 1100 °C. Such an increase in the production of small ash particles is accompanied with the reductions in the formation of large ash cenospheres (>125 µm), which decreases from ~16 % at 600 °C to ~7 % at 1100 °C. The results suggest that ash cenospheres formed during combustion at higher furnace temperatures experience more fragmentation to form smaller ash cenosphere fragments.

Thirdly, the furnace temperature also significantly influences on the ash chemistry of ash cenospheres. As shown in Table 5-1, at 600 °C, there are still significant sulphur present in the ash cenospheres (or their fragments) in all the size-fractioned samples, with Fe:S ratios of ~1:0.23. However, at higher temperatures (900 and 1100 °C), all size fractions contain little sulphur. Such results are consistent with the EDS analyses of individual particles (see results presented in panels e-j of Figures 5-3).

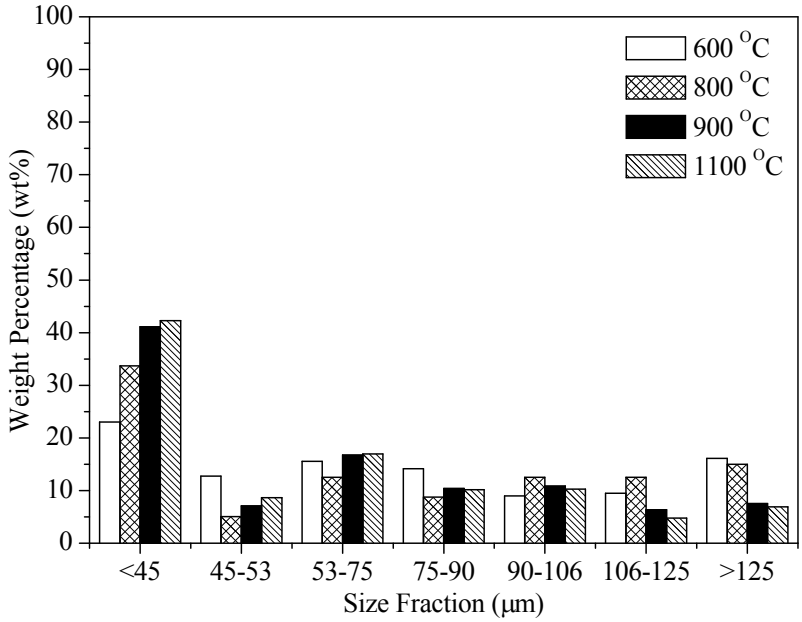

Figure 5-4: Particle size distribution in various size fractions of ash produced from the combustion of pulverized pyrite at furnace temperatures of 600 – 1100 °C.

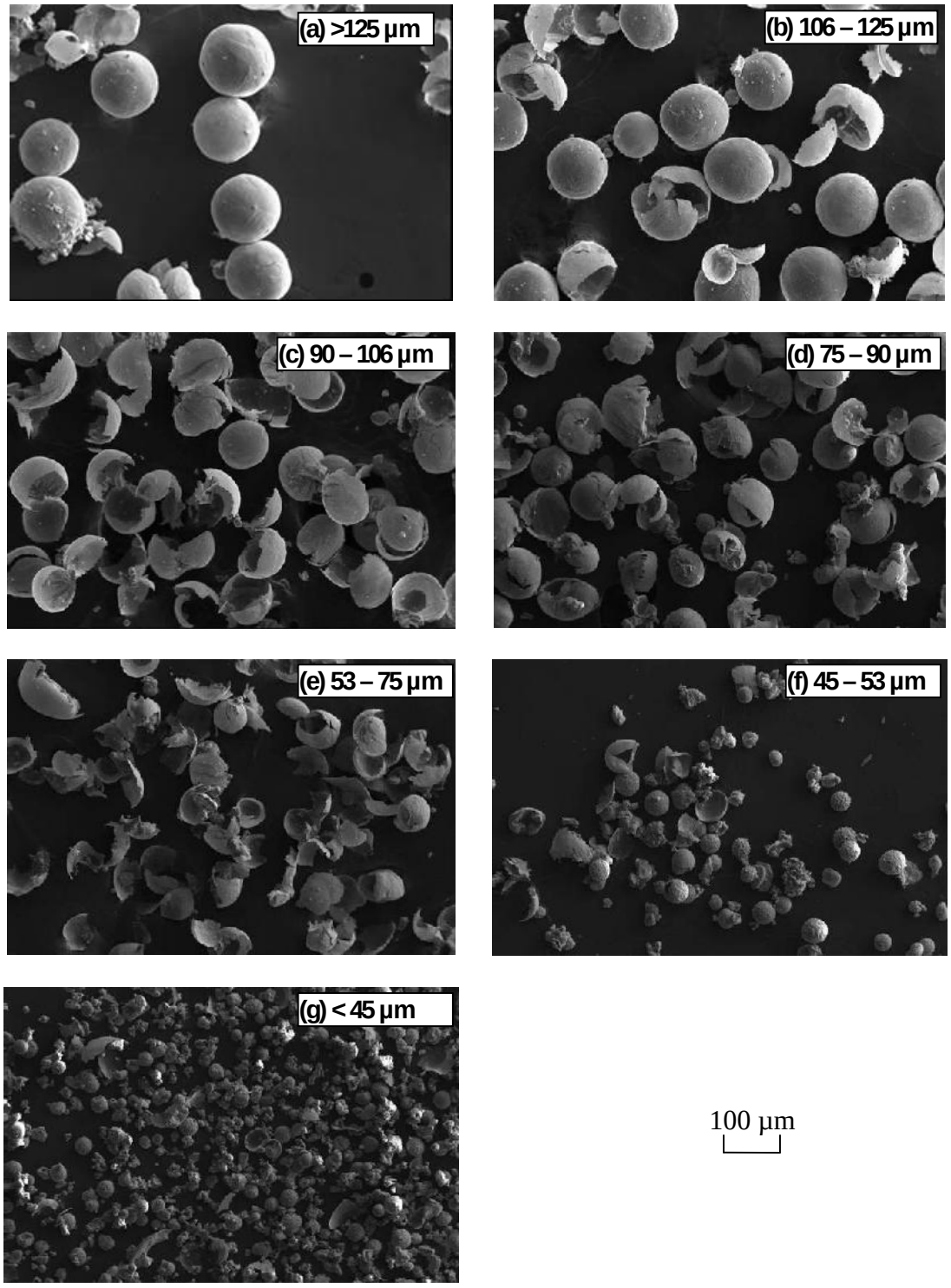

Figure 5-5: SEM images of size-fractioned ash particles produced during the combustion of pulverised pyrite at 900 °C. The scale bar applies for all the images.

Table 5-1: Fe:S molar ratios of different size fractions of ash produced during pulverized pyrite combustion at various furnace temperatures (600, 900 and 1100 °C)

Size fraction	Fe: S molar ratio		
	600 °C	900 °C	1100 °C
<45 µm	1: 0.23	1: 0.01	1: 0.01
45-53 µm	1: 0.24	1: 0.04	1: 0.01
53-75 µm	1: 0.23	1: 0.03	1: 0.01
75-90 µm	1: 0.23	1: 0.03	1: 0.02
90-106 µm	1: 0.22	1: 0.02	1: 0.02
106-125 µm	1: 0.23	1: 0.04	1: 0.02

5.6 Formation Mechanism of Ash Cenospheres during Pulverised Pyrite Combustion

The results presented in Sections 5.2 − 5.5 provide important insights into the formation mechanism of ash cenospheres during pulverized pyrite combustion. On the basis of the above discussion, the mechanism responsible for ash cenosphere formation during the combustion of pulverized pyrite is clarified and summarized in Figure 5-6.

It is important to note that ash cenospheres start to form at 580 °C and become dominant in ash produced at temperatures ≥ 600 °C. To form ash cenospheres, there are two essential conditions to be met. One is that the precursor particles during combustion must have experienced complete melting. The other is that a source of gas must be supplied and enclosed in the molten ash droplet then inflate and expand the molten droplet for producing ash cenospheres after resolidification. At first glance, 580 and 600 °C appear to be too low to enable the formation of molten ash droplets. Particularly, the XRD diffractograms in Figure 5-2 suggest that the phases of the final ash cenospheres are iron oxides, which have high melting points (FeO: 1377 °C; Fe_3O_4: 1548°C; Fe_2O_3: 1566 °C). However, during combustion, pyrite

oxidation reactions are exothermic, so that the temperature of a burning pyrite particle can reach a temperature much higher than the furnace temperature. Our preliminary modelling prediction suggests that, under the conditions in this study, the temperature of a burning pyrite particle is estimated to be ~1000 °C, which, however, is still considerably lower than the melting points of iron oxides. Therefore, ash cenospheres are unlikely formed from iron oxides directly at the temperature. The melting process of the precursor ash particle must have taken place prior to the reacting particles being oxidised to iron oxides.

Figure 5-3 shows that the ash chemistry of individual ash cenospheres at 580 and 600 °C (see panels c-f of Figures 5-3) contains substantial amount of sulphur. It is known that the Fe-S-O system can have a low melting point, depending on the Fe:S:O composition. For example, the eutectic point of an Fe-S-O system can be as low as 915 °C (at an Fe:S:O molar ratio of 1.22:0.76:0.45)[111], much lower than the predicted temperature of burning pyrite particles. It is therefore plausible to reason that, once a suitable Fe-S-O system is established as combustion proceeds, the complete melting of the burning pyrite particles becomes possible. It should be noted that the Fe-S-O melt evolves dynamically. Combustion/oxidation of the molten Fe-S-O melt would then produce sulphur oxides gases and form bubbles inside the Fe-S-O melt. The gas bubbles would coalescence and appear to form a single large bubble and inflate and expand the molten droplet for producing ash cenosphere of thin shells, satisfying the two essential conditions required for ash cenosphere formation.

Therefore, the precursor (Fe-S-O) melt must already be in cenospheric forms. The oxidation of such cenospheric precursors continuously releases sulphur oxides gas products within the cenospheric particles as the particles resolidify to form ash cenospheres. Therefore, the Fe-S-O melt is the precursor, with sulphur oxides gases produced inside the molten Fe-S-O droplet being fundamentally responsible for ash cenospheres formation. At a low temperature (e.g., 580 °C), the reactions are too slow to consume all the sulphur in the precursor particles while solidifying, leading to the formation of ash cenospheres that contain S in the shell and magnetite as the dominant iron oxide (see XRD diffractogram in Figure 5-2). However, at high temperatures (e.g., 900 °C), oxidation reactions are rapid. Not only is the sulphur in the shell of the cenospheric Fe-S-O melt almost consumed completely, but also the

majority of magnetite has been oxidised to hematite, producing ash cenospheres of hematite. It should also be noted that the generation of sulphur oxides gases within the Fe-S-O melt may also lead to the bursting of the precursor cenospheric particles into small Fe-S-O droplets (if still molten) or cenospheric fragments (if not molten). Continuous generation of sulphur oxides gas within the small Fe-S-O droplets would lead to the formation of small ash/cenosphere particles (see Figure 5-5). Depletion of S also leads to the formation of iron oxides, which have much higher melting points, resulting in the resolidification of ash cenospheres. The presence of extensive ash cenosphere fragments in the ash products produced under all combustion conditions (see Figures 5-5 and 5-6) is a clear indication that the ash cenosphere experienced fragmentation during the formation process.

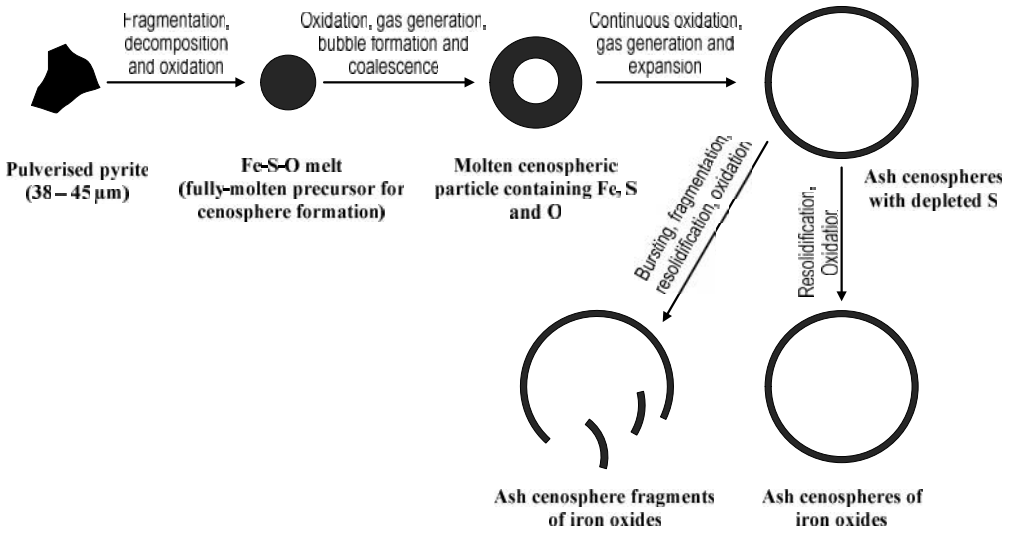

Figure 5- 6: Mechanism of ash cenosphere formation during pulverised pyrite combustion. The process can take place during the combustion of pulverised pyrite at a furnace temperature as low as 580 °C.

5.7 Conclusions

This chapter reports a study on ash cenosphere formation during pulverised pyrite combustion in a DTF under various conditions, to understand the fundamental formation mechanism of ash cenosphere during solid fuels combustion. The main conclusions include:

(1) Ash cenospheres start to form at a furnace temperature as low as 580 °C.

(2) At furnace temperatures ≥600 °C, ash products contain dominantly large ash cenospheres with thin shell and cenosphere fragments.

(3) An increase in furnace temperature leads to enhanced fragmentation of ash cenospheres.

(4) The formation of Fe-S-O melts during pulverised pyrite combustion is essential to ash cenosphere formation.

(5) The molten Fe-S-O droplets trap the sulphur oxides gaseous products within the droplets and inflate to form cenospheric precursors. The cenospheric Fe-S-O precursors are then further oxidised to deplete sulphur and resolidified into ash cenospheres of dominantly iron oxides.

CHAPTER 6 ASH CENOSPHERE FRAGMENTATION AND ITS SIGNIFICANT ROLE IN THE FORMATION OF ASH AND PARTICULATE MATTER DURING PULVERISED PYRITE COMBUSTION

6.1 Introduction

Chapter 5 investigates the fundamental formation mechanism of ash cenospheres through a systematic experimental program using pyrite as the model fuel. The results suggest that substantial amounts of thin-walled ash cenospheres start to be produced at the furnace temperature of 600 °C. The formation of molten ash droplets which trap sulphur oxides gaseous products is essential to ash cenospheres formation during pulverised pyrite combustion. The derived cenospheric Fe-S-O precursor particles are then further reacted and resolidified into ash cenospheres.

The results in Chapter 5 also show the presence of abundant fragments of ash cenospheres in the ash samples. Therefore, fragmentation does take place during the process of ash cenosphere formation and it is strongly temperature dependent. Such fragmentation may influence the formation of both coarse ash particles and fine particulate matter with an aerodynamic diameter less than 10 µm (PM_{10}). While it was speculated that fragmentation of ash cenosphere may contribute to the formation of PM_{10},[34-36] there is no direct experimental evidence to prove such a hypothesis.

Therefore, the objective of this chapter is to investigate the fragmentation behaviour of ash cenosphere and its role in the formation of ash and PM_{10}. This corresponds to the third objective outlined in Chapter 2. Again, pyrite (particle size: 38 – 45 µm) is used as a model fuel in order to provide a simplified combustion system for this study. The combustion experiments were carried out using the drop-tube furnace (DTF) system at 600 °C but different residence times (0.4, 0.7, 0.9, and 1.1 s). Both coarse ash particles and PM_{10} were collected via cyclone and DLPI, respectively. The collected samples were subjected to various analyses including mass-based particle size distributions (PSDs), morphology and chemical composition. The

experimental program in this study enables a mechanistic study on the evolution of PM formation as a result of cenosphere fragmentation. It also provides direct experimental evidences on the roles of ash cenosphere fragmentation in the formation of particulate matter.

6.2 Yields and PSDs of PM_{10} Collected from Pulverised Pyrite Combustion

In this study, the PM samples are reported in 5 size ranges, i.e. PM with aerodynamic diameters in the size ranges of less than 0.1 µm ($PM_{0.1}$), 0.1–1 µm ($PM_{0.1-1}$), less than 1 µm (PM_1), 1–10 µm (PM_{1-10}) and less than 10 µm (PM_{10}), respectively. Figure 6-1 presents the yields of $PM_{0.1}$, $PM_{0.1-1}$, PM_1, PM_{1-10} and PM_{10}, from the combustion of pulverised pyrite at 600 °C and at four different residence times (0.4, 0.7, 0.9, and 1.1 s). The data in Figure 6-1 provide important insights into how the formation of PM evolves with the progress of the combustion of pulverised pyrite.

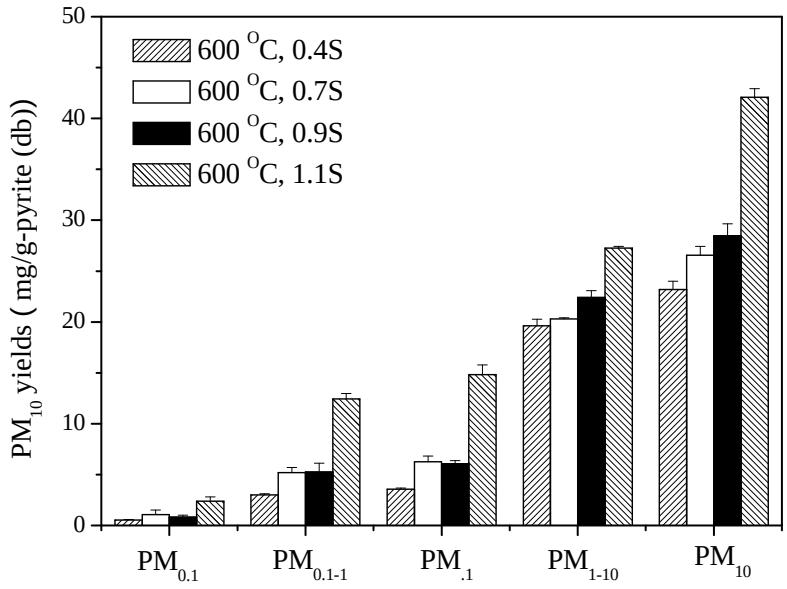

Figure 6-1: Yields of PM with aerodynamic diameters less than 0.1 µm ($PM_{0.1}$), between 0.1 and 1 µm ($PM_{0.1-1}$), less than 1 µm (PM_1), between 1 and 10 µm (PM_{1-10}) and less than 10 µm (PM_{10}) produced during pulverised pyrite combustion at 600 °C but different residence times.

Figure 6-1 clearly shows that at various residence times, the combustion of pulverised pyrite at 600 °C produces substantial amounts of PM_{10}, which are dominated by PM_{1-10}. There are also considerable amounts of PM_1 (including both

$PM_{0.1}$ and $PM_{0.1-1}$) produced under the different conditions. For example, the mass of PM_{1-10} produced from the combustion of pulverised pyrite at 600 °C at the shortest residence time (0.4 s) accounts for ~ 85% of the total PM_{10} mass, while PM_1 only contributes to ~15%. Most importantly, the data also show that the yield of PM clearly evolves as the combustion proceeds, i.e. increasing residence time leads to an increase in the yields of both PM_1 and PM_{1-10}. For example, as the residence time increases from 0.4 to 1.1 s, the yields of PM_1 and PM_{1-10} increase substantially, from 3.6 and 19.6 mg/g_pyrite to 14.8 and 27.3 mg/g_pyrite, respectively.

Further efforts were then taken to investigate the evolution of the mass-based particle size distributions (PSDs) of PM_{10} as the combustion progresses at 600 °C, considering different residence times (see Figure 6-2). There are three important observations in Figure 6-2. Firstly, it is clear that the PSDs of PM_{10} generally show a bimodal distribution, i.e. a fine mode with a mode diameter of 0.26 µm and a coarse mode with mode diameters from 4.4 µm to 6.8 µm. Secondly, the PM_{10} contains mostly PM_{1-10} while the amount of PM_1 is limited, which is consistent with the findings in Figure 6-1. Thirdly, increasing the residence time indeed leads to the increase of the yields of both PM_1 and PM_{1-10}, suggesting the progress of pulverised pyrite combustion plays an important role in the formation of PM_{10}.

Overall, the data in Figures 6-1 and 6-2 indicate that particle residence time significantly affects the yields and PSDs of PM_{10} from pulverised pyrite combustion. The results clearly suggest that the formation of PM is strongly dependent on the progress of combustion. As seen in the next section (Section 6.3), the ash products from pyrite combustion under all conditions in this study include ash cenospheres and their fragments. This in turn indicates that the evolution of ash cenosphere formation plays an important role in PM_{10} formation during pulverised pyrite combustion. These important aspects are discussed in detail in the subsequent Section 6.4.

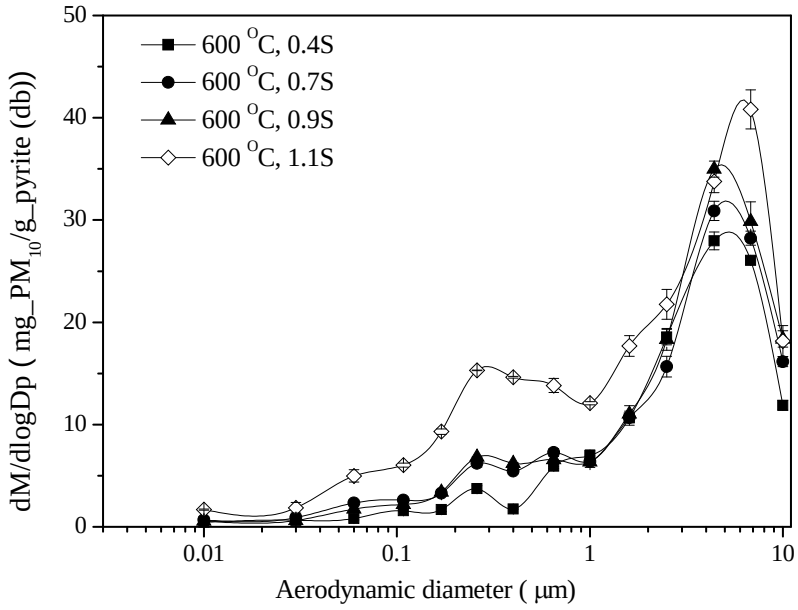

Figure 6-2: Mass-based particle size distributions (PSDs) of PM_{10} produced from the combustion of pulverised pyrite at 600 °C but different residence times.

6.3 Properties of the Ash Collected in the Cyclone

In this study, the ash collecting system collects ash particles with aerodynamic particle size > 10 μm by a cyclone while the PM_{10} is collected via a DLPI system. To further understand the evolution of ash formation during pulverised pyrite combustion, efforts were then taken to investigate the properties of the larger ash particles (>10 μm) collected by the cyclone (hereafter also named as cyclone ashes).

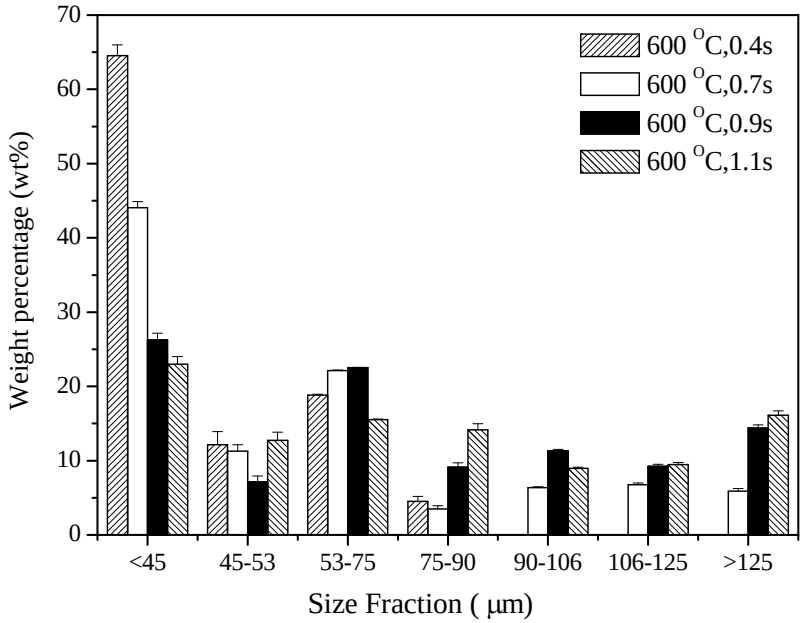

Figure 6-3: Particle size distributions of ash particles collected in cyclone, produced from the combustion of pulverised pyrite at 600 °C but different residence times.

Figure 6-3 presents the PSDs of the cyclone ashes during the combustion of pulverised pyrite at 600 °C but different residence times. As the parent pyrite particles have particle sizes of 38 - 45μm, after combustion, it is safe to conclude that those ash particles > 45 μm must be either ash cenospheres or their fragments. As shown in Chapter 5, at 600 °C and 1.1 s residence time, ash particles in size fractions of 106-125 μm and > 125 μm are dominantly complete ash cenospheres while ash particles in other size fractions > 45 μm are ash cenosphere fragments and/or smaller cenospheres. Similar phenomena are also observed for ash samples collected at residence times of 0.7 and 0.9 s. Figure 6-3 also clearly shows that residence time has a great effect on the PSDs of the cycle ash particles.

On one hand, it is interesting to see in Figure 6-3 that at a residence time of 0.4 s, there are no ash particles of sizes > 90 μm. In other words, there are no large complete ash cenospheres which are generally in the size fractions of both 106-125 μm and > 125 μm. However, as the residence time increases to 0.7 s, ~12 % of cyclone ash particles are in these two size fractions. At residence times of 0.9 and 1.1s, this percentage increases substantially to ~23 % and ~26 %, respectively. Such results clearly demonstrate while there are few ash cenosphere formed at a residence time of 0.4 s, as the combustion progresses to 0.7 s, ash cenosphere formation

becomes significant. Further combustion leads to substantial production of ash cenospheres, especially at a residence time of 1.1 s, the ash product consists of dominantly ash cenospheres and their fragments.

On the other hand, Figure 6-3 also clearly demonstrates that a longer residence time leads to less formation of small ash particles in the size fraction of < 45 µm. For example, ~64 % of cyclone ash particles produced at 0.4s is in this size fraction. As residence time increases to 0.7 s, the percentage of ash particles in the size fraction of <45 µm reduces to ~44 %. At residence times of 0.9 and 1.1 s, only ~26 % and ~23 % of ash particles are <45 µm, respectively. Therefore, it is clear that as residence time increases, the increased proportion of large ash cenospheres is accompanied with a decreased proportion of small ash particles.

Figure 6-4 presents the typical SEM images of size-fractioned cyclone ash particles formed from pulverised pyrite combustion at 600 °C but at various residence times. It can be seen that the morphologies of size-fractioned ash particles are clearly different. For the ash particles in size fractions of 75-90 and 53-75 µm, SEM images in panels a and e of Figure 6-4 show the particles formed at 1.1 s are dominantly the fragments of thin-walled ash cenospheres. However, at shorter residence times, ash particles in these two size fractions are mainly thin-walled cenospheres and the fragments (at 0.9 s), complete spheres with smooth surfaces or adhered with small irregular particles (at 0.7 and 0.4 s), as shown in panels b-d and f-h of Figure 6-4.

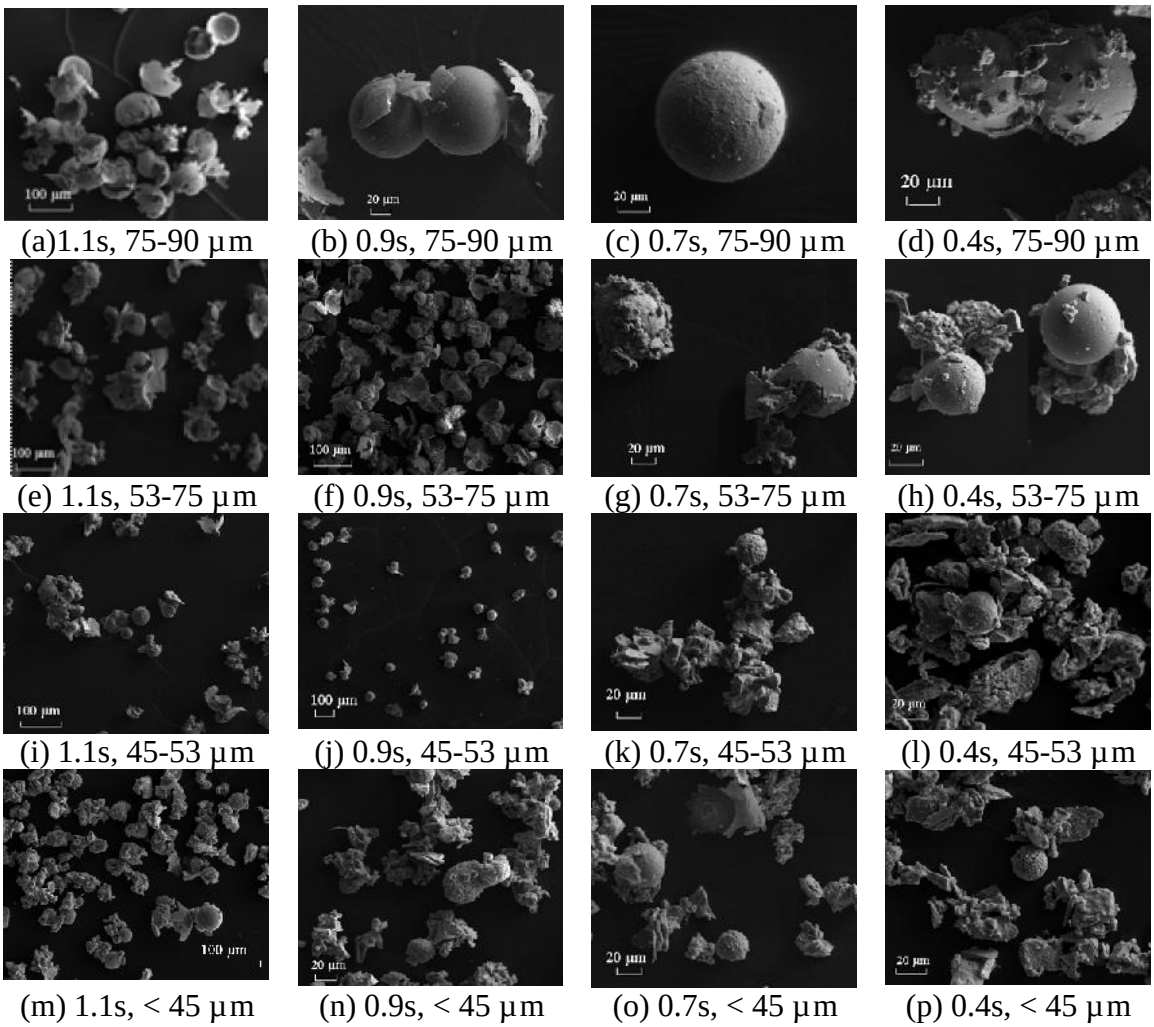

Figure 6-4: Typical SEM images of size-fractioned ash particles produced during pulverised pyrite combustion at 600 °C but different residence times.

In the size fractions of 45-53 and < 45 µm, a substantial proportion of ash particles are small ash cenospheres and/or cenosphere fragments when residence time is 1.1s (see panels i and m of Figure 6-4). As residence time decreases to 0.9 and 0.7 s, SEM images in panels j-k and n-o of Figure 6-4 clearly demonstrate the decrease of the proportion of small ash cenospheres and/or cenosphere fragments. At residence time of 0.4 s, ash particles show remarkable different morphology (see panels l and p of Figure 6-4). Most of the small ash particles are irregular but clearly not the fragments of thin-walled ash cenospheres.

Table 6-1: Fe:S molar ratios of different size fractions of small ash particles produced during pyrite combustion at 600 °C and at different residence times.

Residence time (s)	Fe: S		
	< 45 µm	53–75 µm	>125 µm
0.4	1: 1.17	1: 1.35	NA*
0.7	1: 0.70	1: 0.70	1: 0.80
0.9	1: 0.44	1: 0.53	1: 0.75
1.1	1: 0.23	1: 0.23	1: 0.23

* NA – Not available as there are no ash particles in this size fraction

The chemical compositions of selected ash size fractions were then determined using the methods detailed in Sections 3.4.8 and 3.4.9 of Chapter 3, with the results listed in Table 6-1. At a residence time of 0.4 s, the results in Table 6-1 show that the samples of various size fractions consist of substantial amounts of sulphur. The Fe:S molar ratios of various samples are 1:1.17 for the size fraction < 45 µm and 1:1.35 for the size fraction 53–75µm, respectively. There are no samples having sizes > 90 µm at a residence time of 0.4s, the data suggest that these small ash particles are partially decomposed pyrite particles which would have also experienced at least some degrees of oxidation under the combustion conditions. Table 1 clearly shows that as the combustion proceeds (i.e. at an increasing residence time from 0.4 to 0.7, 0.9 and 1.1 s), the sulphur in the reacting particles of all size fractions is consecutively reduced considerably, obviously as a result of continuous oxidation. Even at a residence time of 1.1 s, complete consumption of sulphur was not achieved during combustion. The data in Table 1 also suggest that at a given residence time, the consumption of sulphur in the reacting particles during pyrite combustion is also dependent on particle size. On one hand, formation of large ash cenosphere particles requires a deep oxidation to generate sufficient gaseous products for expansion. This is evident in the data for ash particle >125 µm. On the other hand, smaller ash particles/fragments would have larger reaction surfaces (per unit mass) available for oxidation reactions, leading to generally lower sulphur contents in the smaller size fractions.

6.4 Roles of Ash Cenosphere Fragmentation in Ash and PM_{10} Formation

The observations from Figures 6-1 to 6-4 and Table 6-1 provide important insights into the evolution of ash cenospheres formation and their roles in the formation of ash and PM_{10} during pulverised pyrite combustion. At residence time of 0.4 s, the combustion of pulverised pyrite at 600 °C produces a large proportion of small ash particles with sizes less than 45 µm, which are most likely to be partially oxidized pyrrhotite (see Table 6-1). Therefore, it seems that the combustion of pulverised pyrite at this condition follows the two-step reaction process as suggested in previous studies.[93, 94, 99-101, 104-106] In this case, the formed pyrrhotite may fragment as reported previously.[21, 89, 90, 105, 106, 109, 110] Indeed, this can be supported by the observation on the morphology of small ash particles as shown in Figure 6-4. During subsequent combustion, at least some of these fragments may further experience melting and form Fe-S-O molten droplets as the cenospheres precursors, leading to the production of ash cenospheres with sizes 53-90 µm. This is supported by the abundant ash cenospheres formed in the samples collected at longer residence times (0.7 – 1.1 s, see Figure 6-3). Clearly, a longer residence time of ash particles during combustion enhances the generation of sulphur-derived gaseous products within the Fe-S-O molten droplets, leading to the production of ash cenospheres as well as the fragmentation of the precursor cenospheric particles. The data also suggest that the fragments appear to melt and expand, resulting in a decrease in the proportions of small ash particles < 45 µm, as shown in Figure 6-3.

There are two important observations from the PSD data presented in Figure 6-3. One is that a substantial proportion of large ash particles with sizes >106 µm are formed during pyrite combustion and these large particles are mainly complete ash cenospheres as observed by SEM. The other is that accompanied with the increase in the yields of large ash cenospheres, the yields of ash particles of 75-106 µm increase substantially with increasing residence time. As discussed above, substantial fragments of thin-walled ash cenospheres are present in these ash particles produced from pyrite combustion.

Two possible mechanisms are expected to be responsible for such fragmentation. One is the bursting of the precursor cenospheric particles due to the generation of sulphur oxide gases within the Fe-S-O melts, leading to the formation of small

Fe-S-O droplets (if still molten) or cenospheric fragments (if at least partially resolidified), as suggested in Chapter 5. Another is due to the fragmentation of the formed ash cenospheres during cooling process. As the cooling process is maintained to be same in this set of experiments, the changes in the properties of ash and PM formation at various residence times are mainly due to the changes in the fragmentation behaviour of the reacting particles during combustion.

To further investigate the formation mechanism of ash and PM, the compositions of selected ash particles were then examined with EDS analysis and shown in Figure 6-5. While some of large ash cenosphere particles contain sulphur, there are also abundant large ash cenospheres (e.g. the one in Figure 6-5a) that mainly consist of Fe and O, i.e., most likely in the form of iron oxides. Ash cenospheres containing S in the shell is attributed to the relatively slow reactions without consuming all of the sulphur in the precursor particles during solidifying.

For the small ash particles (<45 μm), EDS spectra in Figure 6-5 shows that irregular fragment of cenosphere shells consists of Fe, S and O (spectrum 3), while the spherical particle with smooth surface contains only Fe and O (spectrum 4). Therefore, both mechanisms mentioned above are likely to take action in the formation of these particles. The spherical particles may be generated from the bursting of the precursor cenospheric particles, as the first mechanism, leading to the formation of small Fe-S-O droplet, while sulphur in the droplet is continuously oxidised before solidifying. The second mechanism is also plausible. The irregular fragments of ash cenospheres suggest that these fragments are very likely to be formed during cooling after combustion, resulting in the presence of abundant S in these irregular particles.

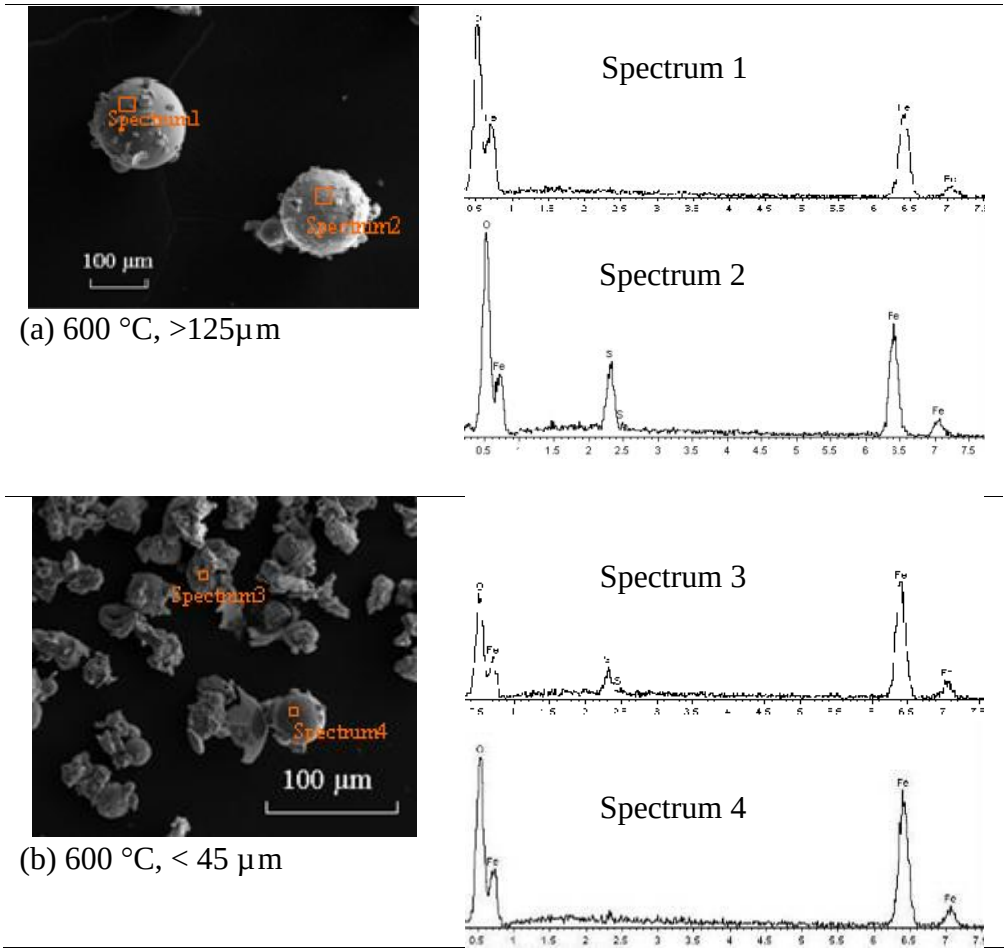

(a) 600 °C, >125µm

(b) 600 °C, < 45 µm

Figure 6-5: Morphology of cyclone ash particles in large (panel a: > 125 µm) and small (panel b: < 45 µm) size fractions collected from pyrite combustion at 600 °C and a residence time of 1.1 s and the EDS results of typical ash particles.

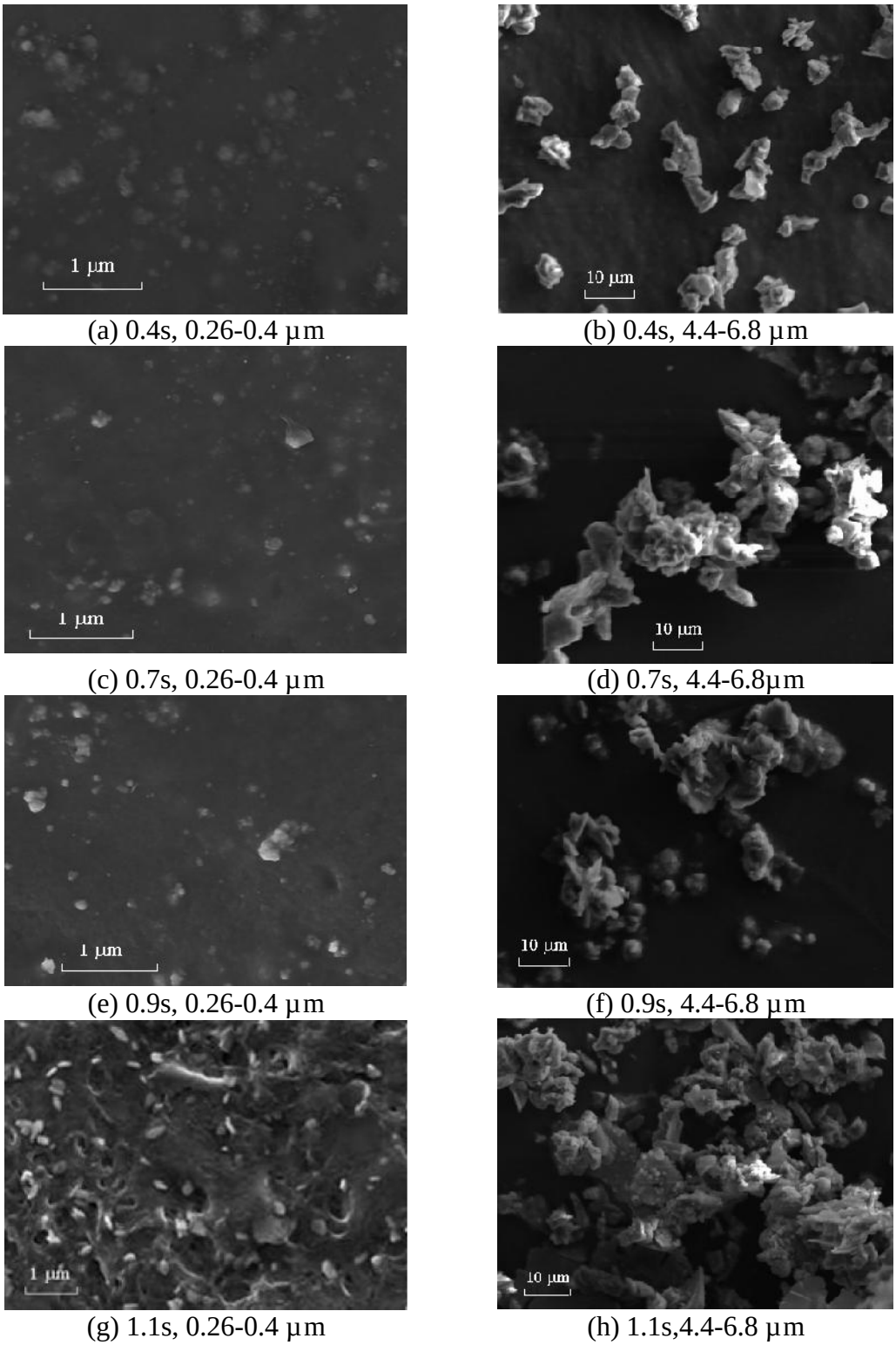

(a) 0.4s, 0.26-0.4 µm (b) 0.4s, 4.4-6.8 µm

(c) 0.7s, 0.26-0.4 µm (d) 0.7s, 4.4-6.8µm

(e) 0.9s, 0.26-0.4 µm (f) 0.9s, 4.4-6.8 µm

(g) 1.1s, 0.26-0.4 µm (h) 1.1s,4.4-6.8 µm

Figure 6-6: Morphology of ash particles collected in DLPI during pyrite combustion at 600 °C under different residence times.

The results presented in Sections 6.2 illustrate the formation of substantial PM_{10} during the combustion of pulverised pyrite under the various conditions. The PSDs of PM_{10} shown in Figure 6-2 are qualitatively in agreement with the observation on PM_{10} produced from the combustion of solid fuels such as coal.[87, 116, 118, 121-127] As suggested in previous studies on solid fuels combustion, particulate matter in submicron and supermicron region has distinct formation mechanisms. Mineral coalescence and char/excluded mineral fragmentation are generally supposed to be responsible for supermicron particles (PM_{1-10}) formation,[87, 110, 114, 119, 121, 124, 125, 130, 132, 133, 137, 140, 148, 149] while vaporization/condensation is the major mechanism of submicron particles (PM_1) formation.[116, 117, 130, 134, 136, 138, 140, 149, 153, 154] However, given that substantial PM_1 formed at the temperature as low as 600 °C, ash vaporisation is unlikely. Therefore, it seems that during pulverised pyrite combustion at 600 °C, not only PM_{1-10} but also PM_1 are produced due to fragmentation mechanism.

Such findings as above are significant. There are several possible routes for fragmentation in this case: the breakup of burning pyrite particles before cenospheric precursors and/or ash cenospheres are formed, the fragmentation of cenospheric precursors and/or ash cenospheres during pyrite combustion, or both. To ascertain this important point, the morphology of PM_{10} collected at the different stages of DLPI during experiments at 600 °C was examined by a Zeiss Neon EsB focused ion beam scanning electron microscope (FIBSEM). The typical images of PM_{10} with size fractions of 0.26-0.4 and 4.4-6.8 µm are presented in Figure 6-6.

As shown in Figure 6-6 a, after pyrite combustion at 600 °C for 0.4s, irregular and individual particles dominate the PM particles in the size fraction of 0.26-0.4 µm. This is very different from the spherical or agglomerated-/aggregated-like morphology of coal-combustion-derived PM_1, as results of vaporization-condensation formation mechanism.[121, 124, 128-130, 132-136] Therefore, it can be deduced that such particles in PM_1 must be formed due to fragmentation mechanism. The results in Section 6.3 indicated that, nearly no large complete ash cenospheres are formed when residence time is 0.4s. Also, there is no ash cenosphere fragments observed in 0.26-0.4 µm ash particles. Therefore, it is expected that the breakup of burning pyrite particles must play a dominant role in PM_1 formation at such a short residence time (0.4 s). This mechanism was proposed in previous

studies,[34-36, 89, 90] speculating the possible contribution of pyrite fragmentation to the formation of PM_1. In addition, for the 4.4-6.8 µm particles produced at 0.4s, the SEM image in Figure 6-6 b illustrates that most of these ash particles are irregular and thick fragments, graphically indicating their possible origination from the fragmentation of burning pyrite particles. The results in present study therefore provide direct experimental evidence to the potential important roles of pyrite fragmentation during combustion in the formation of both PM_{1-10} and PM_1.

The results in Section 6.2 suggest that increasing residence time did not change the shape of the PSDs of PM_{10} (see Figure 6-2), indicating that changing residence time at 600 °C did not change the fragmentation mechanism of PM_{10} formation. This can be further supported by SEM images in panels c-h of Figure 6-6, in which most of PM particles in the size fractions of both 0.26-0.4 and 4.4-6.8 µm show irregular shapes. Furthermore, a closer examination on the morphology of these irregular PM particles, especially those formed at the longest residence time, i.e., 1.1 s (see panels g and h in Figure 6-6), clearly illustrates the presence of fragments of thin-walled shell of ash cenospheres. Therefore, this is direct evidence that the fragmentation of ash cenosphere and/or its precursors contributes the formation of PM_{1-10}, as the first time in the field. It also directly proves that bubble bursting during ash cenosphere formation is an important mechanism for PM_1 formation, which has been long speculated in the literature[34-36] but without direct experimental proof.

Therefore, it is clear that during pulverised pyrite combustion at 600 °C, PM_{10} (including PM_{1-10} and PM_1) is formed from both breakup of burning pyrite before the formation of cenospheric precursors and the fragmentation of cenospheres and/or cenospheric precursors. The data in Figure 6-1 indicate that changing residence time obviously affected the yields of PM_{10} although did not change the PSD pattern of PM_{10}. The higher yields of PM_{1-10} and PM_1 formed at longer residence times appear to coincide with the increase of large ash cenospheres and large cenosphere fragments hence likely intensified ash cenospheres fragmentation. Generally, the fragments of ash cenospheres are irregular and with large physical dimensions. Therefore, during sieving, these fragments might be able to stay on the top of larger sieves, leading to the considerable reduction of ash particles in size fraction < 45 µm when large ash cenospheres and their fragments considerably exist at residence time 1.1 s (see Figure 6-3). However, compared to the fragments of burning pyrite and

cenospheric precursor fragments with comparatively thicker shells formed at shorter residence times, these large cenosphere fragments have relatively lower density hence smaller aerodynamic diameter. This can lead to the emission of more PM_{10} at longer residence times. Indeed, morphology of PM particles shown in Figure 6-6 clearly demonstrates the increased proportions of fragments of thin-walled shell of ash cenospheres formed at longer residence times. Therefore, it can be concluded that during pulverised pyrite combustion at 600 °C, the fragmentation of ash cenospheres and/or cenospheric precursors plays a more significant role in and favours the formation of PM_{10}. Figures 6-1 and 6-2 indicate that increasing the residence time from 0.9 to 1.1 s results in not only a considerable increase in the yield of PM_{1-10} but also a significant increase in the formation of PM_1, particularly $PM_{0.1-1}$. It implies that the fragmentation of cenospheres also makes a great contribution to PM_1 formation.

6.5 Conclusions

This chapter reports a systematic investigation into the fragmentation behaviour of ash cenospheres, to demonstrate its significant role in the evolution of PM emission and provide direct experimental proof as the first time on the effects of ash cenospheres fragmentation on the formation of PM_{10}. The main conclusions include:

(1) Substantial amounts of PM_{10} can be produced during the combustion of pulverised pyrite in DTF under the various conditions.

(2) The PM_{10} collected from the combustion of pulverised pyrite is dominated by PM_{1-10} but also contains considerable amounts of PM_1.

(3) The PSDs of PM_{10} from pulverised pyrite combustion have a bimodal distribution, i.e. a fine mode (mode diameter: 0.26 µm) and a coarse mode (mode diameter: from 4.4 µm to 6.8 µm.

(4) It was found that at 600 °C, the combustion of pulverized pyrite produces a substantial proportion of large ash cenospheres and substantial fragments of thin-walled ash cenospheres, strongly indicating the significant role of ash cenosphere fragmentation in ash formation.

(5) As the first in the field, this study provides direct experimental evidences to

demonstrate the important role of ash cenosphere fragmentation in PM_{10} formation during the combustion of pulverised pyrite.

(6) At a furnace temperature of 600 °C, longer residence time favours the formation of ash cenospheres and intensifies the fragmentation of ash cenospheres and/or cenospheric precursor particles, leading to an increase in PM_{10} yield.

CHAPTER 7 CONCLUSIONS AND RECOMMENDATIONS

7.1 Introduction

This chapter firstly summarizes the main research outcomes from the present study. Overall, the results in this thesis provide original and new insights into the formation mechanism of ash cenospheres and also reveal the significant role of ash cenosphere fragmentation and its contribution to particulate matter emission during the combustion of solid fuels. First, the results in this thesis provide an insightful understanding on the possible formation mechanisms of ash cenospheres during pulverised coal combustion via characterising the ash cenosphere samples collected from a power station. Second, it has clarified the mechanism responsible for the formation of ash cenospheres during the combustion of pulverised pyrite as the model fuel. Third, the thesis also as the first time in the field has reported the direct experimental evidence on the fragmentation behaviour of ash cenosphere and its significant roles in ash and particular matter formation. Lastly, this chapter also concludes with the recommendations for future work in this research area on the basis of the conclusions and evaluations of the present study.

7.2 Conclusions

7.2.1 Possible Formation Mechanisms of Ash Cenospheres from a Coal-fired Power Station

- Thermomechanical analysis shows that the fusion characteristics of ash cenospheres are dependent on the particle size of ash cenospheres. However, the various size-fractioned ash cenospheres do not melt at 1600 °C, suggesting that these ash cenospheres from coal-fired power station are impossible to be formed at temperatures <1600 °C.

- The chemistry of ash cenospheres of various size fractions is dominantly SiO_2, Al_2O_3, TiO_2 and Fe_2O_3, which comprise >99.3 wt% of the total ash chemical compositions. SiO_2/Al_2O_3 ratio decreases with increasing ash cenosphere size,

accompanied with an increase in the sum of TiO_2 and Fe_2O_3 contents (i.e. TiO_2+Fe_2O_3).

- The gas products locked inside ash cenospheres of all size fractions are dominantly CO_2 and some N_2, with trace amount of CO. The average gas pressure inside the individual ash cenosphere particles decreases from 0.227 atm to 0.172 atm (NTP) as particle size increases from 63-75 µm to 150-250 µm.

- The characteristics of molten ash cenosphere precursors derived from the ash chemistry of individual cenospheres indicate that the optimum particle temperature for cenosphere formation is from ~ 1640 to 1800 °C. Under these conditions, molten ash droplets can be formed and trap a certain amount of gas generated within the ash droplets.

- The wide range of viscosity of molten cenosphere precursors together with the force of surface tension, which is demonstrated to be inversely proportional to the viscosity of molten droplets, governs the growth of cenosphere precursors and producing ash cenospheres with various wall thicknesses.

- In addition to Fe_2O_3, the data also appear to suggest that TiO_2 may play a role in ash cenosphere formation.

7.2.2 Formation Mechanism of Ash Cenosphere from the Combustion using Pulverised Pyrite as a Model Fuel

- Ash cenospheres start to form at a furnace temperature as low as 580 °C during pulverised pyrite combustion. These ash cenospheres typically have small sizes (20−45 µm in diameter), with shells of thickness 2−10 µm.

- At furnace temperatures ≥ 600 °C, ash products of pyrite combustion consist of dominantly large ash cenospheres (up to 130 µm in diameter) with thin shells (1−3 µm) and ash cenosphere fragments of various sizes.

- Furnace temperature has significant influences on the size distributions and ash chemistry of ash cenospheres. An increase in furnace temperature during pyrite combustion results in enhanced ash cenosphere fragmentation and the reduction of sulphur presented in the ash cenospheres or their fragments.

- The formation of molten Fe-S-O droplets during pyrite combustion is essential to ash cenosphere formation.

- The molten Fe-S-O droplets trap the sulphur oxides gases within the droplets and inflate to form cenospheric precursors. Further oxidation and resolidification transforms these cenospheric Fe-S-O precursors into final ash cenospheres that also experience fragmentation and contain dominantly iron oxides.

7.2.3 Ash Cenosphere Fragmentation and its Significant Role in the Formation of Ash and Particulate Matter during Pulverised Pyrite Combustion

- Substantial amounts of PM_{10} are produced during the combustion of pulverised pyrite in DTF under the various conditions.

- The PM_{10} collected from the combustion of pulverised pyrite under the various conditions is dominated by $PM_{1\text{-}10}$ but also contains considerable amounts of PM_1 (including both $PM_{0.1}$ and $PM_{0.1\text{-}1}$).

- The PSDs of PM_{10} from pulverised pyrite combustion under the various conditions have a bimodal distribution, i.e. a fine mode with a mode diameter of 0.26 µm and a coarse mode with mode diameters from 4.4 µm to 6.8 µm.

- Particle residence time significantly affects the yields and PSDs of PM_{10} from pulverised pyrite combustion, suggesting that the formation of PM is strongly dependent on the progress of combustion.

- It was found that at 600 °C, the combustion of pulverized pyrite produces a substantial proportion of large ash cenospheres and substantial fragments of thin-walled ash cenospheres, strongly indicating the significant role of ash cenosphere fragmentation in ash formation.

- As the first in the field, this study provides direct experimental evidences to demonstrate the important role of ash cenosphere fragmentation in PM_{10} formation during the combustion of pulverised pyrite.

- At a furnace temperature of 600 °C, longer residence time favours the formation of ash cenospheres and intensifies the fragmentation of ash cenospheres and/or cenospheric precursor particles, leading to an increase in PM_{10} yield.

7.3 Recommendations

On the basis of the conclusions of the present study, the future work in this research area is recommended:

(1) Combustion conditions such as cooling rate can be important factors controlling ash cenosphere formation and fragmentation during solid fuel combustion. Future research is needed to study these aspects, particularly the effect of cooling rate on the formation and fragmentation of ash cenosphere and its role in PM formation via experiments using pyrite as a model fuel.

(2) Pyrite is used a model fuel for study ash cenosphere formation during solid fuel combustion. Future work should be extended to investigate ash cenosphere formation during the combustion of other pulverised solid fuels, considering parent fuels with various characteristics.

(3) It is also important to carry out mathematical modelling on the formation and fragmentation behaviour of ash cenospheres during solid fuels combustion, using the experimental data in this thesis for model validation.

REFERENCES

1. IEA, International Energy Outlook. *U.S. Energy Information Administration* **2010**.
2. Borm, P. J. A., Toxicity and occupational health hazards of coal fly ash (CFA). A review of data and comparison to coal mine dust. *Annals of Occupational Hygiene* **1997,** 41, (6), 659-676.
3. van Hook, R. I., Potential health and environmental effects of trace elements and radionuclides from increased coal utilization. *Environmental Health Perspectives* **1979,** 33, 227-247.
4. Santhanam, C. J.; Lunt, R. R.; Johnson, S. L.; etc., Health and environmental impacts of increased generation of coal ash and FGD sludges. *Environmental Health Perspectives* **1979,** 33, 131-157.
5. Adriano, D. C.; Page, A. L.; Elseewi, A. A.; Chang, A. C.; Straughan, I., Utilization and Disposal of Fly Ash and Other Coal Residues in Terrestrial Ecosystems: A Review. *J. Environ. Qual.* 9, (3), 333-344.
6. Gupta, D.; Rai, U.; Tripathi, R.; Inouhe, M., Impacts of fly-ash on soil and plant responses. *Journal of Plant Research* **2002,** 115, (6), 401-409.
7. Torrey, S., *Coal Ash Utilization: Fly Ash, Bottom Ash and Slag*. Noyes Data Corporation: New Jersey, 1978.
8. Iyer, R. S.; Scott, J. A., Power station fly ash — a review of value-added utilization outside of the construction industry. *Resources, Conservation and Recycling* **2001,** 31, (3), 217-228.
9. Wang, S.; Wu, H., Environmental-benign utilisation of fly ash as low-cost adsorbents. *Journal of Hazardous Materials* **2006,** 136, (3), 482-501.
10. *Annual Membership Survey Results*; 2010.
11. Elliot, A.; Zhang, D., Australia coal ash-a valuable resources: current state and future directions. *CRC for Coal in Sustainable Development: Perth* **2003**.
12. Heidrich, C., Ash Utilisation - an Australian Perspective. In *2003 International Ash Utilization Symposium*, Univeristy of Kentuchy: 2003.
13. Anshits, N. N.; Mikhailova, O. A.; Salanov, A. N.; Anshits, A. G., Chemical composition and structure of the shell of fly ash non-perforated cenospheres produced from the combustion of the Kuznetsk coal (Russia). *Fuel* **2010,** 89, (8), 1849-1862.
14. Carlile, J., Cenospheres from various sources. *Fuel in Science and Practice* **1943,** 22, 87-95.
15. Fisher, G. L.; Chang, D. P. Y.; Brummer, M., Fly Ash Collected from Electrostatic Precipitators: Microcrystalline Structures and the Mystery of the Spheres. *Science* **1976,** 192, (4239), 553-555.
16. Jang, H.; Etsell, T. H., Morphological and Mineralogical Characterization of Oil Sands Fly Ash. *Energy & Fuels* **2005,** 19, 2121-2128.
17. Kruger, R.; Toit, P., Recovery and characterization of cenospheres from South African power plants. *Proceedings of Ninth International Ash Use Symposium* **1991,** 3, 1-20.
18. Lauf, R. J., Cenospheres in fly ash and conditions favouring their formation. *Fuel* **1981,** 60, (12), 1177-1179.

19. Ngu, L.-n.; Wu, H.; Zhang, D.-k., Characterization of Ash Cenospheres in Fly Ash from Australian Power Stations. *Energy & Fuels* **2007,** 21, (6), 3437-3445.
20. Raask, E., Cenospheres in pulverized-fuel ash. *Journal of the Institute of Fuel* **1968,** 43, 339-344.
21. Raask, E., *Mineral impurities in coal combustion-behaviour, problems, and remedial measures*. Hemisphere Publishing Corporation: Leatherhead, 1985.
22. Vassilev, S. V.; Menendez, R.; Diaz-Somoano, M.; Martinez-Tarazona, M. R., Phase-mineral and chemical composition of coal fly ashes as a basis for their multicomponent utilization. 2. Characterization of ceramic cenosphere and salt concentrates. *Fuel* **2004,** 83, (4-5), 585-603.
23. Zhao, Y.; Zhang, J.; Tian, C.; Li, H.; Shao, X.; Zheng, C., Mineralogy and Chemical Composition of High-Calcium Fly Ashes and Density Fractions from a Coal-Fired Power Plant in China. *Energy & Fuels* **2010,** 24, 834-843.
24. Kruger, R. A., Fly ash beneficiation in South Africa: creating new opportunities in the market-place. *Fuel* **1997,** 76, (8), 777-779.
25. Vassilev, S. V.; Vassileva, C. G., Mineralogy of combustion wastes from coal-fired power stations. *Fuel Processing Technology* **1996,** 47, (3), 261-280.
26. Barbare, N.; Shukla, A.; Bose, A., Uptake and loss of water in a cenosphere-concrete composite material. *Cement and Concrete Research* **2003,** 33, (10), 1681-1686.
27. Cardoso, R. J.; Shukla, A.; Bose, A., Effect of particle size and surface treatment on constitutive properties of polyester-cenosphere composites. *Journal of Materials Science* **2002,** 37, (3), 603-613.
28. Chalivendra, V. B.; Shukla, A.; Bose, A.; Parameswaran, V., Processing and mechanical characterization of lightweight polyurethane composites. *JOURNAL OF MATERIALS SCIENCE* **2003**
38, 1631-1643.
29. McBride, S. P.; Shukla, A.; Bose, A., Processing and characterization of a lightweight concrete using cenospheres. *Journal of Materials Science* **2002,** 37, (19), 4217-4225.
30. Rohatgi, P.; Guo, R., Opportunities of using fly ash particles for synthesis of composites. *Proceedings of the American Power Conference* **1997,** 59, (2), 828-833.
31. Souvignier, C.; Sercombe, T.; Huo, S.; Calvert, P.; Schaffer, G., Freeform fabrication of aluminum metal-matrix composites. *Journal of Materials Research* **2001,** 16, (9), 2613-2618.
32. Huffman, G. P.; Huggins, F. E.; Levasseur, A. A.; Chow, O.; Srinivasachar, S.; Mehta, A. K., Investigation of the transformations of pyrite in a drop-tube furnace. *Fuel* **1989,** 68, (4), 485-490.
33. ten Brink, H. M.; Eenkhoorn, S.; Hamburg, G., A fundamental investigation of the flame kinetics of coal pyrite. *Fuel* **1996,** 75, (8), 945-951.
34. Ramsden, A. R., Microscopic investigation into the formation of fly-ash during the combusiton of a pulverized bituminous coal. *Fuel* **1969,** 48, (2), 121-137.
35. Smith, R. D., The trace element chemistry of coal during combustion and the emissions from coal-fired plants
Progress in Energy and Combustion Science **1980,** 6, (1), 53-119.
36. Smith, R. D.; Campbell, J. A.; Nielson, K. K., Characterization and formation of submicron particles in coal-fired plants. *Atmospheric Environment (1967)* **1979,** 13, (5), 607-617.
37. Newall, H.; Sinnatta, F., The carbonisation of coal in the form of fine particles. I. The production of cenospheres. *Fuel in Science and Practice* **1924,** 3, 424-434.

38. Newall, H.; Sinnatta, F., The combustion of coal in air. The study of cenospheres. II. . *Fuel Science and Practice* **1926,** 5, (8), 335-339.
39. Newall, H.; Sinnatta, F., The carbonisaiton of particles of coal. The study of cenospheres.III. *Fuel in Science and Practice* **1927,** 6, (3), 118-120.
40. Anshits, A.; Sharonova, O.; Kovalev, A., The recovery of magnetic microspheres and cenospheres of the stabilized composition from coal power plant fly ash. *Proceedings of the International Technical Conference on Coal Utilication and Coal systems* **2001,** 26th, 1053-1062.
41. Blanco, F.; García, P.; Mateos, P.; Ayala, J., Characteristics and properties of lightweight concrete manufactured with cenospheres. *Cement and Concrete Research* **2000,** 30, (11), 1715-1722.
42. Drozhzhin, V.; Piculin, I.; Kuvayev, M., Natural silicate microspheres: properties and production methods. *Journal of the Moscow Physical Society* **1999,** 9, (3), 215-222.
43. Ignaszak, Z.; Baranowsi, A.; Hycnar, J.; Maria, A., Heat-insulating, high-temperature materials on cenosphere base. *ASTM Special Technical Publication* **1990,** 1030, 741-747.
44. Matsunaga, T.; Kim, J. K.; Hardcastle, S.; Rohatgi, P. K., Crystallinity and selected properties of fly ash particles *Materials Science and Engineering A* **2002,** 325, 333-343.
45. Rohatgi, P.; Huang, P.; Guo, R.; Keshavaram, N.; Golden, D., morphology and selected properities of fly ash. *American Concrete Institute* **1996,** 1, 459-478.
46. Sarkar, A.; Rano, R.; Mishra, K. K.; Mazumder, A., Characterization of Cenospheres Collected from Ash-pond of a Super Thermal Power Plant. *Energy Sources, Part A: Recovery, Utilization, and Environmental Effects* **2008,** 30, (3), 271-283.
47. Wandell, T., Cenospheres: from waste to profits. *American Ceramic Society Bulletin* **1996,** 75, (6), 79-81.
48. Yih, S.; Tu, C., Recovery of cenospheres and application to the manufacture of insulation materials. *Journal of the Chinese Institute of Chemical Engineers* **1988,** 19, (1), 23-29.
49. Jewad, M. A.; Probert, S. D., The thermal conductivity of pulverised-fuel ash cenospheres. *Applied Energy* **1976,** 2, 67-76.
50. Kolay, P. K.; Singh, D. N., Physical, chemical, mineralogical, and thermal properties of cenospheres from an ash lagoon. *Cement and Concrete Research* **2001,** 31, (4), 539-542.
51. Pedlow, J. W., *Coal ash utilization: fly ash, bottom ash, and slag.* Noyes Data Corp.: Park Ridge, 1978; p 353-363.
52. Russak, M. A.; Tobin, A.; Feldman, C., Development and characterization of a closed pore insulation material. *American Ceramic Society Bulletin* **1976,** 55, (5), 504-507.
53. Zhang, Q.; Li, Z. l.; Wang, H., A study on the benefication and application of fly ash from power plants. *The Australian Institute of Mining and Metallurgy* **1993,** 5, 1447-1452.
54. Sokol, E. V.; Maksimova, N. V.; Volkova, N. I.; Nigmatulina, E. N.; Frenkel, A. E., Hollow silicate microspheres from fly ashes of the Chelyabinsk brown coals (South Urals, Russia). *Fuel Processing Technology* **2000,** 67, (1), 35-52.
55. Bibby, D. M., Composition and variation of pulverized fuel ash obtained from the combustion of sub-bituminous coals, New Zealand. *Fuel* **1977,** 56, 427-431.

56. Vassilev, S. V.; Menendez, R.; Borrego, A. G.; Diaz-Somoano, M.; Rosa Martinez-Tarazona, M., Phase-mineral and chemical composition of coal fly ashes as a basis for their multicomponent utilization. 3. Characterization of magnetic and char concentrates. *Fuel* **2004,** 83, (11-12), 1563-1583.
57. ChavezAlcala, J.; MoralesDavila, R.; LastraQuintero, R., Recovery of cenospheres and magnetite from coal burning power plant fly ash. *Transactions ISIJ* **1987,** 27, 531-538.
58. Lilkov, V.; Djabarov, N.; Bechev, G.; Petrov, O., Properties and hydration products of lightweight and expansive cements Part II: Hydration products. *Cement and Concrete Research* **1999,** 29, (10), 1641-1646.
59. Shukla, S.; Seal, S.; Akesson, J.; Oder, R.; Carter, R.; Rahman, Z., Study of mechanism of electroless copper coating of fly-ash cenosphere particles. *Applied Surface Science* **2001,** 181, (1-2), 35-50.
60. Fisher, G.; Prentice, B.; Silberman, D.; Ondov, J., physical and morphological studies of size-classified coal fly ash. *Environmental Science and Technology* **1978,** 12 (4), 447-451.
61. Gupta, N.; Woldesenbet, E.; Mensah, P., Compression properties of syntactic foams: effect of cenosphere radius ratio and specimen aspect ratio. *Composites Part A: Applied Science and Manufacturing* **2004,** 35, (1), 103-111.
62. Hiel, C.; Dittman, D.; Ishai, O., Composite sandwich construction with syntactic foam core: a practical assessment of post-impact damage and residual strength. *Composites* **1993,** 24, (5), 447-450.
63. Johnson, A. A.; Mukherjee, K.; Schlosser, S.; Raask, E., The behaviour of a cenosphere-resin composite under hydrostatic pressure. *Ocean Engineering* **1970,** 2, (1), 45-46, IN3-IN4, 47-48.
64. Shutov, F., *Syntactic polymeric foams*. Hanser Publisher: New York, 1991; p 355-374.
65. Bardella, L.; Genna, F., Elastic design of syntactic foamed sandwiches obtained by filling of three-dimensional sandwich-fabric panel. *International Journal of Solids Structure* **2000,** 38, (2), 307-333.
66. Dou, Z.; Jiang, L.; Wu, G.; Zhang, Q.; Xiu, Z.; Chen, G., High strain rate compression of cenosphere pure aluminum syntactic foam. *Reinforced Plastics* **2007,** 46, (10), 16.
67. Shao, Y.; Jia, D.; Zhou, Y.; Liu, B., Novel method for fabrication of silicon nitrides/silicon oxynitride composite ceramic foams using fly ash cenosphere as a pore forming agent. *Journal of America Ceramic Society* **2008,** 91, (11), 3781-3785.
68. Parameswaran, V.; Shukla, A., Processing and characterization of a model functionally gradient material. *Journal of Materials Science* **2000,** 35, (1), 21-29.
69. Rousseau, C.; Tippur, H., Evaluation of crack tip fields and stress intensity factors in functionally graded elastic materials: Cracks parallel to elastic gradient. *International Journal of Fracture* **2002,** 114, 87-111.
70. Rohatgi, P. K.; Guo, R. Q.; Iksan, H.; Borchelt, E. J.; Asthana, R., Pressure infiltration technique for synthesis of aluminum-fly ash particulate composite. *Materials Science and Engineering A* **1998,** 244, (1), 22-30.
71. Anshits, A. G.; Kondratenko, E. V.; Fomenko, E. V.; Kovalev, A. M.; Anshits, N. N.; Bajukov, O. A.; Sokol, E. V.; Salanov, A. N., Novel glass crystal catalysts for the processes of methane oxidation. *Catalysis Today* **2001,** 64, (1-2), 59-67.
72. Anshits, A. G.; Kondratenko, E. V.; Fomenko, E. V.; Kovalev, A. M.; Bajukov, O. A.; Anshits, N. N.; Sokol, E. V.; Kochubey, D. I.; Boronin, A. I.; Salanov, A. N.; Koshcheev, S. V., Physicochemical and catalytic properties of glass crystal catalysts

for the oxidation of methane. *Journal of Molecular Catalysis A: Chemical* **2000,** 158, (1), 209-214.
73. Bartake, P.; Singh, D., Determination of crushing strength of cenospheres. *Journal of ASTM International* **2005,** 2, (7), 1-9.
74. Prashanth, T.; Kumar, M.; SuryaNarayan, Evaluation of sliding wear properties of fly ash cenosphere aluminum composite. *International Conference on Advanced Materials and Composites* **2007**, 490-495.
75. Drozhzhin, V.; Piculin, I.; Alexandrovich, R.; Aushev, A., Microspheres of natural silicates as fillers of composite materials. *Journal of the Moscow Physical Society* **1999,** 9, (3), 209-214.
76. Montgomery, D.; Diamond, S., The influence of fly ash cenospheres on the details of cracking in flyash-bearing cement pastes. *Cement and Concrete Research* **1984,** 14, (6), 767-775.
77. Pervez, S.; Pandey, G., Cenosphere-load in coal-ash discharge of thermal power plant. *Research and Industry* **1993,** 38, 99-100.
78. Vassilev, S. V.; Menendez, R.; Alvarez, D.; Diaz-Somoano, M.; Martinez-Tarazona, M. R., Phase-mineral and chemical composition of coal fly ashes as a basis for their multicomponent utilization. 1. Characterization of feed coals and fly ashes[small star, filled]. *Fuel* **2003,** 82, (14), 1793-1811.
79. Ghosal, S.; Self, S. A., Particle size-density relation and cenosphere content of coal fly ash. *Fuel* **1995,** 74, (4), 522-529.
80. Gurupira, T.; Jone, C. L.; Howard, A.; Lockert, C.; Wandell, T.; Stencel, J. M., New products from coal combustion ash: Selective extraction of particle with density <2. In *International Ash Utilization Symposium*, Centre for Applied Energy Research: Univeristy of Kentucky, 2001.
81. Honaker, R., Generating products from coal combustion fly ash using physical separations. *Environmental Issues and Waste Management in Energy and Mineral Production, Proceedings of the International Symposium on Environmental Issues and Waste Management in Energy and Mineral Production, 5th, Ankara* **1998**, 565.
82. Sarofim, A. F.; Howard, J. B.; Padia, A. S., The Physical Transformation of the Mineral Matter in Pulverized Coal Under Simulated Combustion Conditions. *Combustion Science and Technology* **1977,** 16, (3), 187-204.
83. Srinivasachar, S.; Helble, J. J.; Boni, A. A.; Shah, N.; Huffman, G. P.; Huggins, F. E., Mineral behavior during coal combustion 2. Illite transformations. *Progress in Energy and Combustion Science* **1990,** 16, (4), 293-302.
84. Fisher, G.; Natusch, D., Academic Press: New York, 1979; Vol. 3, p 489-541.
85. Hubbard, F.; McGILL, R., Clay and pytire transformations during ignition of pulverized coal. *Mineralogical Magzine* **1984,** 48, 251-256.
86. Spears, D. A., Role of clay minerals in UK coal combustion. *Applied Clay Science* **2000,** 16, (1-2), 87-95.
87. Wibberley, L. J.; Wall, T. F., An Investigation of Factors Affecting the Physical Characteristics of Flyash Formed in a Laboratory Scale Combustor. *Combustion Science and Technology* **1986,** 48, (3-4), 177-190.
88. Fenelonov, V. B., The properties of cenospheres and the mechanism of their formation during high-temperature coal combustion at thermal power plants. *KONA Powder & Particle* **2010,** 28, 189-208.
89. Bryers, R. W., Fireside slagging,fouling,and high-temperature corrosion of heat-thansfer surface due to impurities in steam raising fuels
Progress in Energy and Combustion Science
1996, 22, 29-120.

90. Miller, S. F.; Schobert, H. H., Effect of the occurrence and composition of iron compounds on ash formation, composition, and size in pilot-scale combustion of pulverized coal and coal-water slurry fuels. *Energy & Fuels* **1993,** 7, (6), 1030-1038.
91. Baxter, L. L., The evolution of mineral particle size distributions during early stages of coal combustion. *Progress in Energy and Combustion Science* **1990,** 16, (4), 261-266.
92. Baxter, L. L.; Mitchell, R. E.; Fletcher, T. H., Release of inorganic material during coal devolatilization. *Combustion and Flame* **1997,** 108, (4), 494-502.
93. Bool Iii, L. E.; Peterson, T. W.; Wendt, J. O. L., The partitioning of iron during the combustion of pulverized coal. *Combustion and Flame* **1995,** 100, (1-2), 262-270.
94. McLennan, A. R.; Bryant, G. W.; Bailey, C. W.; Stanmore, B. R.; Wall, T. F., An Experimental Comparison of the Ash Formed from Coals Containing Pyrite and Siderite Mineral in Oxidizing and Reducing Conditions. *Energy & Fuels* **2000,** 14, (2), 308-315.
95. Srinivasachar, S. H., J. J.; Boni, A. A.; , Mineral behavior during coal combustion 1. pyrite transformations. *Progress in Energy and Combustion Science* **1990,** 16, (4), 281-292.
96. ten Brink, H. M. t.; Smart, J. P.; Vleeskens, J. M.; Williamson, J., Flame transformations and burner slagging in a 2.5 MW furnace firing pulverized coal: 1. Flame transformations. *Fuel* **1994,** 73, (11), 1706-1711.
97. Zeng, T.; Helble, J. J.; Bool, L. E.; Sarofim, A. F., Iron transformations during combustion of Pittsburgh no. 8 coal. *Fuel* **2009,** 88, (3), 566-572.
98. Bhargava, S. K.; Garg, A.; Subasinghe, N. D., In situ high-temperature phase transformation studies on pyrite. *Fuel* **2009,** 88, (6), 988-993.
99. Dunn, J. G.; De, G. C.; O'Connor, B. H., The effect of experimental variables on the mechanism of the oxidation of pyrite: Part 2. Oxidation of particles of size 90-125 [mu]m. *Thermochimica Acta* **1989,** 155, 135-149.
100. Dunn, J. G.; De, G. C.; O'Connor, B. H., The effect of experimental variables on the mechanism of the oxidation of pyrite: Part 1. Oxidation of particles less than 45 [mu]m in size. *Thermochimica Acta* **1989,** 145, 115-130.
101. Jorgensen, F. R. A.; Jorgensen, F., Phases formed during the thermal analysis of pyrite in air. *Journal of thermal analysis* **1982,** 25, (2), 473.
102. Schwab, G.-M.; Philinis, J., Reactions of Iron Pyrite: Its Thermal Decomposition, Reduction by Hydrogen and Air Oxidation. *Journal of the American Chemical Society* **1947,** 69, (11), 2588-2596.
103. Hu, G.; Dam-Johansen, K.; Wedel, S.; Hansen, J. P., Decomposition and oxidation of pyrite. *Progress in Energy and Combustion Science* **2006,** 32, (3), 295-314.
104. Hong, Y.; Fegley, B., The kinetics and mechanism of pyrite thermal decomposition. *Berichte der Bunsengesellschaft für physikalische Chemie* **1997,** 101, (12), 1870-1881.
105. Srinivasachar, S.; Boni, A. A., A kinetic model for pyrite transformations in a combustion environment. *Fuel* **1989,** 68, (7), 829-836.
106. Srinivasachar, S.; Helble, J. J.; Boni, A. A., Mineral behavior during coal combustion 1. Pyrite transformations. *Progress in Energy and Combustion Science* **1990,** 16, (4), 281-292.
107. Bryers, R. W., Physical and chemical characteristics of pyrites and their influence on fireside problems in steam generators. *Journal Name: J. Eng. Power;*

(United States); Journal Volume: 98:4; Conference: ASME winter annual meeting, Houston, TX, USA, 30 Nov 1975 **1976**, Medium: X; Size: Pages: 517-527.
108. Groves, S. J.; Williamson, J.; Sanyal, A., Decomposition of pyrite during pulverized coal combustion. *Fuel* **1987,** 66, (4), 461-466.
109. Sheng, C.; Lin, J.; Li, Y.; Wang, C., Transformation behaviors of excluded pyrite during O2/CO2 combustion of pulverized coal. *Asia-Pacific Journal of Chemical Engineering* **2010,** 5, (2), 304-309.
110. Yan, L.; Gupta, R.; Wall, T., Fragmentation Behavior of Pyrite and Calcite during High-Temperature Processing and Mathematical Simulation. *Energy & Fuels* **2001,** 15, (2), 389-394.
111. Naldrett, A. J., A Portion of the System Fe-S-O between 900 and 1080 °C and its Application to Sulfide Ore Magmas. *Journal of Petrology* **1969,** 10, (2), 171-201.
112. Lighty, J., combustin aerosols: factors govering their size and composition and implications to human health
Journal of the Air & Waste Management Association **2000,** 50, (9), 1565-1618.
113. Davison, R. L.; Natusch, D. F. S.; Wallace, J. R.; Evans, C. A., Trace elements in fly ash. Dependence of concentration on particle size. *Environmental Science & Technology* **1974,** 8, (13), 1107-1113.
114. Damle, A. S.; Ensor, D. S.; Ranade, M. B., Coal Combustion Aerosol Formation Mechanisms: A Review. *Aerosol Science and Technology* **1982,** 1, (1), 119-133.
115. Gladney, E. S.; Small, J. A.; Gordon, G. E.; Zoller, W. H., Composition and size distribution of in-stack particulate material at a coal-fired power plant. *Atmospheric Environment (1967)* **1976,** 10, (12), 1071-1077.
116. Kauppinen, E. I.; Pakkanen, T. A., Coal combustion aerosols: a field study. *Environmental Science & Technology* **1990,** 24, (12), 1811-1818.
117. Linak, W. P.; Yoo, J.-I.; Wasson, S. J.; Zhu, W.; Wendt, J. O. L.; Huggins, F. E.; Chen, Y.; Shah, N.; Huffman, G. P.; Gilmour, M. I., Ultrafine ash aerosols from coal combustion: Characterization and health effects. *Proceedings of the Combustion Institute* **2007,** 31, (2), 1929-1937.
118. Lind, T.; Valmari, T.; Kauppinen, E. I.; Sfiris, G.; Nilsson, K.; Maenhaut, W., Volatilization of the Heavy Metals during Circulating Fluidized Bed Combustion of Forest Residue. *Environmental Science & Technology* **1998,** 33, (3), 496-502.
119. Yu, D.; Xu, M. H.; Liu, X.; Huang, J.; Li, G., Mechanisms of Submicron and Residual Ash Particle Formation during Pulverised Coal Combustion: A Comprehensive Review. *Developments in Chemical Engineering and Mineral Processing* **2005,** 13, (3-4), 467-482.
120. Esmen, N. A.; Corn, M., Residence time of particles in urban air. *Atmospheric Environment (1967)* **1971,** 5, (8), 571-578.
121. Lind, T.; Kauppinen, E. I.; Maenhaut, W.; Shah, A.; Huggins, F., Ash Vaporization in Circulating Fluidized Bed Coal Combustion. *Aerosol Science and Technology* **1996,** 24, (3), 135-150.
122. Liu, X.; Xu, M.; Yao, H.; Yu, D.; Gao, X.; Cao, Q.; Cai, Y., Effect of Combustion Parameters on the Emission and Chemical Composition of Particulate Matter during Coal Combustion. *Energy & Fuels* **2006,** 21, (1), 157-162.
123. McElroy, M. W.; Carr, R. C.; Ensor, D. S.; Markowski, G. R., Size distribution of fine particles from coal combustion. *Science* **1982,** 215, (4528), 13-19.
124. Sheng, C.; Li, Y.; Liu, X.; Yao, H.; Xu, M., Ash particle formation during O2/CO2 combustion of pulverized coals. *Fuel Processing Technology* **2007,** 88, (11-12), 1021-1028.

125. Takuwa, T.; Mkilaha, I. S. N.; Naruse, I., Mechanisms of fine particulates formation with alkali metal compounds during coal combustion. *Fuel* **2006,** 85, (5-6), 671-678.
126. Zhang, L.; Ninomiya, Y., Emission of suspended PM10 from laboratory-scale coal combustion and its correlation with coal mineral properties. *Fuel* **2006,** 85, (2), 194-203.
127. Gao, X.; Wu, H., Effect of Sampling Temperature on the Properties of Inorganic Particulate Matter Collected from Biomass Combustion in a Drop-Tube Furnace. *Energy & Fuels* **2010,** 24, (8), 4571-4580.
128. Linak, W. P.; Miller, C. A.; Seames, W. S.; Wendt, J. O. L.; Ishinomori, T.; Endo, Y.; Miyamae, S., On trimodal particle size distributions in fly ash from pulverized-coal combustion. *Proceedings of the Combustion Institute* **2002,** 29, (1), 441-447.
129. Seames, W. S., An initial study of the fine fragmentation fly ash particle mode generated during pulverized coal combustion. *Fuel Processing Technology* **2003,** 81, (2), 109-125.
130. Yu, D.; Xu, M.; Yao, H.; Liu, X.; Zhou, K., A new method for identifying the modes of particulate matter from pulverized coal combustion. *Powder Technology* **2008,** 183, (1), 105-114.
131. Kang, S. G. Fundamental studies of mineral matter transformation during pulverized coal combustion: residual ash formation. MIT, 1991.
132. Sheng, C.; Lu, Y.; Gao, X.; Yao, H., Fine Ash Formation during Pulverized Coal Combustion A Comparison of O2/CO2 Combustion versus Air Combustion *Energy & Fuels* **2006,** 21, (2), 435-440.
133. Yu, D.; Xu, M.; Yao, H.; Sui, J.; Liu, X.; Yu, Y.; Cao, Q., Use of elemental size distributions in identifying particle formation modes. *Proceedings of the Combustion Institute* **2007,** 31, (2), 1921-1928.
134. Ninomiya, Y.; Zhang, L.; Sato, A.; Dong, Z., Influence of coal particle size on particulate matter emission and its chemical species produced during coal combustion. *Fuel Processing Technology* **2004,** 85, (8-10), 1065-1088.
135. Sadakata, M.; Mochizuki, M.; Sakai, T.; Okazaki, K.; Ono, M., Formation and behavior of submicron fly ash in pulverized coal combustion furnace. *Combustion and Flame* **1988,** 74, (1), 71-80.
136. Zhang, L.; Ninomiya, Y.; Yamashita, T., Formation of submicron particulate matter (PM1) during coal combustion and influence of reaction temperature. *Fuel* **2006,** 85, (10-11), 1446-1457.
137. Xu, M.; Yu, D.; Yao, H.; Liu, X.; Qiao, Y., Coal combustion-generated aerosols: Formation and properties. *Proceedings of the Combustion Institute* **2011,** 33, (1), 1681-1697.
138. Flagan, R. C.; Friedlander, S. K., *Recent developments in aerosol science*. John Wiley and Sons: New York, 1978.
139. Quann, R. J.; Sarofim, A. F., A scanning electron microscopy study of the transformations of organically bound metals during lignite combustion. *Fuel* **1986,** 65, (1), 40-46.
140. Buhre, B. J. P.; Hinkley, J. T.; Gupta, R. P.; Nelson, P. F.; Wall, T. F., Fine ash formation during combustion of pulverised coal-coal property impacts. *Fuel* **2006,** 85, (2), 185-193.
141. Helble, J. J.; Srinivasachar, S.; Boni, A. A., Factors influencing the transformation of minerals during pulverized coal combustion. *Progress in Energy and Combustion Science* **1990,** 16, (4), 267-279.

142. Baxter, L. L., Char fragmentation and fly ash formation during pulverized-coal combustion. *Combustion and Flame* **1992,** 90, (2), 174-184.
143. Helble, J. J.; Sarofim, A. F., Influence of char fragmentation on ash particle size distributions. *Combustion and Flame* **1989,** 76, (2), 183-196.
144. Sundback, C. A.; BeÃ©r, J. M.; Sarofim, A. F., Fragmentation behavior of single coal particles in a fluidized bed. *Symposium (International) on Combustion* **1985,** 20, (1), 1495-1503.
145. Mitchell, R. E.; Akanetuk, A. E. J., The impact of fragmentation on char conversion during pulverized coal combustion. *Symposium (International) on Combustion* **1996,** 26, (2), 3137-3144.
146. Liu, G.; Benyon, P.; Benfell, K. E.; Bryant, G. W.; Tate, A. G.; Boyd, R. K.; Harris, D. J.; Wall, T. F., The porous structure of bituminous coal chars and its influence on combustion and gasification under chemically controlled conditions. *Fuel* **2000,** 79, (6), 617-626.
147. Wu, H.; Wall, T.; Liu, G.; Bryant, G., Ash Liberation from Included Minerals during Combustion of Pulverized Coal: The Relationship with Char Structure and Burnout. *Energy & Fuels* **1999,** 13, (6), 1197-1202.
148. Helble, J.; Neville, M.; Sarofim, A. F., Aggregate formation from vaporized ash during pulverized coal combustion. *Symposium (International) on Combustion* **1988,** 21, (1), 411-417.
149. Helble, J. J.; Sarofim, A. F., Factors determining the primary particle size of flame-generated inorganic aerosols. *Journal of Colloid and Interface Science* **1989,** 128, (2), 348-362.
150. Quann, R. J.; Sarofim, A. F., vaporization of refractory oxides during pulverized coal combustion. *Nineteenth Symposium (International) on Combustion/ The Combustion Institute*
1982, 1429-1440.
151. Wall, T. F.; Lowe, A.; Wibberley, L. J.; MacStewart, I., Mineral matter in coal and the thermal performance of large boilers. *Process in Energy and Combustion Science* **1979,** 5, 1-29.
152. Neville, M.; Quann, R. J.; Haynes, B. S.; Sarofim, A. F., Vaporization and condensation of mineral matter during pulverized coal combustion. *Symposium (International) on Combustion* **1981,** 18, (1), 1267-1274.
153. Buhre, B. J. P.; Hinkley, J. T.; Gupta, R. P.; Wall, T. F.; Nelson, P. F., Submicron ash formation from coal combustion. *Fuel* **2005,** 84, (10), 1206-1214.
154. Liu, X.; Xu, M.; Yao, H.; Yu, D.; Lv, D.; Zhou, K., The Formation and Emission of Particulate Matter during the Combustion of Density Separated Coal Fractions. *Energy & Fuels* **2008,** 22, (6), 3844-3851.
155. Xu, M.; Yan, R.; Zheng, C.; Qiao, Y.; Han, J.; Sheng, C., Status of trace element emission in a coal combustion process: a review. *Fuel Processing Technology* **2004,** 85, (2-3), 215-237.
156. Holve, D. J., In Situ Measurements of Flyash Formation from Pulverized Coal. *Combustion Science and Technology* **1986,** 44, (5-6), 269-288.
157. Zhang, L.; Ninomiya, Y.; Yamashita, T., Occurrence of Inorganic Elements in Condensed Volatile Matter Emitted from Coal Pyrolysis and Their Contributions to the Formation of Ultrafine Particulates during Coal Combustion. *Energy & Fuels* **2006,** 20, (4), 1482-1489.
158. Kang, S.-G.; Helble, J. J.; Sarofim, A. F.; Beér, J. M., Time-resolved evolution of fly ash during pulverized coal combustion. *Symposium (International) on Combustion* **1989,** 22, (1), 231-238.

159. Quann, R. J.; Neville, M.; Janghorbani, M.; Mims, C. A.; Sarofim, A. F., Mineral matter and trace-element vaporization in a laboratory-pulverized coal combustion system. *Environmental Science & Technology* **1982,** 16, (11), 776-781.
160. Wang, Q.; Zhang, L.; Sato, A.; Ninomiya, Y.; Yamashita, T., Interactions among Inherent Minerals during Coal Combustion and Their Impacts on the Emission of PM10. 1. Emission of Micrometer-Sized Particles. *Energy & Fuels* **2007,** 21, (2), 756-765.
161. Yip, K.; Tian, F.; Hayashi, J.-i.; WU, H., Effect of alkali and alkaline earth metallic species on biochar reactivity and syngas compositions during steam gasification. *Energy & Fuels* **2010,** 24, (1), 173-181.
162. Li, C.Z.; Sathe, C; Kershaw, J. R; Pang, Y., Fates and roles of alkali and alkaline earth metals during the pyrolysis of a Victorian brown coal. *Fuel* **2000**, 79, (3-4), 427-438.
163. Gao, X.; Wu, H., Combustion of Volatiles Produced in Situ from the Fast Pyrolysis of Woody Biomass: Direct Evidence on Its Substantial Contribution to Submicrometer Particle (PM1) Emission. *Energy & Fuels* **2011,** 25, (9), 4172-4181.
164. Gao, X.; Wu, H., Biochar as a Fuel: 4. Emission Behavior and Characteristics of PM1 and PM10 from the Combustion of Pulverized Biochar in a Drop-Tube Furnace. *Energy & Fuels* **2011,** 25, (6), 2702-2710.
165. Winegartner, E.; Rhodes, B., An expirical study of the relation of chemical properties to ash fusion temperatures. *Journal of Engineering for Power* **1975**, 395-406.
166. Hoy, H., Behaviour of mineral matter in slagging gasification processes. *Journal of Institution of Gas Engineers* **1965,** 5, (6), 444-469.
167. van Dyk, J. C.; Waanders, F. B.; Benson, S. A.; Laumb, M. L.; Hack, K., Viscosity predictions of the slag composition of gasified coal, utilizing FactSage equilibrium modelling. *Fuel* **2009,** 88, (1), 67-74.
168. Yan, L.; Gupta, R. P.; Wall, T. F., A mathematical model of ash formation during pulverized coal combustion. *Fuel* **2002,** 81, (3), 337-344.
169. Raask, E., Creation, capture and coalescence of mineral species in coal flames. *Journal of the Institute of Energy* **1984,** 57, (430), 231.
170. Hansen, J. P. PhD Thesis, Technical University of Denmark, 2003.

Every reasonable effort has been made to acknowledge the owners of copyright material. I would be pleased to hear from any copyright owner who has been omitted or incorrectly acknowledged.